Modulation and Coding Techniques for Infrared Wireless Local Area Networks

by

Ubolthip Sethakaset

B.Eng., Kasetsart University, 1998
M.Eng., Kasetsart University, 2000

A Dissertation Submitted in Partial Fulfillment of the Requirements
for the Degree of

DOCTOR OF PHILOSOPHY

in the Department of Electrical and Computer Engineering

Modulation and Coding Techniques for Infrared Wireless Local Area Networks

by

Ubolthip Sethakaset

Ph.D, University of Victoria, 2006

Supervisory Committee

Dr. T. Aaron Gulliver, Supervisor (Department of Electrical and Computer Engineering)

Dr. Adam Zielinski, Department Member (Department of Electrical and Computer Engineering)

Dr. Michael McGuire, Department Member (Department of Electrical and Computer Engineering)

Dr. Kui Wu, Outside Member (Department of Computer Science)

Supervisory Committee

Dr. T. Aaron Gulliver, Supervisor (Department of Electrical and Computer Engineering)

Dr. Adam Zielinski, Department Member (Department of Electrical and Computer Engineering)

Dr. Michael McGuire, Department Member (Department of Electrical and Computer Engineering)

Dr. Kui Wu, Outside Member (Department of Computer Science)

ABSTRACT

Because of low-cost optical devices and virtually unlimited bandwidth, optical wireless communications (OWC) for indoor wireless local area networks (WLANs) have recently become an attractive alternative to radio frequency systems. Since optical signals cannot penetrate through walls or other opaque barriers, the security of infrared WLANs is very high and there is no interference between rooms. Subsequently, cell planning is simple and easy, and the potential capacity of an optical-based network in a building is extremely high. However, the system link is susceptible to path loss and multipath dispersion. In addition, the average transmit power is constrained by eye-safety regulations and power consumption concerns. Hence, most recent research deals with the physical layer aspects such as modulation, equalization and error-control coding in order to cope with these drawbacks, especially the effects of multipath dispersion. The objective of this thesis is to study practical signaling techniques capable of eliminating the effects of intersymbol interference (ISI).

Regarding the drawbacks of OWC, modulation schemes which are power and bandwidth efficient are considered. Pulse-position modulation (PPM) has been employed for IrDA and IEEE802.11 standards because it offers high power efficiency. However, it requires high bandwidth so that its performance is considerably degraded when the channel

is more corrupted by ISI. A number of modified PPM techniques have been proposed to improve bandwidth efficiency. This thesis introduces a hybrid between pulse-amplitude modulation (PAM) and differential pulse-position modulation (DPPM), named differential amplitude pulse-position modulation (DAPPM), in order to gain a better compromise between power and bandwidth efficiency. It yields better bandwidth and/or power efficiency than PAM, PPM and DPPM depending on the number of amplitude levels (A), and the maximum length (L) of a symbol.

The channel capacity of PPM, DPPM and DAPPM systems is investigated. Since these modulation schemes over an ISI channel can be represented by a trellis diagram, their channel capacity is determined using a method for calculating the capacity of a Markov process channel. Over a soft-output channel, DAPPM achieves a higher capacity and is less sensitive to multipath dispersion than PPM and DPPM. Moreover, the comparison of hard-decision decoding (HDD) and soft-decision decoding (SDD) for PPM and DPPM systems shows that the performance of SDD is superior to that of HDD, especially when the channel is dispersive.

Then, some soft-decision techniques for DPPM system are considered. Although maximum-likelihood sequence detection (MLSD) is the optimal SDD for DPPM system, its complexity is extremely high. This thesis examines SDDs which are less complex than MLSD, but have performance close to that with MLSD. As the DPPM system is a Markov process, maximum a posteriori (MAP), Max-Log-MAP and the soft-output Viterbi algorithm (SOVA) are adopted. In addition, a novel very low complexity soft-decision decoding algorithm is introduced. The performance of the proposed algorithm is independent of the knowledge of the channel model, while the performance of the optimal and suboptimal MAP algorithms is impaired when the receiver has no information about the channel.

Finally, to achieve lower power requirements, error-control coding in an OWC system is investigated. Because insertion and deletion errors exist in DPPM systems, conventional coding techniques cannot be used. This thesis presents the concatenation of marker and Reed-Solomon codes which is able to correct such errors. The coded systems with HDD

and SDD are examined by analysis and simulation.

Table of Contents

List of Tables

List of Figures

List of Abbreviations

WLANs	wireless local area networks
OWC	optical wireless communications
IM/DD	intensity modulation and direct detection
AWGN	additive white Gaussian noise
ISI	intersymbol interference
OOK	on-off keying
PPM	pulse-position modulation
MPPM	multiple pulse-position modulation
OPPM	overlapping pulse-position modulation
DPPM	differential pulse-position modulation
DAPPM	differential amplitude pulse-position modulation
DH-PIM	dual header pulse interval modulation
PAPR	peak-to-average power ratio
SNR	signal-to-noise ratio
BER	bit error rate
FER	frame error rate
MLSD	maximum-likelihood sequence detection
MAP	maximum a posteriori
SOVA	soft-output Viterbi algorithm
RS-M	concatenated Reed-Solomon and marker codes
bps	bits per second

Acknowledgement

I could go through the doctoral program at University of Victoria because of these people whom I can never thank enough.

Firstly, I would like to acknowledge and thank my supervisor, Professor T. Aaron Gulliver, for accepting me as his student and generously giving me support and guidance. I would also like to express my deepest gratitude to Dr. Poramate Tarasak, who was the key to my success. You are the one who introduced optical wireless communications to me and always give me helpful discussions on my work. Because of you and my parents, who have always been there to support, encourage and believe in me, I could pursue my education. Many thanks are due to my friends and staff for lots of help. Finally, I am grateful to the University of Victoria Fellowship and UVic-Anand Fund for financial support.

Dedication

Dedicated to my parents, Roongchip (Chin-Long) Sethakaset and Su-Yei Peng; my brother, Davis (Guo-Song) Peng; and my sister, Viyada (Guo-Mei) Peng.

Chapter 1

Introduction

Recently, the use of mobile devices, e.g., laptops, cell phones and PDAs, has become ubiquitous. Users expect to access very high-speed backbone networks and be able to communicate with other users, and share common resources such as printers and scanners, through an ad-hoc network at high transfer data rates. As a consequence, wireless local area networks (WLANs) have been introduced and attract more attention from researchers. WLANs are subject to more noise and interference compared with wired-line systems. Because users are sharing the same high-speed network channel, high data security and extremely high bandwidth are in demand. From a user's point of view, power consumption, size, weight and cost of portable devices are major concerns. Thus, WLAN design is more challenging than for a cable backbone network.

In general, WLANs have adopted radio wave-based technology, for example Bluetooth, IEEE802.11 and ultra wideband (UWB). The demand for access to the network is growing rapidly, yet radio bandwidth is limited. In the future, radio frequencies may be insufficient to accommodate a large number of users or devices. Accordingly, Gfeller and Bapst [1] recommended utilization of infrared in indoor wireless communications in 1979, and this has been received wide interest. The most attractive point of infrared WLANs is that they provide virtually unlimited and worldwide unregulated bandwidth because the infrared frequencies range from 300 GHz to approximately 300 THz. The optical transceiver can be made smaller and cheaper than an RF transceiver module. In addition, the optical circuitry consumes little power; therefore the battery life can be very long. A comparison of dif-

ferent communications standards, e.g., IEEE802.11, UWB, Bluetooth and an optical link in terms of power consumption and bit rate was given in [2]. It was shown that optical systems achieve the highest bit rate and the least energy consumption normalized by the bit rate (J/Bits). Since optical signals cannot penetrate through walls or other opaque barriers, the security of infrared WLANs is very high and there is no interference between rooms. Consequently, the cell planning is simple and easy, and the potential capacity of an optical-based network in a building is extremely high. Infrared WLANs can be used in radiowave prohibited environments such as hospitals, airplanes and laboratories as there is no electromagnetic interference (EMI).

An optical system is expected to operate at very high data rates (several Gbps) within approximately a 10-meter range. However, the crucial factor which hinders the rate of data transmission is multipath dispersion caused by reflections from ceilings and walls. The misalignment between transmitter and receiver caused by objects and people degrades the performance of the system. Optical wireless communications (OWC) are also susceptible to ambient optical noise such as sunlight and illuminating lights. Hence, most recent research deals with the physical layer aspects of optical systems such as modulation, equalization and error-control coding, in order to cope with these drawbacks, especially the effects of multipath dispersion [3, 4, 5, 6].

The object of this thesis is to develop modulation schemes and error-control coding techniques in order to improve the performance of indoor optical wireless communications. Both the bit error rate (BER) and channel capacity are investigated.

1.1 Optical Wireless Communications (OWC)

Since a coherent optical system is difficult to implement because of the need for an accurate local oscillator and requires expensive coherent optical sources, an optical wireless system widely uses intensity modulation and direct detection (IM/DD) which is simply implemented, as shown in Fig. 1.1. Furthermore, the advantage of using IM/DD is its spatial

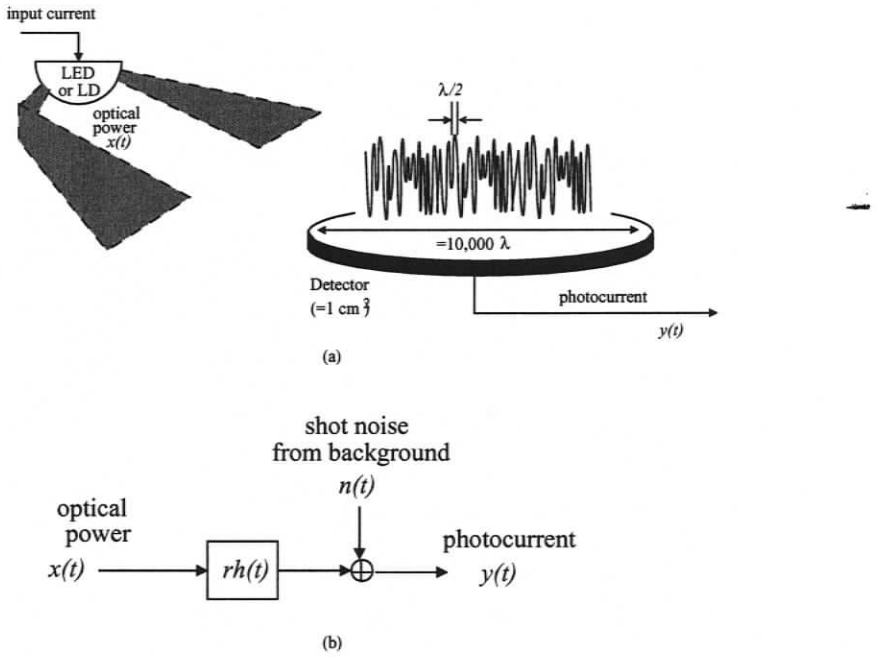

Figure 1.1. *(a) Transmitter and receiver in an infrared link with intensity modulation and direct detection (IM/DD). (b) The channel can be modeled as a time-invariant system having impulse response $h(t)$, with additive white Gaussian noise $n(t)$. The photodetector has responsivity r.*

diversity. Intensity modulation means that the intensity of the light wave $x(t)$ is modulated according to the transmitted data. The intensity of the light-emitter, i.e. either a laser diode or a light-emitting diode (LED), can be adjusted by varying its bias current. The transmitted light signal, represented as power, must be a nonnegative value unlike in radio-frequency communications, i.e.

$$x(t) \geq 0, \tag{1.1}$$

and its average is constrained by eye-safety regulations according to International Electrotechnical Commission (IEC) standards [7] since optical radiation can cause harm to the eyes. The average transmitted optical power P_t

$$P_t = \lim_{T \to \infty} \frac{1}{2T} \int_{-T}^{T} x(t)dt \tag{1.2}$$

must be less than the Laser Safety Standard IEC60825-1: class 1 allowable exposure limit (AEL) which depends on the wavelength and size of the source. The allowed average optical power increases with wavelength.

At the receiver, a large-area photodiode with photodetector responsivity r (A/W) is used to detect the transmitted optical signal. The use of a large square-law detector operating on a short wavelength can mitigate the multipath fading. Output electrical current $y(t)$ is induced proportional to the light intensity impinging on its surface. The output current $y(t)$ generated by the photodetector can be written as

$$y(t) = rh(t) * x(t) + n(t), \tag{1.3}$$

where $*$ denotes convolution and $h(t)$ is the channel impulse response with path loss $H(0) = \int_{-\infty}^{\infty} h(t)dt$. Since the room configuration does not change, the optical wireless link with IM/DD can be considered as a linear time-invariant channel. The ambient background light from illuminating lights and sunlight induces a high intensity shot noise in the photodetector, so that the received noise $n(t)$ can be modeled as additive white Gaussian noise (AWGN) with double-sided power-spectral density N_0 [3, 8]. The performance of a wireless optical link at bit rate R_b is related to the received electrical signal-to-noise ratio

(SNR)

$$SNR = \frac{r^2 H(0)^2 P_t^2}{R_b N_0}. \tag{1.4}$$

1.2 Transceiver

In an optical system, a low-cost light emitter and photodetector which operate at wavelengths between 850-950 nm are usually chosen to be the transmitter and receiver [3, 9]. At the transmitter, either a light-emitting diode (LED) or a laser diode can be used. The light beam generated from the LED is approximately proportional to the drive current, while the laser diode emits light proportional to the current when it is larger than the threshold. A laser diode has a number of advantages over LEDs. A laser diode can be modulated faster and the electrical power is converted to optical power more efficiently. It also emits a narrow beam of concentrated light so that it is suitable for use in an OWC system with line-of-sight. However, a laser diode has some drawbacks such as its characteristic can change drastically as a function of temperature or age of the device and it is more expensive than LEDs. A laser diode requires special circuitry for threshold and temperature compensation; therefore the transmitter using a laser diode is more complicated than that using a LED. When the cost is the first concern, a LED is preferable. Nonetheless, the selection of either a LED or a laser diode depends on the specifications of the system.

A photodetector is a transducer capable of converting incident light into an electrical current containing the same information as in the transmitted light. Two practical options for a photodetector are a p-intrinsic-n (PIN) diode and an avalanche photodiode (APD). Although the photocurrent gain of an APD is greater than that of a PIN diode, a PIN diode is preferable because it is cheaper and easier to bias. Furthermore, an APD generates excess shot noise due to the current flowing in the device. Besides the photodetector, a filter and concentrator are required at the receiver [3, 10]. A bandpass optical filter is used to eliminate ambient light noise and the concentrator provides higher gain at the receiver.

Recently, a transceiver for OWC operating at 155 Mbps has been implemented using

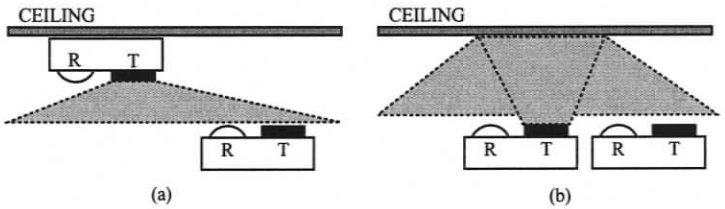

Figure 1.2. *Non-directed link configurations (a) Line-of-sight link (b) Diffuse link.*

integrated technology [11]. The transmitter is an array of resonant cavity LED emitters operating at 980 nm and the receiver is a detector array flip-chip bonded to a CMOS integrated circuit. Later, Sekai *et al* [12] developed a micro module of size D12 x W19 x H14 mm for an indoor full-duplex beam optical wireless communications system which can operate at more than 1.25 Gbps over distances exceeding 10 meters. The module consists of a vertical-cavity surface-emitting laser, photodiodes and beam splitters for separating the receiving beam from the transmitted beam.

1.3 Channel Model

An OWC channel can be categorized as a directed or a non-directed link. The transmitter and receiver used on a directed link have a narrow-beam radiation pattern and a narrow field of view, respectively. On the other hand, a non-directed link adopts a transmitter with a broad-beam radiation pattern and a receiver with a wide field of view. When the transmitter is aimed directly at the receiver, the link is called line-of-sight (LOS). Conversely, a non-LOS link utilizes the reflection characteristic of light, i.e. the transmitter is pointed up and the received optical power is that scattered from the ceiling and walls [3]. The directed LOS link has been adopted for long distance optical wireless systems. Since the optical power is concentrated into narrow optical beams and the ambient background light noise and the multipath dispersion cannot corrupt the system due to the narrow field of view of the receiver, the system can operate at extremely high data rates on the order of 1-2.5 Gbps [13, 14]. However, the requirement of alignment between transmitter and receiver means

a directed LOS link is not suitable for WLANs. Therefore the non-directed link shown in Fig. 1.2, using either a LOS or a diffuse configuration, is preferable for infrared WLANs. A hybrid link configuration for LOS and diffuse links, called quasi-diffuse link, has been proposed [15, 16, 17]. In a quasi-diffuse link, a holographic beam splitter is used at the transmitter to split the emitted light into multiple narrow beams instead of a large wide beam as with a diffuse link. The transmitted signal is less attenuated but the channel is more susceptible to shadowing compared with a diffuse link due to the low beam scatter.

According to the results in [18], a non-directed LOS link needs less transmit power than a diffuse link. However, if the alignment between transmitter and receiver is obstructed, the LOS link performs worse than the diffuse link. Exploiting the diffuse link in an indoor infrared wireless system was first proposed by Gfeller and Bapst [1]. Their research showed that the ceiling and office materials are well-approximated by an ideal Lambertian reflector, so that the incident infrared energy will re-radiate in all directions with appreciable energy. Hence, this provides a number of paths between the transmitter and receiver that make the diffuse channel difficult to be interrupted by shadowing.

The channel impulse response of a diffuse link has been studied through simulation and experimental results under different indoor environment [19, 20, 21]. It was shown that the channel model depends on room sizes, transmitter and receiver locations and orientations.

In 1997, a closed form expression was introduced by Carruthers and Kahn to represent the intersymbol interference (ISI) in an indoor wireless optical channel. Afterwards, a ceiling-bounce model was widely used to investigate optical wireless communication performance. Note that this model will be used throughout this thesis. The impulse response of a diffuse link can be represented as [20]

$$h(t) = H(0)\frac{6a^6}{(t+a)^7}u(t), \tag{1.5}$$

where $u(t)$ is the unit step function and a depends on the room size and the transmitter and receiver position. a is related to the rms delay spread D_{rms} by [20]

$$D_{rms} = \frac{a}{12}\sqrt{\frac{13}{11}}. \tag{1.6}$$

In addition, we define D_T as the ratio of rms delay spread to bit duration T_b, i.e. $D_T = D_{rms}/T_b$ [22]. The channel model is characterized by two parameters, rms delay spread D_{rms} and optical path loss $H(0)$, which cause intersymbol interference and signal attenuation, respectively.

1.4 Survey of Current Applications of Optical Wireless Communications

Besides using OWC inside buildings, it can be used to transmit data outdoors. Optical wireless communications for outdoor applications, normally referred to as free space optics (FSO), are also rapidly gaining attention. Therefore in this section, a survey of recent applications of optical wireless communications for both indoors and outdoors is reviewed.

1.4.1 Indoor applications

The standards of infrared WLANs were completed by two major organizations, IrDA and IEEE. The Infrared Data Association (IrDA) [23] was formed in 1994 in order to establish an open standard and develop the applications and protocols for infrared data communications. The Infrared Financial Messaging (IrFM), which is a universal wireless payment standard, is one development by IrDA. IrFM allows to high secure payments to be made at point of sales (POS) terminals and vending machines, and transfer the transaction record at high speed using infrared. The current transfer data rates of IrDA standards, so called IrBURST, are 115.2 kbps, 4 Mbps and 16 Mbps, with 100 Mbps under development. Moreover, an Ultra Fast Infrared (UFIR) special interest group has been established in order to support IrBURST requirements for digital content transfer rates up to 500 Mbps. A WLAN specification for an optical wireless physical layer has also been proposed by IEEE802.11 [24]. According to the specification, the infrared physical layer can support two data rates: 1 Mbps with 16-PPM and 2 Mbps with 4-PPM.

Instead of using a frequency in the infrared range, Tanaka proposed the use of a white LED as a transmitter and he renamed OWC as visible-light communications [10]. Soon, most electric lights will be replaced by white LEDs. White LEDs offer advantages and properties such as high brightness, reliability, lower power consumption and a long life-time. Besides use as illumination, LEDs can be used as a communication device. Visible-light communications can be integrated with power-line communications [10, 25] to reduce the requirements of installing a wired network. In June 2005, [26] a visible light system was installed at Kansai Airport, Japan, for passengers to be able to receive information about departures, shops and facilities, and to download music and video at rate of several Mbps from an LED. Optical wireless systems have also gained high interest in audio-visual equipment, especially for home multimedia. In 1997, NEC [27] announced the success of OWC in multimedia networks with transmission rates up to 125 Mbps over a maximum distance of 10 meters. Later, JVC [28] adopted optical wireless transmission technology to transmit high definition (HD) television signals between a source device and a display in 2004. The system operates at a data rate of 1.5 Gbps within a 10-meter area.

Since radiowaves from mobile RF-emitting devices have the potential to interrupt the normal operation of medical and avionic equipment, optical wireless communications have received much attention from hospitals and aircraft companies. In 1999, Clarinet Systems [29] released PDA-based infrared networking solutions for the healthcare market. It allows physicians, clinicians, staff, faculty, and students to access the network via both PocketPC and PDAs. The network has been successfully installed at many healthcare centers in North America. Schmitt [30] presented the use of OWC in aircraft cabins for in-flight entertainment. The first laboratory demonstration showed that data rates up to 10 Mbps over a diffuse link can be achieved.

1.4.2 Outdoor applications

Outdoor optical wireless systems with LOS provide the ability to transmit data between buildings up to several Gbps over a few-kilometers distance (1 to 5 km) [31, 32], as shown

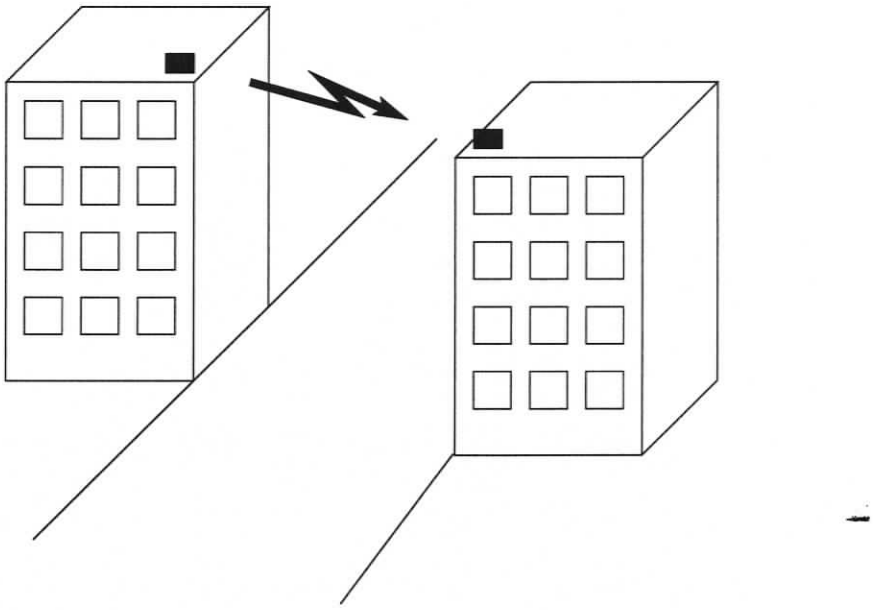

Figure 1.3. *Free space optic (FSO) transmission between buildings.*

in Fig. 1.3. However, the channel is subject to severe weather fluctuations due to fog, snow and rain. Current products offer bit rates from 1.5 Mbps up to 1.5 Gpbs over distances between 250 meters and 5.5 kilometers [33, 34, 35, 36]. The availability of the connections is about 99.999%. In Japan, an information system with LED traffic lights has been introduced [37]. The driver can receive real-time traffic information about traffic jams, traffic restrictions, accidents, construction and parking lots from LED traffic lights.

Since an optical wireless system can be quickly installed and the optical frequency range is unlicensed and unregulated, it can also be used on a temporary basis. For example, during the Olympic games in 2000, a free-space optical link was used to transmit eight broadcast video channels over a distance of 0.89 kilometers [38]. Aljada *et al* suggested that when existing networks are damaged in a disaster area, OWC can be exploited to connect between the disaster information center and the evacuation locations [39].

Optical wireless communications have also been adopted for deep space communications. The design of a system with a high data rate and small antennas is difficult due to a

great distance in deep space and limited room on spacecrafts. In a comparison amongst all technology candidates, an optical system is preferable because OWC achieves very high data rates and offers less beam spread and a smaller transceiver than RF systems. As a result, OWC has been developed for use in deep space communications for decades at Jet Propulsion Laboratory (JPL) [40]. Furthermore, the first high-speed deep space optical communications system will be on board NASA's Mars Telecommunications Orbiter to be launched in 2009 [41].

1.5 Thesis Structure

The main drawback of an optical wireless link is dispersion, which causes ISI and effectively limits the data rates of the system. Therefore this thesis focuses on signaling techniques which are able to diminish ISI and are also practicable. This thesis is organized as follows.

In Chapter 2, the modulation schemes for OWC are discussed. A system with intensity modulation and direct detection normally uses baseband modulation, e.g., on-off keying (OOK) and pulse-position modulation (PPM) since it is simple to adjust the intensity of the light. In addition, modulation schemes which are adapted from PPM have been proposed. Differential pulse-position modulation (DPPM) is one obtained by modifying PPM. Its advantages over PPM are that it provides more power efficiency and/or bandwidth efficiency and throughput. Moreover, symbol synchronization is not required so that the design of receiver can be simpler. As pulse amplitude modulation (PAM) offers better bandwidth efficiency, a hybrid of DPPM and PAM termed differential amplitude pulse-position modulation (DAPPM) is proposed. The performance of DAPPM will be analyzed and compared with other modulation schemes over non-dispersive and dispersive links.

In Chapter 3, it is shown that modulation schemes such as PPM, DPPM and DAPPM over an ISI channel can be represented as Markov processes. Accordingly, the channel capacity of the modulation schemes with hard- and soft-decision decoding is investigated by

using expectation-maximization. Soft-decision decoding achieves more power gain than hard-decision decoding, especially when the channel is subject to dispersive multipath. Thus, soft-decision techniques for a DPPM system which have performance close to optimal soft-decision decoding are proposed in Chapter 4.

DPPM using a non-zero pulse to identify the symbol boundary provides better bandwidth efficiency and the receiver can be simply implemented. However, this technique introduces a class of errors called insertion and deletion errors. An insertion error occurs when an extra symbol which was not transmitted is detected at the receiver. In contrast, a deletion error occurs when a transmitted symbol is not detected at the receiver. Therefore in Chapter 5, a concatenated code which can handle these errors is introduced and applied to a DPPM system. The performance of coded DPPM systems is evaluated by analysis and simulation. Finally, Chapter 6 presents a summary of the thesis, future work and extensions.

Chapter 2

Modulation for Optical Wireless Communications

For indoor applications, a non-directed diffuse link, exploiting the light-reflection characteristics for transmitting data to a receiver, has been considered as a suitable configuration because alignment of the transmitter and receiver is not required and it is robust against shadowing. On the other hand, these advantages lead to the major drawbacks of a diffuse link. First, the lack of a direct link between transmitter and receiver increases path loss. The second disadvantage is multipath dispersion caused by reflections of light from walls and room objects. In addition, the transmit power is constrained by power consumption concerns and eye-safety regulations [7]. Consequently, a power and bandwidth efficient modulation scheme is desirable. The comparison of several modulation schemes for optical wireless communications was presented in [41, 42, 43, 44, 45, 46, 47]. Next, the modulation schemes which are employed in OWC are summarized.

Normally, an optical wireless system adopts a baseband modulation scheme such as on-off keying (OOK) or pulse-position modulation (PPM) because the transceiver can be simply implemented as a pulse of light is sent for an "on" chip and no light is sent for an "off" chip. In a PPM system, each symbol interval is partitioned into L chips and only one "on" chip is sent during a symbol duration. The pulse position is indicated by binary representation. Because PPM has a low duty cycle which offers improved power efficiency, it has been utilized in IrDA and IEEE802.11 standards. Although the optical power requirement

can be made small when L is large, the bandwidth efficiency is significantly decreased. At the high data rate, the number of symbols affected by intersymbol interference increases so PPM performs worse over a dispersive channel. As a result, several variations of PPM such as multiple PPM (MPPM) and overlapping PPM (OPPM) have been developed in order to gain higher bandwidth efficiency, i.e. the effect of intersymbol interference is mitigated when the channel is dispersive. In multiple PPM (MPPM), a group of $\lfloor \log_2 \left[{L \atop n} \right] \rfloor$ bits is mapped to n pulses in L chip positions. The pulse positions are assigned such that MPPM is orthogonal signaling. The transmission bandwidth is about half that of PPM and the peak power is also reduced. When the n pulses are constrained to be consecutive, MPPM is defined as overlapping PPM (OPPM); however, OPPM is not orthogonal. Note that the length of PPM, MPPM and OPPM symbols is fixed.

The bandwidth requirements can be also reduced by using modulation schemes in which the number of chips per symbol is variable. Examples of such schemes are differential pulse-position modulation (DPPM), digital pulse interval modulation (DPIM) and dual header pulse interval modulation (DH-PIM$_\alpha$). The DPPM waveform is obtained from PPM by deleting the "off" chips following the "on" chip. One of the advantages of DPPM over PPM is that it does not require symbol synchronization since the "on" chip indicates a symbol boundary. Accordingly, the symbol length varies from 1 to L. It has been shown that DPPM achieves a good compromise between power efficiency and bandwidth efficiency, and provides twice the throughput of PPM [41, 48, 49]. DPIM [50, 51, 52] is an inverted version of DPPM. Dual header pulse interval modulation (DH-PIM$_\alpha$) [22, 53] is a modified version of DPIM. DH-PIM$_\alpha$ has less transmission bandwidth than DPIM at the expense of a higher average power requirement and α denotes number of pulses in header two. Also, DH-PIM$_\alpha$ has built-in symbol synchronization.

The improved PPM schemes as discussed above are only binary (two) level. The bandwidth efficiency can be also achieved by using multilevel modulation schemes at the cost of higher power requirements. The simplest multilevel modulation scheme is pulse amplitude modulation (PAM). A PAM symbol is represented as a single pulse with an amplitude cor-

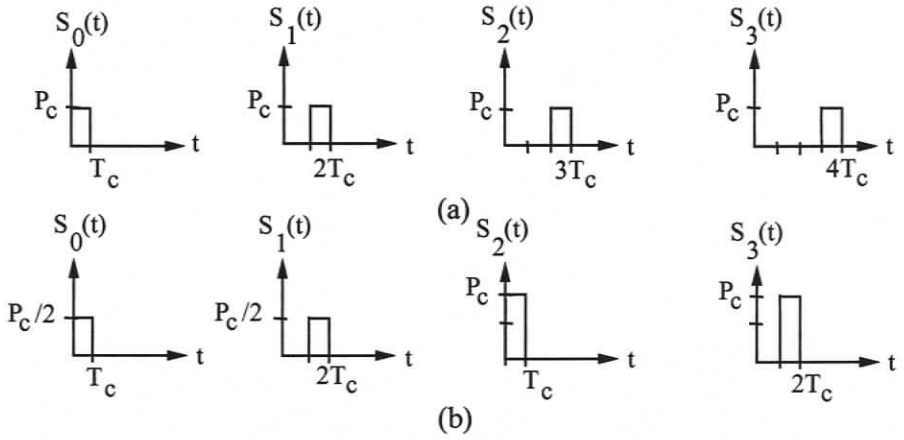

Figure 2.1. *The symbol structure for $M = 2$ bits/symbol with (a) $4-$DPPM and (b) $2 \times 2-$DAPPM.*

responding to a group of M transmitted data bits. A new modulation scheme, adaptively biased quadrature amplitude modulation (AB-QAM), was proposed and it was shown that it offers a 3 dB improvement in SNR over PAM for the same bandwidth efficiency [54].

In this chapter, a novel hybrid modulation technique called differential amplitude pulse-position modulation (DAPPM) is proposed. DAPPM is a combination of pulse amplitude modulation (PAM) and differential pulse-position modulation (DPPM). In the next sections, the symbol structure and properties of DAPPM, e.g., peak-to-average power ratio (PAPR), bandwidth requirements, and throughput, are discussed. The power spectral density is also derived and compared to that of other modulation schemes. The performance of DAPPM with hard-decision detection on non-dispersive and dispersive channels is examined by analysis and simulation.

2.1 Differential Amplitude Pulse-Position Modulation

Differential amplitude pulse-position modulation (DAPPM) is a combination of PAM and DPPM. Therefore the symbol length and pulse amplitude are varied according to the infor-

Table 2.1. *Mapping of 3-bit OOK words into PPM, DPPM, DH-PIM$_2$ and DAPPM symbols.*

OOK	PPM (L=8)	DPPM (L=8)	DH-PIM$_2$ (L=8)	DAPPM (A=2,L=4)	DAPPM (A=4,L=2)
000	10000000	1	100	1	1
001	01000000	01	1000	01	01
010	00100000	001	10000	001	2
011	00010000	0001	100000	0001	02
100	00001000	00001	110000	2	3
101	00000100	000001	11000	02	03
110	00000010	0000001	1100	002	4
111	00000001	00000001	110	0002	04

mation being transmitted. A set of DAPPM waveforms is shown in Fig. 2.1. A block of $M = \log_2(A \times L)$ input bits is mapped to one of 2^M distinct waveforms, each of which has one "on" chip which is used to indicate the end of the symbol. The amplitude of the "on" chip is selected from the set $\{1, 2, \ldots, A\}$ and the length of a DAPPM symbol is from the set $\{1, 2, \ldots, L\}$. Alternatively, the DAPPM encoder transforms an information symbol into a chip sequence according to a DAPPM coding rule such as the one shown in Table 2.1. The transmitted DAPPM signal is then

$$x(t) = \sum_{k=-\infty}^{\infty} \left(\frac{P_c}{A}\right) b_k p(t - kT_c), \tag{2.1}$$

where $b_k \in \{0, 1, \ldots, A\}$, P_c is the peak transmit power and $p(t)$ is a unit-amplitude rectangular pulse shape with a duration of one chip, i.e.

$$T_c = \frac{MT_b}{\bar{L}}, \tag{2.2}$$

where T_b is the bit duration and $\bar{L}$ is the average DAPPM symbol length given by

$$\bar{L} = \frac{L+1}{2}. \tag{2.3}$$

Therefore

$$T_c = \frac{2M}{(L+1)R_b}, \tag{2.4}$$

where R_b represents the data bit rate. The PAPR of DAPPM is then

$$\text{PAPR} = \frac{P_c}{P_t} = \frac{L+1}{A+1}. \tag{2.5}$$

The required first-null bandwidth of DAPPM to support communications at bit rate R_b is given by

$$W = \frac{1}{T_c} = \frac{(L+1)R_b}{2M}. \tag{2.6}$$

The bit rate of DAPPM is not constant due to the variable-length symbols. We assume that the symbol length is random and equiprobable. The average bit rate $\bar{R}_b$ with variable-length symbols is defined as the average number of information bits per transmitted chip

Table 2.2. *Peak-to-average power ratio (PAPR), bandwidth requirements and throughput of PPM, DPPM, DH-PIM$_\alpha$ and DAPPM, where M represents the number of bits/symbol.*

Modulation scheme	PPM	DPPM	DH-PIM$_\alpha$	DAPPM
PAPR	2^M	$\frac{2^M+1}{2}$	$\frac{2(2^{M-1}+2\alpha+1)}{3\alpha}$	$\frac{2^M+A}{A(A+1)}$
Bandwidth requirement (Hz)	$\frac{2^M R_b}{M}$	$\frac{(2^M+1)R_b}{2M}$	$\frac{(2^{M-1}+2\alpha+1)R_b}{2M}$	$\frac{(2^M+A)R_b}{2MA}$
Throughput	M	$\frac{M2^{M+1}}{(2^M+1)}$	$\frac{M2^{M+1}}{(2^{M-1}+2\alpha+1)}$	$\frac{MA2^{M+1}}{(2^M+A)}$

[53]. Therefore the average bit rate with DAPPM is

$$\bar{R}_b = \frac{M}{\bar{L}T_c} = \frac{2M}{(L+1)T_c}. \tag{2.7}$$

We define the throughput as the average number of information bits which can be transmitted during the time required to transmit M bits for OOK. We now compare the throughput of PPM, DPPM, DH-PIM$_\alpha$ and DAPPM assuming that they have the same chip duration equal to the chip duration of PPM. The throughput of DAPPM is then

$$\text{Throughput} = \frac{MA2^{M+1}}{(2^M + A)}. \tag{2.8}$$

The properties of PPM, DPPM [46, 49], DH-PIM$_\alpha$ [22, 53] and DAPPM are summarized in Table 2.2. Compared to the other modulation schemes, DAPPM provides better bandwidth efficiency, higher throughput and a lower peak-to-average power ratio. Fig. 2.2 shows that the throughput of DAPPM approaches $2A$ times and A times that of PPM and DPPM, respectively, as the number of bits/symbol increases. The throughput of DH-PIM$_2$ is about the same as DAPPM (A=2). However, DAPPM requires better threshold detection accuracy than DPPM in the system components.

Next, the power spectral density of DAPPM is derived. From (2.1), $x(t)$ can be viewed as a cyclostationary process [55, 56] with a power spectral density (PSD) given by $S(f) =$

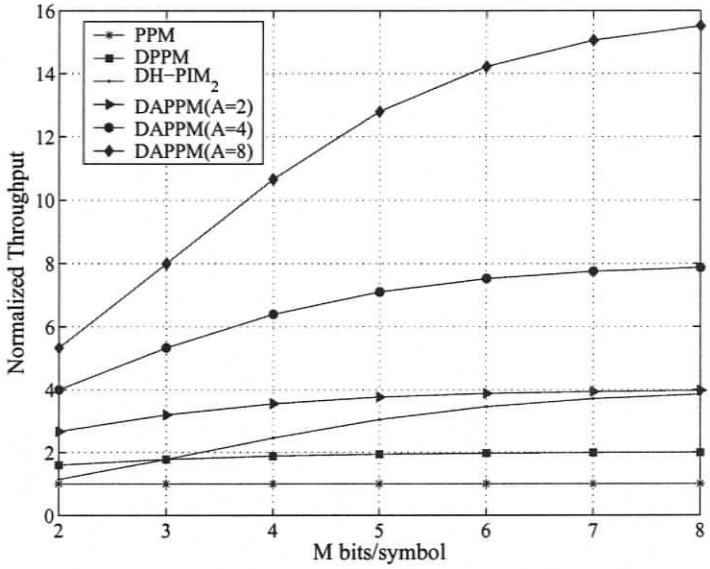

Figure 2.2. *The throughput of PPM, DPPM, DH-PIM$_2$ and DAPPM normalized to the throughput of OOK (M bits/symbol).*

$(1/T_c)|P(f)|^2 S_b(f)$. For a rectangular pulse $p(t)$, $|P(f)|^2 = T_c^2 \text{sinc}^2(fT_c)$. $S_b(f)$ is the discrete-time Fourier transform of the chip autocorrelation function R_k, which is defined by $R_{n-m} = E[b_n b_m]$. The autocorrelation of the chip sequence R_k is

$$R_0 = \frac{(A+1)(2A+1)}{3(L+1)}, \tag{2.9}$$

and

$$R_k = \begin{cases} \frac{(A+1)^2(L+1)^{k-2}}{2L^k}, 1 \leq k \leq L \\ \frac{1}{AL}\sum_{i=1}^{L} R_{k-i}, k > L \end{cases} . \tag{2.10}$$

R_k converges to $E[b]^2$ where $E[b] = (A+1)/(A(L+1))$, as k increases, so the continuous and discrete components of the PSD can be approximated as

$$S_c(f) \approx \sum_{k=-5L}^{5L} [R_k - E[b]^2] \exp(-j2\pi k f T_c), \tag{2.11}$$

and

$$S_d(f) = \frac{E[b]^2}{T_c} \sum_{k=-\infty}^{\infty} \delta\left(f - \frac{k}{T_c}\right), \tag{2.12}$$

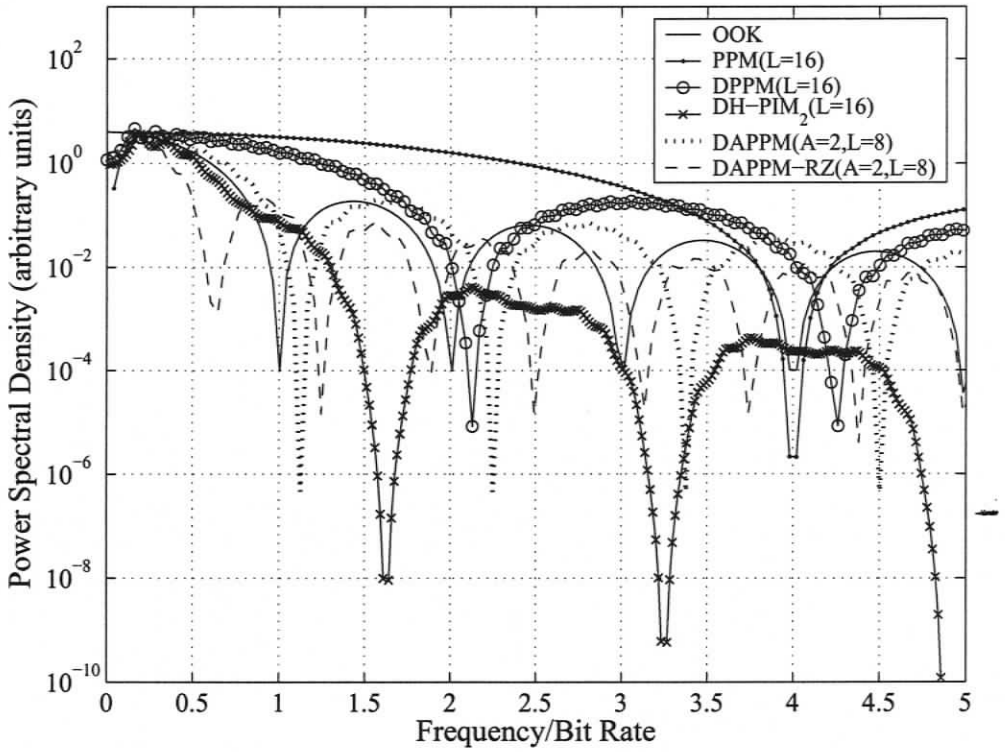

Figure 2.3. *The power spectral density of OOK, PPM, DPPM, DH-PIM$_2$ and DAPPM with the discrete spectral portion omitted when $M = 4$ bits/symbol. All curves represent the same average transmitted optical power with a rectangular pulse shape.*

respectively. An estimate of the power spectral density of DAPPM is compared with those of other modulation schemes [49, 53] is illustrated in Fig. 2.3. Given the same number of bits/symbol, the PSD of DAPPM is similar to those of DPPM and DH-PIM$_2$. In addition, DAPPM requires less bandwidth but is more susceptible to baseline wander [51] because the PSD of DAPPM has the larger signal around DC.

2.2 Error Probability Analysis of DAPPM

A block diagram of the DAPPM transmitter is shown in Fig. 2.4(a). Each block of M input bits is converted into one of the $2^M = A \times L$ possible symbols. Each chip b_k is input

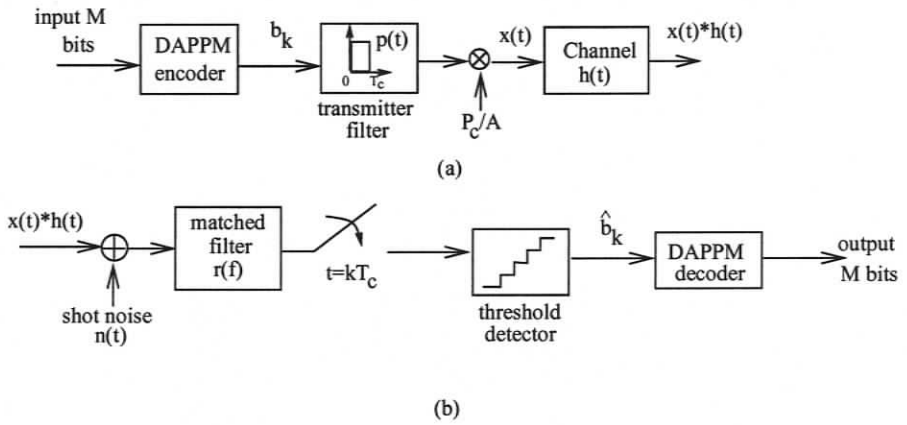

Figure 2.4. *(a) Block diagram of a DAPPM transmitter. The data bit sequence is transformed to the chip sequence* (b_k) *according to the DAPPM coding rule. An "on" chip induces the generation of a rectangular pulse* $p(t)$ *with amplitude* $(b_k P_c)/A$*. The resulting optical signal* $x(t)$ *is transmitted through a channel with impulse response* $h(t)$*. (b) Block diagram of an unequalized hard-decision DAPPM receiver comprised of a receive filter* $r(t) = p(-t)$*, matched to the transmitted pulse shape, and an optimum threshold detector.*

to a transmit filter with a unit-amplitude rectangular pulse shape and multiplied by P_c/A. Then, the light signal $x(t)$ is transmitted through a channel with impulse response $h(t)$ in (1.5) and it is corrupted by white Gaussian noise $n(t)$. The received signal passes through a receive filter $r(t) = p(-t)$ matched to the transmitted pulse. The output of the receive filter is sampled and converted into a chip sequence by comparing the samples with an optimal threshold as shown in Fig. 2.4(b). The filter output r_k is compared to the optimal detection thresholds $\{\theta_1, \ldots, \theta_A\}$ (which are relative to P_c) to estimate the transmitted chip b_k as

$$\hat{b}_k = \begin{cases} 0, & \text{for } r_k < \theta_1, \\ i, & \text{for } \theta_i \leq r_k < \theta_{i+1}, \text{ where } i = 1, 2, \ldots, A-1, \\ A, & \text{for } r_k \geq \theta_A. \end{cases} \tag{2.13}$$

The equivalent discrete-time impulse response of the system can be written as

$$f_k = f(t)|_{t=kT_c} = \frac{P_c}{A} p(t) * h(t) * r(t)|_{t=kT_c}. \tag{2.14}$$

In an optical wireless system, we compare the performance of modulation schemes by evaluating the power penalty, which is the average power required normalized by the average power required to transmit the data over a non-dispersive channel using OOK modulation at the same error probability. The power penalty can be calculated as

$$\text{Power penalty} = \frac{P(\text{BER}, h(t), N_0, \text{Modulation Scheme})}{P(\text{BER}, \delta(t), N_0, OOK)}, \tag{2.15}$$

where the bit error rate (BER) for OOK is

$$\text{BER}_{OOK} = Q\left(\frac{rH(0)P_t}{\sqrt{R_b N_0}}\right), \tag{2.16}$$

and $P(\text{BER}, h(t), N_0, \text{Modulation Scheme})$ represents the average power required to achieve a specific error probability with a modulation scheme over a channel with impulse response $h(t)$ and additive white Gaussian noise with two-sided noise N_0. We only consider the effects of noise and multipath dispersion, so it is assumed there is no path loss, $H(0) = 1$, and the photodetector responsivity is $r = 1$.

2.2.1 Non-dispersive channels

We first consider the performance of DAPPM over a non-dispersive channel, i.e. $h(t) = \delta(t)$. The input symbols are assumed to be independent, and identically distributed. Let p_0 denote the probability of receiving an "off" chip, and p_A the probability of receiving a pulse with nonzero amplitude. Then the probability of chip error is given by

$$\begin{aligned} P_{ce} &= p_0 Q\left\{\frac{\theta_1 P_c}{A\sqrt{N_0 W}}\right\} \\ &+ p_A \sum_{i=1}^{A-1}\left(Q\left\{\frac{(i-\theta_i)P_c}{A\sqrt{N_0 W}}\right\} + Q\left\{\frac{(\theta_{(i+1)}-i)P_c}{A\sqrt{N_0 W}}\right\}\right) \\ &+ p_A Q\left\{\frac{(A-\theta_A)P_c}{A\sqrt{N_0 W}}\right\}. \end{aligned} \tag{2.17}$$

Similar to DPPM, the "on" chip indicates a symbol boundary. Therefore the DAPPM receiver is simpler than that for PPM since symbol synchronization is not required (but chip synchronization is still needed). However, since there is no fixed symbol boundary, a single chip error affects not only the current symbol, but also the next symbol. Therefore we cannot compare its performance with other types of modulation in terms of bit error rate (BER) but we use frame error rate (FER) instead. To transmit an F-bit frame, the average DAPPM chip sequence length is

$$\bar{N} = \frac{F(L+1)}{2M}. \tag{2.18}$$

For very small values of P_{ce}, the frame error rate can be approximated by [22]

$$\text{FER} = 1 - (1 - P_{ce})^{\bar{N}} \approx \bar{N} P_{ce}. \tag{2.19}$$

Power requirements are normalized to the power required to send a 1000-bit frame using OOK at an average frame error rate of 10^{-6}. Fig. 2.5 shows the average optical power and bandwidth requirements of OOK, PAM, PPM, DPPM, DH-PIM$_2$ and DAPPM. DAPPM can give better bandwidth and/or power efficiency than PAM, PPM, DPPM and DH-PIM$_2$ depending on the number of amplitude levels (A) and the maximum length (L) of a symbol. Given the same power penalty as PPM $(L = 4)$ (which has been adopted as

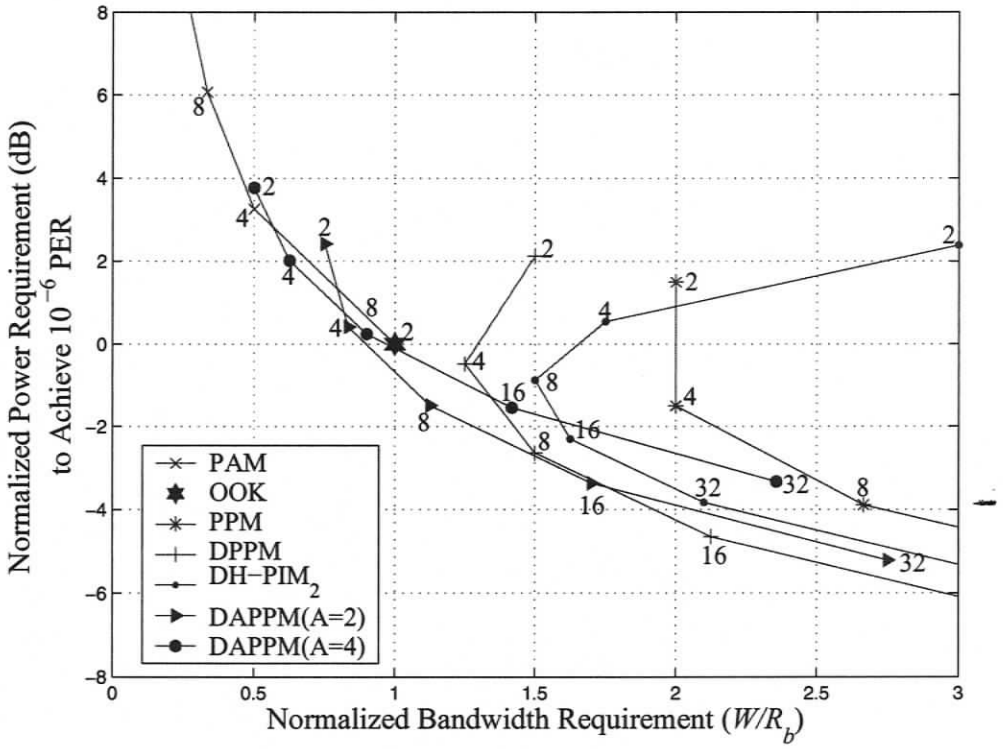

Figure 2.5. *The normalized optical power and bandwidth required for OOK, PAM, PPM, DPPM, DH-PIM$_2$ and DAPPM over a non-dispersive channel. Each point of DAPPM represents the maximum length (L) of symbol. For other modulation schemes, each point represents the number of possible symbols (2^M).*

an IrDA standard [23]), DAPPM $(A = 2, L = 8)$ and DAPPM $(A = 4, L = 16)$ provide better bandwidth efficiency, throughput and PAPR. In particular, DAPPM $(A = 2, L = 16)$ yields better power efficiency and double the throughput of DPPM $(L = 8)$, albeit at a slightly lower bandwidth efficiency.

2.2.2 Dispersive channels

In this section, we consider the performance of DAPPM over a dispersive channel which has impulse response given in (1.5) and causes intersymbol interference. Thus, when the

bit rate increases, the performance of the system will be degraded. Here, we focus our attention on the effects of ISI caused by multipath dispersion, and assume that the timing recovery is perfect, decision thresholds are optimized and the receiver and transmitter are co-located.

Note that the discrete-time dispersive channel (f_k) contains a zero tap, a single precursor tap, and possibly multiple postcursor taps. Suppose that the channel contains m taps. Let s_j be an m-chip segment randomly taken from a DAPPM sequence, $p(s_j)$ be the probability of occurrence of s_j, and $I(s_j)$ the receiver filter output (excluding noise) of the next-to-last chip of s_j. The probability of chip error is

$$P_{ce} = \sum_j p(s_j)\epsilon(s_j), \tag{2.20}$$

where

$$\epsilon(s_j) = \begin{cases} Q\left(\frac{(\theta_1 - I(s_j))P_c}{A\sqrt{N_0 W}}\right) & , b_k = 0, \\ Q\left(\frac{(I(s_j)-\theta_i)P_c}{A\sqrt{N_0 W}}\right) + Q\left(\frac{(\theta_{i+1}-I(s_j))}{A\sqrt{N_0 W}}\right) & , b_k = i, \\ Q\left(\frac{(I(s_j)-\theta_A)P_c}{A\sqrt{N_0 W}}\right) & , b_k = A. \end{cases} \tag{2.21}$$

Fig. 2.6 shows the power required by DAPPM compared to the other modulation schemes to transmit an optical signal in a room with a 3.5 m-height at different bit rates. Given the same number of bits/symbol $(M = 2)$, DAPPM provides better power efficiency compared to PAM because the "off" chips between "on" chips of the symbols reduce the influence of ISI. Note that DH-PIM$_2$ requires less power than DAPPM.

Next, we compare the performance of DAPPM with PPM, DPPM and DH-PIM$_2$ when the maximum length of a symbol is the same. DAPPM requires about 1 dB more transmit power than DPPM and 2 dB more than PPM when the bit rate is lower than 50 Mbps. When the bit rate is over 50 Mbps, the average optical power required with DAPPM is about 1.5 dB more than DPPM and 1 dB more than PPM. On the other hand, DH-PIM$_2$ requires more power than DAPPM. Intuitively, DAPPM has better bandwidth efficiency and so is more susceptible to corruption by noise, but the influence of ISI is less than with PPM and DPPM at high bit rates. This is because the effects of ISI are alleviated by the longer

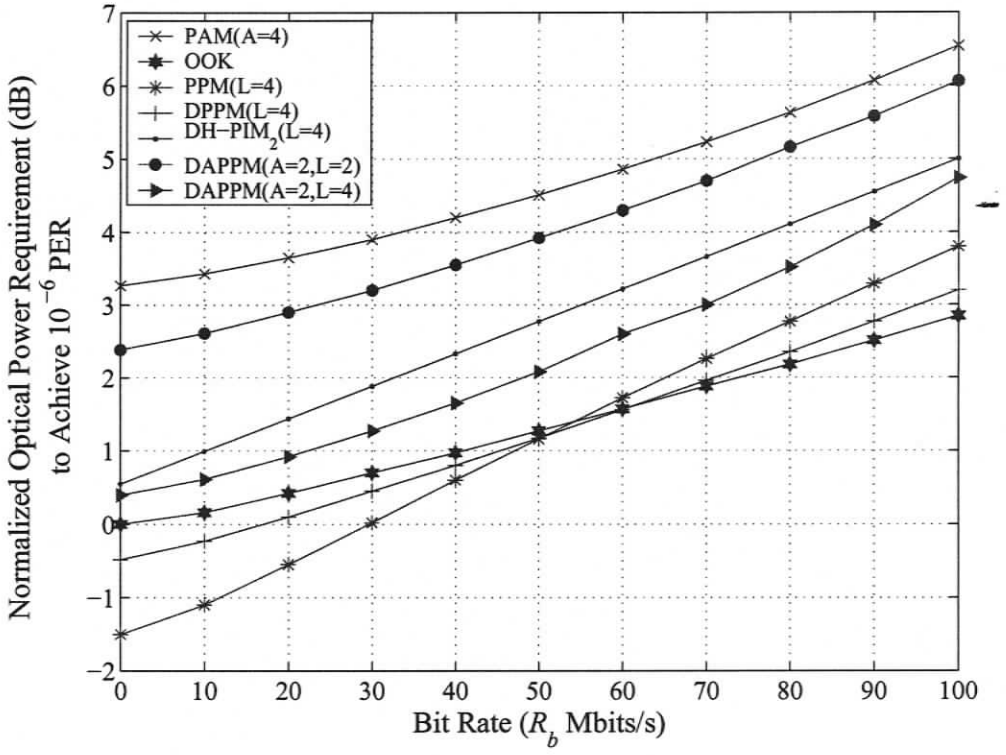

Figure 2.6. *Average optical power requirement of PAM, OOK, PPM, DPPM, DH-PIM$_2$ and DAPPM versus bit rate R_b (in Mbps) over a dispersive channel.*

symbol duration of DAPPM compared to that with PPM and DPPM. However, as shown in Fig. 2.6, DAPPM has less power efficiency and requires more average optical power than PPM and DPPM.

2.3 Conclusions

We introduced DAPPM and investigated its performance over an indoor wireless optical link. DAPPM provides several advantages. A DAPPM receiver is simple because it does not need symbol synchronization. We compared DAPPM with PPM DPPM and DH-PIM$_\alpha$ on the basis of required bandwidth, throughput, peak-to-average power ratio and required power over non-dispersive and dispersive channels. It was shown that DAPPM requires less bandwidth when the number of amplitude levels is high. Furthermore, the throughput of DAPPM converges to $2A$ times and A times that of PPM and DPPM, respectively, when the number of bits/symbol increases. The throughput of DH-PIM$_2$ is about the same as DAPPM ($A = 2$). Hence, given the same symbol duration, DAPPM can provide a higher data rate than PPM, DPPM and DH-PIM$_\alpha$. Also, DAPPM achieves a lower peak-to-average power ratio. However, it requires more average optical power than PPM, DPPM and DH-PIM$_\alpha$ to achieve the same error probability.

Over a dispersive channel, given the same number of bits/symbol, DAPPM with an unequalized receiver provides better performance than PAM but it requires more power than DH-PIM$_2$. For the same maximum length, although DAPPM has better bandwidth efficiency, it requires more average optical power than PPM and DPPM but less power when compared to DH-PIM$_2$.

Chapter 3

Channel Capacity for Indoor Optical Wireless Communications

3.1 Introduction

Optical wireless communications have the potential for extremely high data rates of up to tens of Gbps. However, this capacity still cannot be achieved because of the physical limitations of optical devices and the channel which exhibits path loss, noise from ambient light and the receiver, and the multipath dispersion from multiple reflections off walls and other objects in a room. In addition, the signal which represents optical power must be positive and its average is subject to eye-safety regulations [7]. Therefore the object in this chapter is to investigate the effects of the presence of noise and intersymbol interference on the channel capacity of an indoor optical wireless system.

The channel capacity of PPM over memoryless and multipath channels was examined in [57, 58, 59]. However, the capacity of DPPM and DAPPM over such channels has not yet been investigated. In this chapter, we show that PPM, DPPM and DAPPM can be represented as Markov processes. The channel capacity of these modulation schemes over both memoryless and multipath channels can be evaluated using the expectation-maximization method described in [60]. Furthermore, the capacity over a noiseless channel is computed. We also compare the channel capacity achievable with hard- and soft-decision decoding.

In the next sections, the algorithms to determine the capacity for Markov sources over

noiseless and noisy channels are reviewed. Then, they are applied to calculate the channel capacity of L-PPM, L-DPPM and $A \times L$-DAPPM. Finally, performance results are presented and discussed.

3.2 Capacity of Markov Process

Denote the input channel sequence by $\boldsymbol{b}_1^\tau = (\boldsymbol{b}_1, \boldsymbol{b}_2, \ldots, \boldsymbol{b}_\tau)$ where $\boldsymbol{b}_k$ is the input vector signal chosen from a finite alphabet and state sequence which produces $\boldsymbol{b}_1^\tau$ denoted by $\boldsymbol{s}_1^\tau = (s_1, s_2, \ldots, s_\tau)$ where s_k is chosen from a finite set of states $\mathcal{S}$. Note that $n(\mathcal{S})$ is the number of states in the set $\mathcal{S}$. The input sequence is defined as a Markov process of memory one if the current state s_k depends only on the past state s_{k-1} [61]. The Markov process can be described by a state-transition matrix **B** where

$$B_{ij} = \begin{cases} 1, & \text{for valid transition} \\ 0, & \text{for invalid transition} \end{cases} \tag{3.1}$$

where valid transition means that there is a transition from state i to j; otherwise, it is defined as an invalid transition, and the transition probability matrix is **P** where

$$P_{ij} = P(s|s') = \Pr(s_k = j | s_{k-1} = i) \tag{3.2}$$

is the probability of a transition from previous state $(s' = s_{k-1})$ to current state $(s = s_k)$. Let $P(s)$ be the probability of being at state $(s_k = i)$ with

$$P(s) = \Pr(s_k = i) = \sum_{s'} P(s')P(s|s'), \tag{3.3}$$

and

$$\sum_{s} P(s) = 1. \tag{3.4}$$

3.2.1 Noiseless channels

It has been shown that the capacity of a Markov source over a noiseless channel can be calculated from the state-transition matrix **B** [62], so that

$$C = \log_2 \lambda_{max}, \tag{3.5}$$

where λ_{max} is the largest real eigenvalue of **B**. Alternatively, the capacity is the largest real root of the characteristic equation of **B**.

3.2.2 Noisy channels

The channel capacity of a Markov source transmitted through a channel with memory, e.g., an intersymbol interference channel with m taps, has been studied in [60, 63]. The state transitions depend only on the previous channel state and the channel input. The mapping between the transitions and inputs is one-to-one. Consequently, the channel capacity can be expressed as

$$C = \lim_{\tau\to\infty} \sup_{P(\boldsymbol{b}_k)} \frac{1}{\tau} I\left(\boldsymbol{b}_1^\tau : \boldsymbol{r}_1^\tau\right) = \lim_{\tau\to\infty} \sup_{P(s)} \frac{1}{\tau} I\left(\boldsymbol{s}_1^\tau : \boldsymbol{r}_1^\tau\right), \tag{3.6}$$

where $I\left(\boldsymbol{b}_1^\tau : \boldsymbol{r}_1^\tau\right)$ is the mutual information rate between the input channel sequence $\boldsymbol{b}_1^\tau$ and the output channel sequence $\boldsymbol{r}_1^\tau$, and $\boldsymbol{s}_1^\tau$ is the trellis state sequence which produces $\boldsymbol{b}_1^\tau$. Since the beginning state s_0 does not affect the mutual information and $P(s)$ depends on $P(s|s')$, the capacity can be rewritten as [60]

$$C = \max_{P(s|s')} \lim_{\tau\to\infty} \frac{1}{\tau} I\left(\boldsymbol{s}_1^\tau : \boldsymbol{r}_1^\tau | s_0\right), \tag{3.7}$$

and the mutual information can be expressed as

$$I\left(\boldsymbol{s}_1^\tau : \boldsymbol{r}_1^\tau | s_0\right) = \sum_{k=1}^{\tau} P(s')P(s|s') \left[\log \frac{1}{P(s|s')} + T(s', s)\right], \tag{3.8}$$

and

$$T(s', s) = \lim_{\tau\to\infty} \frac{1}{\tau} \sum_{k=1}^{\tau} \left[\log \frac{P_k(s', s|\boldsymbol{r}_1^\tau)^{\frac{P_k(s', s|\boldsymbol{r}_1^\tau)}{P(s')P(s|s')}}}{P_k(s'|\boldsymbol{r}_1^\tau)^{\frac{P_k(s'|\boldsymbol{r}_1^\tau)}{P(s')}}}\right], \tag{3.9}$$

which can be calculated using a modified BCJR algorithm [64] as follows.

First, define

$$\alpha_k(s) = \Pr(s_k = j|\boldsymbol{r}_1^k), \tag{3.10}$$

$$\beta_k(s) = \frac{\Pr(\boldsymbol{r}_{k+1}^\tau|s_k = j)}{\Pr(\boldsymbol{r}_{k+1}^\tau|\boldsymbol{r}_1^k)}, \tag{3.11}$$

and

$$\begin{aligned}\gamma_k(s', s) &= \Pr(\boldsymbol{r}_k|s_k = j, s_{k-1} = i) \cdot \Pr(s_k = j|s_{k-1} = i) \\ &= P(\boldsymbol{r}_k|s, s')P(s|s'),\end{aligned} \tag{3.12}$$

where $P(\boldsymbol{r}_k|s, s')$ is the probability of received signal $\boldsymbol{r}_k$ when there is a transition from s' to s. Since the transition is caused by the transmitted signal $\boldsymbol{b}_k$

$$P(\boldsymbol{r}_k|s, s') = P(\boldsymbol{r}_k|\boldsymbol{b}_k), \tag{3.13}$$

which is the transition probability of the channel. Consequently, $\alpha_k(s)$ and $\beta_k(s)$ can be calculated recursively as

$$\alpha_k(s) = \frac{\sum_{s'} \gamma_k(s', s)\alpha_{k-1}(s')}{\sum_{s',s} \gamma_k(s', s)\alpha_{k-1}(s')} \tag{3.14}$$

$$\beta_k(s') = \frac{\sum_{s} \gamma_k(s', s)\beta_{k+1}(s)}{\sum_{s',s} \gamma_k(s', s)\alpha_k(s')}. \tag{3.15}$$

Now, $P_k(s'|\boldsymbol{r}_1^\tau)$ and $P_k(s', s|\boldsymbol{r}_1^\tau)$ in (3.9) can be computed from

$$\begin{aligned}P_k(s'|\boldsymbol{r}_1^\tau) &= \Pr(s_{k-1} = i|\boldsymbol{r}_1^\tau) \\ &= \alpha_{k-1}(s') \cdot \beta_{k-1}(s'),\end{aligned} \tag{3.16}$$

and

$$\begin{aligned}P_k(s', s|\boldsymbol{r}_1^\tau) &= \Pr(s_{k-1} = i, s_k = j|\boldsymbol{r}_1^\tau) \\ &= \frac{\alpha_{k-1}(s') \cdot \gamma_k(s', s) \cdot \beta_k(s)}{p(\boldsymbol{r}_k)},\end{aligned} \tag{3.17}$$

where

$$p(\boldsymbol{r}_k) = \sum_s \sum_{s'} \gamma_k(s', s)P(s'). \tag{3.18}$$

After using the modified BCJR algorithm and calculating $T(s', s)$ in (3.9), the noisy adjacency matrix $\boldsymbol{A}$ is computed as [60]

$$A(s', s) = \begin{cases} 2^{T(s',s)}, & \text{for valid transition} \\ 0, & \text{for invalid transition.} \end{cases} \tag{3.19}$$

Then, the channel capacity is given by $C = \log_2 \lambda_{\max}$ where $\lambda_{\max}$ is the maximum eigenvalue of matrix $\boldsymbol{A}$.

3.3 Channel Model

According to the receiver shown in Fig. 2.4, besides the previous transmitted symbols, the pulse-shape of the transmitted symbol is also affected by the next transmitted symbol. In this chapter, we modify the receiver by using a whitened-matched filter [65] at the front-end of the receiver as shown in Fig. 3.1. This filter consists of a matched filter $r(t) = p(-t) \otimes h(-t)$ followed by a sampler and a whitening filter w_k which whitens the noise and also eliminates the anti-causal part of the ISI channel. Assuming perfect timing recovery, the discrete-time impulse response is

$$f_k = f(t)|_{t=kT_c} = \frac{P_c}{A} p(t) \otimes h(t) \otimes p(-t) \otimes h(-t)|_{t=kT_c}, \tag{3.20}$$

with $2m - 1$ taps and a maximum at f_0. Hence, the equivalent discrete-time system

$$g_k = f_k \otimes w_k \tag{3.21}$$

has only m taps, and the transmitted signal is corrupted only by the $m - 1$ past signals.

A method for determining the coefficients of a whitening filter w_k was proposed in [65]. First, we define $x(D) = x_0 + x_1 D + x_2 D^2 + \cdots$. Since $f(D)$ is a symmetric function and has $2m - 1$ nonzero terms, it has $2m - 2$ roots. $f(D)$ can be factored as

$$f(D) = W(D)W(D^{-1}), \tag{3.22}$$

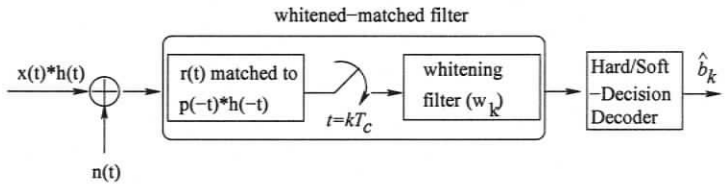

Figure 3.1. *Block diagram of a receiver with whitened-matched filter.*

where $W(D)$ has $m-1$ roots inside the unit circle and $W(D^{-1})$ has $m-1$ roots which are the inverse-complex conjugate of the roots inside the unit circle. Hence, the whitening filter coefficients w_k are the coefficients of $(1/W(D^{-1}))$.

3.4 Capacity of Pulse-Position Modulation

The capacity of PPM has been widely investigated in the literature. It has been shown that the channel capacity of PPM over a noiseless channel is [58, 59]

$$\begin{aligned} C_{\text{PPM}} &= \log_2 L \text{ bits/symbol} \\ &= \frac{\log_2 L}{L} \text{ bits/sec/Hz.} \end{aligned} \tag{3.23}$$

Next, we determine the capacity of PPM with hard- and soft-decision decoding when the system is corrupted by noise and intersymbol interference.

If the PPM symbol is transmitted over a channel with hard-decision decoding, the PPM symbol having an "on" chip at the same position as the largest element in the received sequence is chosen. The transition probability for the channel is [58, 59]

$$P(\boldsymbol{r}_k|\boldsymbol{b}_k) = \begin{cases} 1-p_L, & \boldsymbol{r}_k = \boldsymbol{b}_k \\ \frac{p_L}{L-1}, & \boldsymbol{r}_k \neq \boldsymbol{b}_k \end{cases}, \tag{3.24}$$

where P_L is the probability of incorrect symbol detection. Then, the capacity of PPM with hard-decision decoding is calculated as [58, 59]

$$C_{\text{PPM}} = \frac{\log_2 L}{L} + \frac{(1-P_L)}{L}\log_2(1-P_L) + \frac{P_L}{L}\log_2\left(\frac{P_L}{L-1}\right) \text{ bits/sec/Hz.} \tag{3.25}$$

The capacity of PPM with soft-decision decoding when the system is corrupted by noise and intersymbol interference is determined by using Monte carlo integration in [57, 58, 59]. Nonetheless, we can exploit the expectation-maximization method described in Section 3.2.2 to calculate the capacity of PPM over a noisy channel as follows. Let $\boldsymbol{b}_k$ be a PPM symbol chosen from an orthogonal set

$$\underbrace{\{\overbrace{100\ldots00}^{L \text{ chips}}, 010\ldots00, \ldots, 000\ldots01\}}_{L \text{ symbols}}. \tag{3.26}$$

The set of states $\mathcal{S}$ is assigned in order to store the memory of the channel with m taps. If $(m-1) \leq L$, the states are simply assigned as the input channel symbols as shown in Fig. 3.2(a) and the number of states is equal to $n(\mathcal{S}) = L$. Otherwise, the states denote all possible $\lceil (m-1)/L \rceil$ subsequent symbols as shown in Fig. 3.2(b). In addition, the number of states is equal to $n(\mathcal{S}) = L^{\lceil (m-1)/L \rceil}$.

The maximum mutual information rate in (3.6) is achieved if the probability of a PPM symbol and the probability at state $(s_k = i)$ are uniform, i.e. $P(\boldsymbol{b}_k) = 1/L$ and $P(s) = 1/n(\mathcal{S})$. Consequently, the probability of a state-transition is determined as

$$P(s|s') = \begin{cases} \frac{1}{n(\mathcal{S})L}, & \text{for valid transition} \\ 0, & \text{for invalid transition} \end{cases}. \tag{3.27}$$

Furthermore, the probability transition of the discrete-input, continuous-output channel is given as

$$P(\boldsymbol{r}_k|\boldsymbol{b}_k) = \left(\frac{1}{\sqrt{2\pi}\sigma}\right)^L \exp\left[-\frac{\sum_{i=1}^{L}\left(r_{(k,i)} - \sum_{j=0}^{m-1} g_j b_{(k,i)-j}\right)^2}{2\sigma^2}\right], \tag{3.28}$$

where g_k is the discrete-time channel model described in (3.21) and σ^2 is the variance of the additive white Gaussian noise. Then, the channel capacity of PPM with soft-decision decoding can be determined by using the algorithm for a noisy channel in Section 3.2.2.

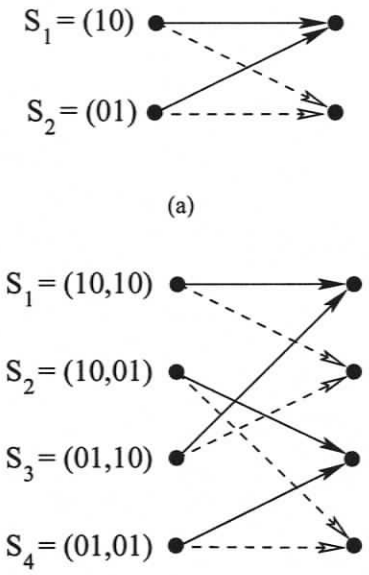

Figure 3.2. *Trellis diagrams for 2-PPM over a dispersive channel with (a)* $0 \leq m \leq 3$ *taps and (b)* $4 \leq m \leq 5$ *taps. The dashed and solid lines represent transitions between two states forced by* $\mathbf{b}_k = \{01\}$ *and* $\{10\}$*, respectively.*

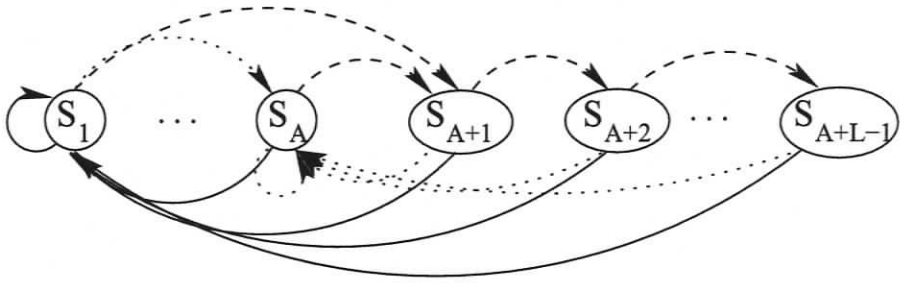

Figure 3.3. *State diagram of $A \times L$-DAPPM, the dashed, solid and dotted lines represent transitions between two states forced by $b_k = 0, 1$ and A, respectively.*

3.5 Capacity of Differential Amplitude Pulse-Position Modulation

First, we consider the channel capacity of DAPPM over a noiseless channel. Because the number of consecutive zeros is constrained, DAPPM is a Markov process of memory one. Consequently, DAPPM can be represented by the state diagram shown in Fig. 3.3. The transition to state $s_1, s_2, \ldots, s_A$ corresponding to the current channel input $b_k = 1, 2, \ldots, A$ is shown. $s_{A+1}, \ldots, s_{A+L-1}$ denotes that there are $1, \ldots, L-1$ consecutive zeros immediately after the "on" chip. Hence, the number of states is $n(\mathcal{S}) = A + L - 1$. Note that L-DPPM is equivalent to $1 \times L$-DAPPM. From the state diagram, the state-transition matrix can be written as

$$\mathbf{B} = \begin{bmatrix} \mathbf{O}_{(A+L-1)\times A} & \mathbf{C}_{A\times(L-1)} \\ & \mathbf{D}_{(L-1)\times(L-1)} \end{bmatrix}, \tag{3.29}$$

where $\mathbf{O}_{(A+L-1)\times A}$ is an $(A+L-1)\times A$ matrix of ones

$$\mathbf{C}_{A\times(L-1)} = \underbrace{\left[\begin{array}{ccccc} 1 & 0 & 0 & \dots & 0 \\ 1 & 0 & 0 & \dots & 0 \\ \vdots & \vdots & \vdots & \ddots & \vdots \\ 1 & 0 & 0 & \dots & 0 \end{array}\right]}_{L-1 \text{ columns}} \Bigg\} A \text{ rows}, \tag{3.30}$$

and

$$\mathbf{D}_{(L-1)\times(L-1)} = \underbrace{\left[\begin{array}{cccccc} 0 & 1 & 0 & \dots & 0 & 0 \\ 0 & 0 & 1 & \dots & 0 & 0 \\ \vdots & \vdots & \vdots & \ddots & \vdots & \vdots \\ 0 & 0 & 0 & \dots & 0 & 1 \\ 0 & 0 & 0 & \dots & 0 & 0 \end{array}\right]}_{L-1 \text{ columns}} \Bigg\} L-1 \text{ rows}. \tag{3.31}$$

Then, the characteristic equation of matrix **B** is

$$f(X) = X^{L+1} - (A+1)X^L + A = 0, \tag{3.32}$$

and the capacity is the base-two logarithm of its largest real root. Fig. 3.4 shows the capacity of PPM, DPPM and DAPPM over a noiseless channel as a function of L. As shown by Kato and Zeger [66], the capacity of a $(0,k)$ run-length code (in terms of storage), is equivalent to the capacity of L-DPPM which from Fig. 3.4 is 1 bit/sec/Hz when L is large, and the rate of convergence is $\left(\frac{1}{4}\log_2 e\right)/2^L$. We extend their work to find the capacity limit of DAPPM when L is large. From the figure, this capacity converges to $\log_2(A+1)$, i.e.

$$\lim_{L\to\infty} C_{\text{DAPPM}} = \log_2(A+1) \text{ bits/sec/Hz}, \tag{3.33}$$

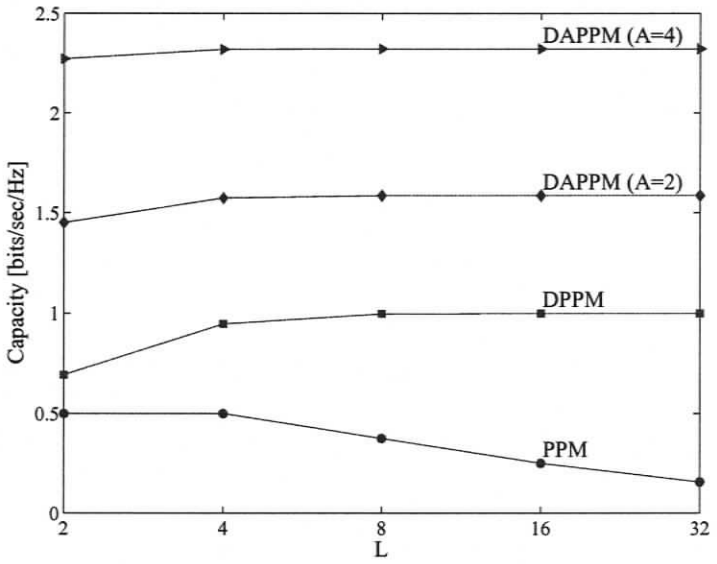

Figure 3.4. *Capacity of PPM, DPPM, DAPPM as a function of L.*

and the convergence rate is

$$\frac{A \log_2 e}{(A+1)^{L+1}}. \tag{3.34}$$

The proof of (3.33) and (3.34) are given in Appendix A. As shown in Fig. 3.4, the capacity converges to the limit faster when A is higher. Note that the capacity of PPM tends to be zero when L is large.

Next, we examine the capacity of DPPM and DAPPM systems over a multipath dispersion channel with m taps. Because the DAPPM signal is a Markov process of memory one and the channel has memory $(m-1)$, the set of states $\mathcal{S}$ is assigned in order to store the channel memory and the symbol memory. Both DPPM and DAPPM schemes over a dispersive channel with m taps can be represented by a trellis diagram as shown in Fig. 3.5. This represents the possible $(m-1)$-chip sequences preceding b_k, i.e. $S_n \leftrightarrow (b_{k-m+1}, \cdots, b_{k-1})$.

If $(m-1) > (L-1)$, the states must not contain any run of zeros exceeding $L-1$. For example, the 2×2-DAPPM trellis over a channel with 3 taps given in Fig. 3.5(a) does not have state $(0,0)$, and there is no transition when the current state is S_3 or S_6 and $b_k = 0$. Conversely, if $(m-1) \leq (L-1)$, the number of states is $n(\mathcal{S}) = (A+1)^{m-1} + L - m$.

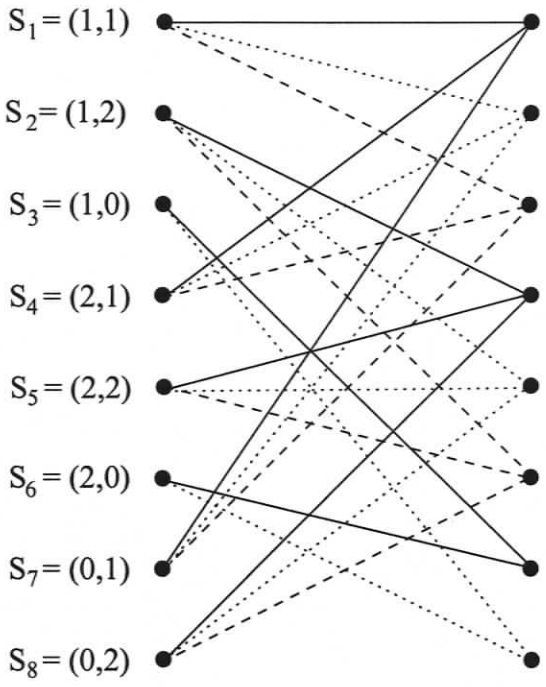

(a)

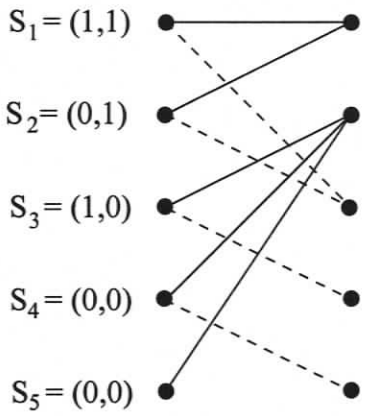

(b)

Figure 3.5. *Trellis diagrams for (a)* 2×2*-DAPPM and (b)* 4*-DPPM systems over a dispersive channel with three taps. The dashed, solid and dotted lines represent transitions between two states forced by* $b_k = 0, 1$ *and* 2*, respectively.*

The extra $(L-m)$ states containing $(m-1)$ consecutive zeros are required to limit the number of consecutive zeros so that there is no run of zeros exceeding $(L-1)$, which is the constraint imposed by the DPPM and DAPPM sequences. For example, the 4-DPPM trellis over a channel with 3 taps in Fig. 3.5(b) has state $(0,0)$. States S_4 and S_5 represent runs of two and three zeros preceding the current channel input. Also, there is no transition when the current state is S_5 and $b_k = 0$.

Although the DAPPM symbol is identically and independently distributed (i.i.d), each DAPPM symbol has different number of chips and format. As a result, each chip in a DAPPM symbol is not i.i.d. and the probabilities $P(s|s')$ which maximize the mutual information is not uniform. These probabilities can be determined iteratively using the expectation-maximization method described in [60, 63] until the transition probabilities converge. First, arbitrary $P(s|s')$ are selected according to the state transitions. The input channel sequence is generated and transmitted through the channel under consideration. Then, using the modified BCJR algorithm, $T(s',s)$ in (3.9) is calculated to determine the noisy adjacency matrix $\boldsymbol{A}$. The transition probabilities are updated as

$$P(s|s') = \frac{v_s}{v_{s'}} \cdot \frac{A(s',s)}{\lambda_{\max}}, \tag{3.35}$$

where $\lambda_{\max}$ is the maximum eigenvalue of matrix $\boldsymbol{A}$ and $\boldsymbol{v}$ is the eigenvector corresponding to the maximum eigenvalue. After convergence, the capacity is given by $C = \log_2 \lambda_{\max}$.

Next, the transition probabilities are calculated for the discrete-input, discrete-output channel. Since the input chips b_k are not equiprobable and depend on the transition probabilities $P(s|s')$, the conditional probabilities $P(r_k|b_k)$ are not symmetric.

Here, we consider the transition probabilities for DPPM over a channel with hard-decision decoding. Suppose that the channel contains m taps. Let s_j be an m-chip segment randomly taken from a DPPM sequence, $\Pr(s_j)$ be the probability of occurrence of segment s_j, and $I(s_j)$ be the receiver filter output (excluding noise) of the last chip of s_j. The probability of detecting "0" as "1" can be calculated as

$$P(r_k|b_k) = \Pr(r_k = 1|b_k = 0) = \sum_{s_j} \Pr(s_j) Q\left(\frac{P_c(\theta - I(s_j))}{\sqrt{N_0 W}}\right), \tag{3.36}$$

when the last chip of the segment s_j is "0". On the other hand, the probability of detecting "1" as "0" can be calculated as

$$P(r_k|b_k) = \Pr(r_k = 0|b_k = 1) = \sum_{s_j} \Pr(s_j) Q\left(\frac{P_c(I(s_j) - \theta)}{\sqrt{N_0 W}}\right), \tag{3.37}$$

when the last chip of the segment s_j is "1".

If the receiver uses soft-decision decoding, the transition probabilities of the channel are

$$P(r_k|s, s') = \left(\frac{1}{\sqrt{2\pi}\sigma}\right) \exp\left[-\frac{\left(r_k - \sum_{i=0}^{m-1} g_i b_{k-i}\right)^2}{2\sigma^2}\right], \tag{3.38}$$

where g_k is the discrete-time channel model described in (3.21) and σ^2 is the variance of the additive white Gaussian noise.

3.6 Performance Results

Figs. 3.6 through 3.8 show the channel capacity for PPM and DPPM with hard-decision and soft-decision decoding when $L = 2, 4$ and 8. Over an AWGN channel ($D_T = 0.01$), the soft-output channel offers about a 2-dB advantage compared with hard-output channel. Moreover, its performance is superior to hard-decision decoding when D_T is high, i.e. approximately a 10-dB gain can be obtained.

The capacity of DPPM and DAPPM with soft-decision decoding over dispersive channels with $D_T = 0.01$ and 0.3 are compared with that of PPM in Figs. 3.9 through 3.13. Note that the channel capacities of 2-PPM and 4-PPM converge to the same values when the SNR is large. However, at low SNRs, the capacity of 4-PPM is higher than that of 2-PPM because 4-PPM has better power efficiency.

In Figs. 3.9 and 3.10, there is a cross-over point between DAPPM and DPPM at low SNR. Although it has better bandwidth efficiency than DPPM, DAPPM achieves less capacity at low SNRs because it is more susceptible to corruption by noise. However, the

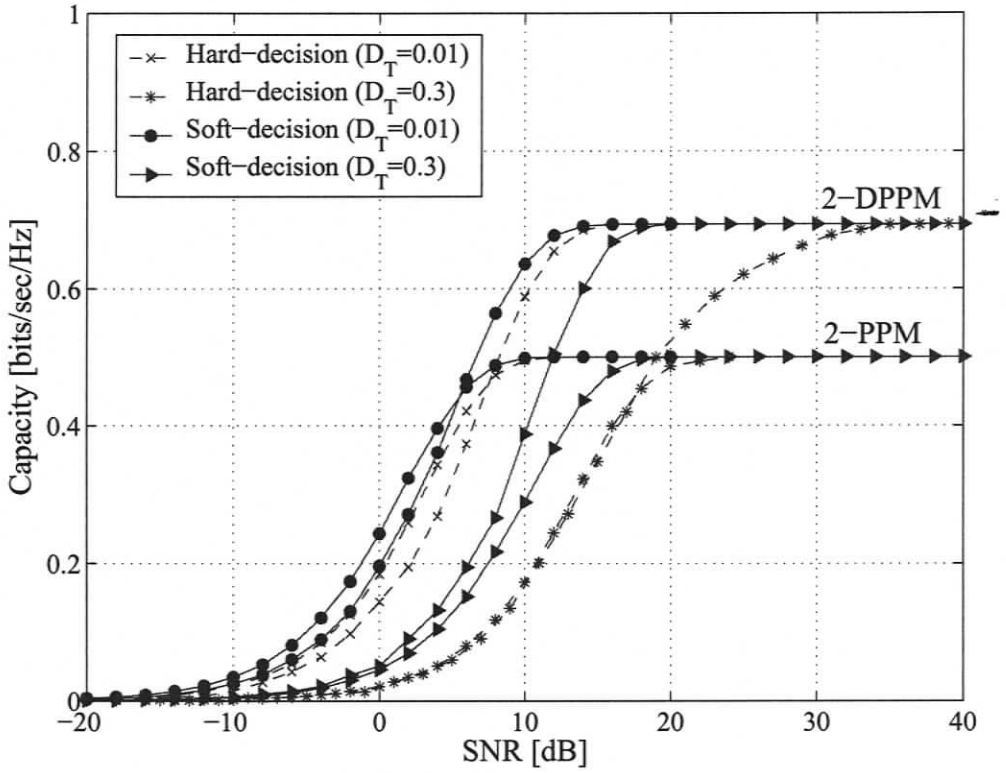

Figure 3.6. *Capacity of* 2*-PPM and* 2*-DPPM as a function of SNR over a dispersive channel with* $D_T = 0.01$ *and* 0.3.

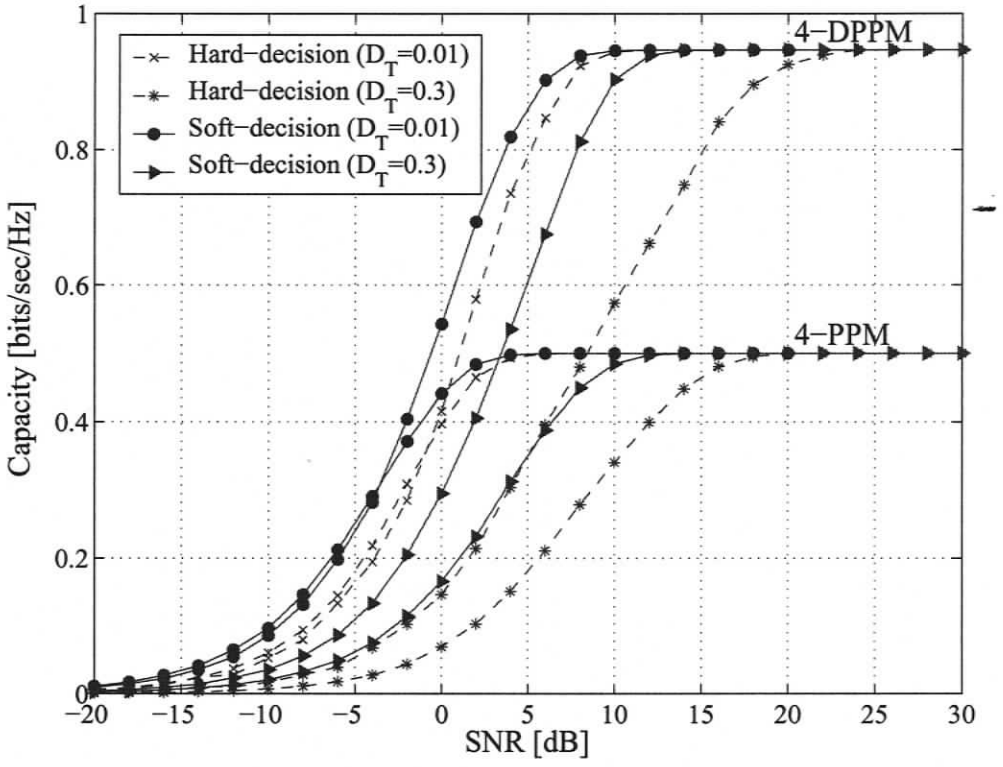

Figure 3.7. *Capacity of* 4*-PPM and* 4*-DPPM as a function of SNR over a dispersive channel with* $D_T = 0.01$ *and* 0.3.

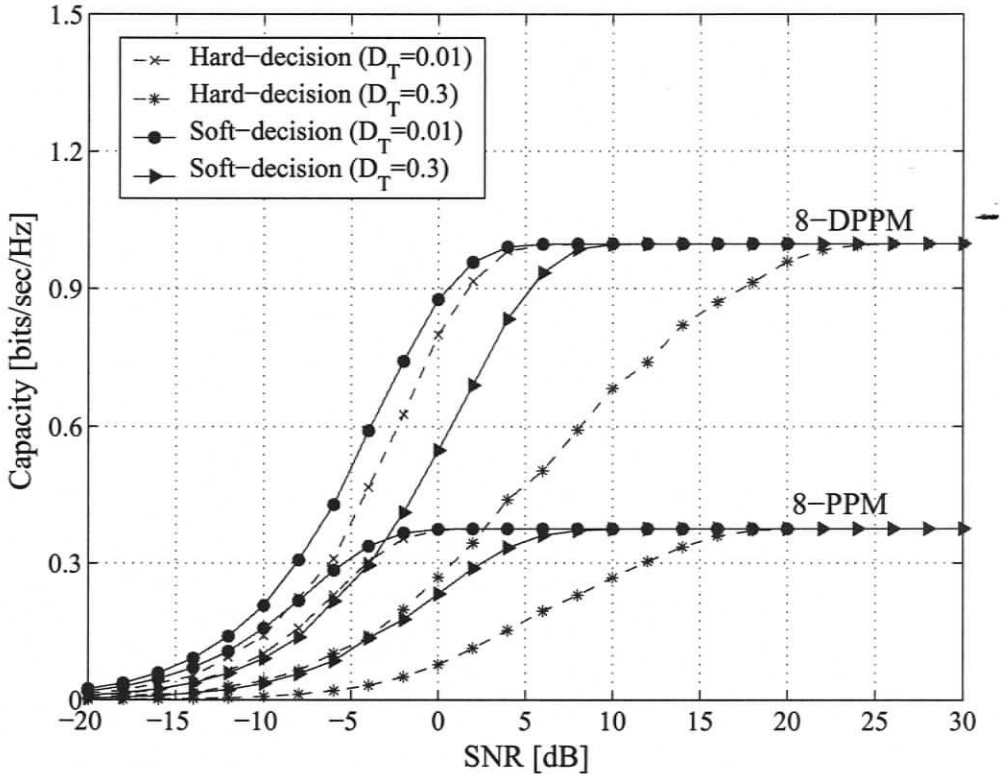

Figure 3.8. *Capacity of* 8*-PPM and* 8*-DPPM as a function of SNR over a dispersive channel with* $D_T = 0.01$ *and* 0.3.

cross-over point between DAPPM and DPPM occurs at low SNR when D_T is higher since DAPPM is less sensitive to ISI.

At high SNRs, 4-DPPM can provide $C = 0.95$ while 4-PPM gives only $C = 0.5$, so DPPM yields about twice the capacity of PPM. Considering PPM, DPPM and DAPPM systems with $L = 2$, the capacity of 2-DPPM, 2×2-DAPPM and 4×2-DAPPM are $C = 0.69$, $C = 1.45$ and $C = 2.27$, respectively, while 2-PPM yields only $C = 0.5$ at high SNR as shown in Fig. 3.11. Thus, the higher A is, the higher the channel capacity that can be achieved. The channel capacities for modulation schemes with $L = 4$ and $L = 8$ are similar to that for modulation schemes with $L = 2$ as shown in Figs. 3.12 and 3.13.

Considering the effect of multipath dispersion on capacity, 8-PPM over a channel with $D_T = 0.3$ requires about 10 dB more SNR to yield the highest capacity compared with when $D_T = 0.01$, while 8-DPPM requires only about 4 dB more as shown in Fig. 3.13. The difference in SNR for 2-PPM, 2-DPPM, 2×2-DAPPM and 4×2-DAPPM to achieve the highest capacity when $D_T = 0.01$ and $D_T = 0.3$ is 9.5, 4.5, 3 and 2 dB, respectively, as shown in Fig. 3.11. The difference between the power required to achieve the highest capacity in a DAPPM system over a channel with $D_T = 0.01$ and $D_T = 0.3$ decreases as A increases. This is because DAPPM is more bandwidth efficient and suffers less from inter-symbol interference than PPM. Therefore the capacity of PPM is more severely degraded compared to that with DPPM and DAPPM over a dispersive channel with high D_T.

3.7 Conclusions

In this chapter, it was shown that L-DPPM and $A \times L$-DAPPM systems over a dispersive channel can be represented by a trellis diagram. The corresponding capacity was determined by exploiting a method for calculating the capacity of a Markov process channel. The channel capacity of the modulation schemes was determined and compared with that of L-PPM. Over a noiseless channel, the capacity of DAPPM converges to $\log_2(A+1)$, while the capacity of PPM converges to zero when L is large. Over a noisy channel, DAPPM

can provide greater capacity than PPM and DPPM. Performance results show that DAPPM systems are more robust to multipath dispersion than PPM and DPPM systems because DAPPM is more bandwidth efficient.

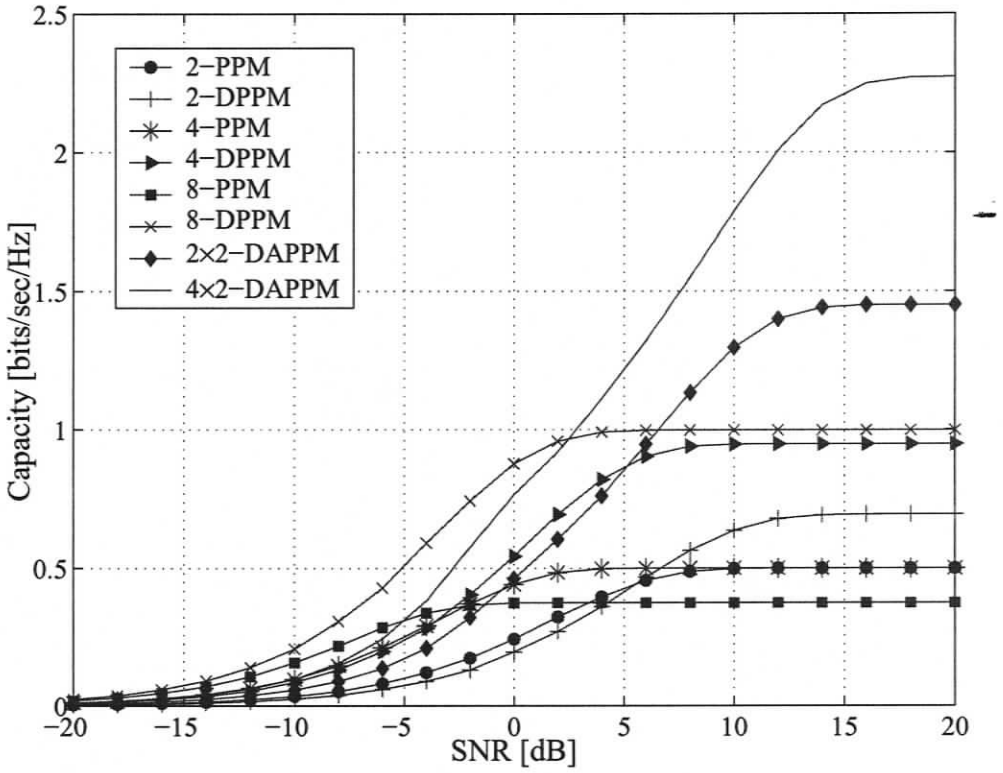

Figure 3.9. *Capacity of PPM and DPPM with* $L = 2, 4, 8$ *and* 2×2*-DAPPM and* 4×2*-DAPPM in bits/sec/Hz as a function of SNR over a dispersive channel with* $D_T = 0.01$.

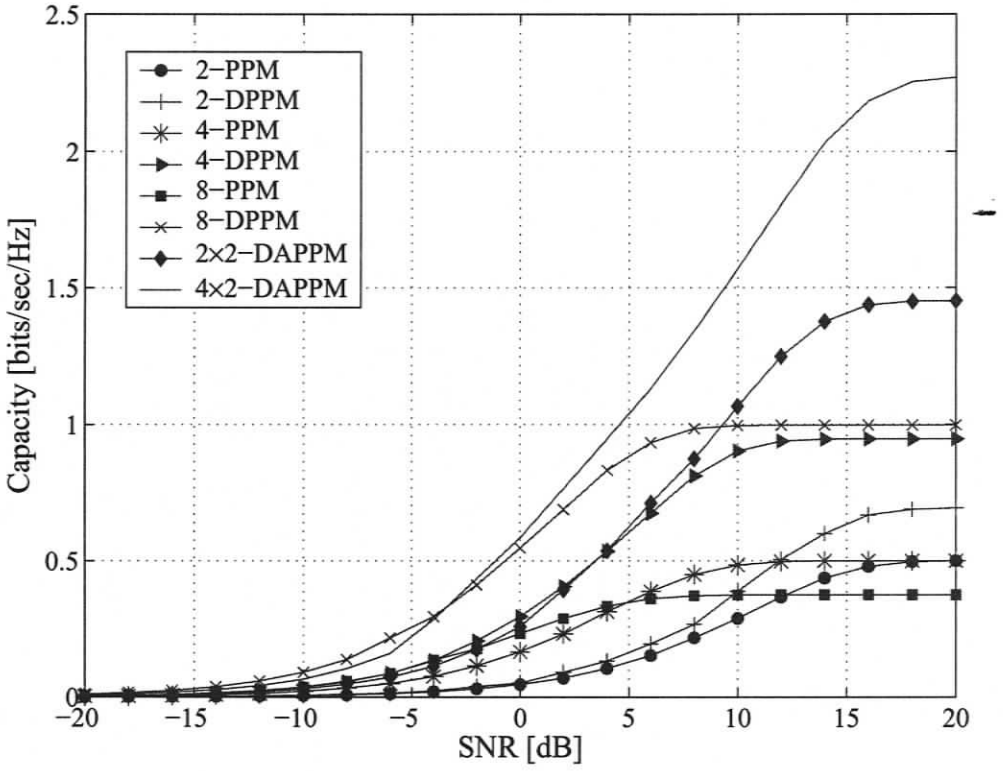

Figure 3.10. *Capacity of PPM and DPPM with* $L = 2, 4, 8$ *and* 2×2*-DAPPM and* 4×2*-DAPPM in bits/sec/Hz as a function of SNR over a dispersive channel with* $D_T = 0.3$.

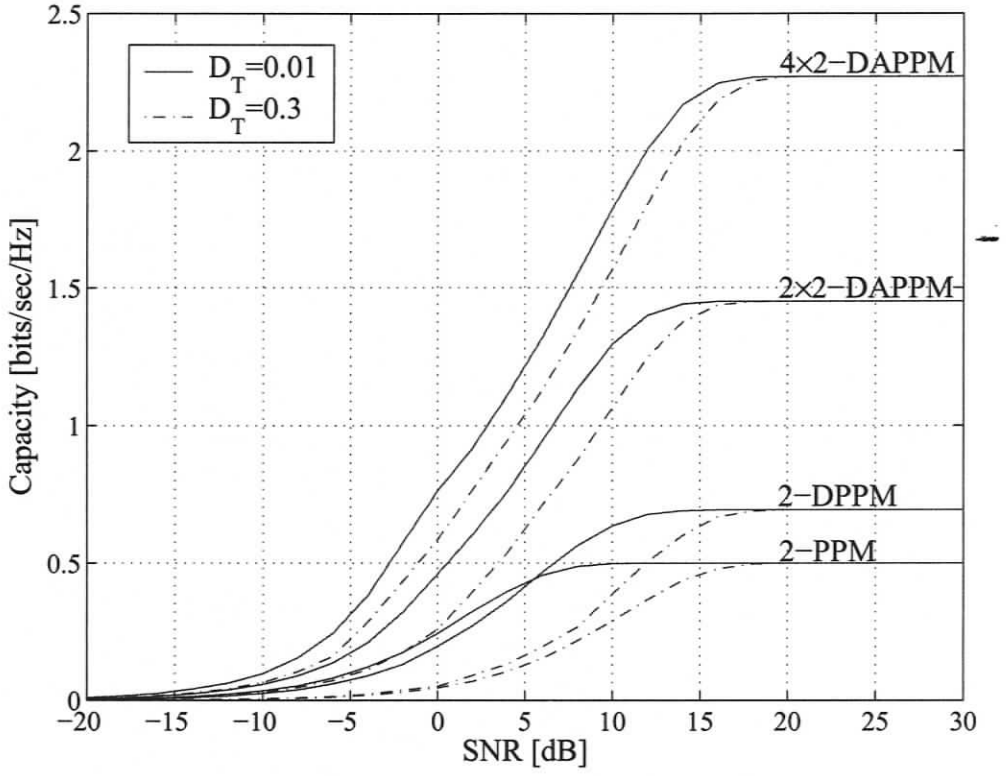

Figure 3.11. *Capacity of* 2*-PPM,* 2*-DPPM,* 2×2*-DAPPM and* 4×2*-DAPPM with soft-decision decoding as a function of SNR over a dispersive channel with* $D_T = 0.01$ *and* 0.3.

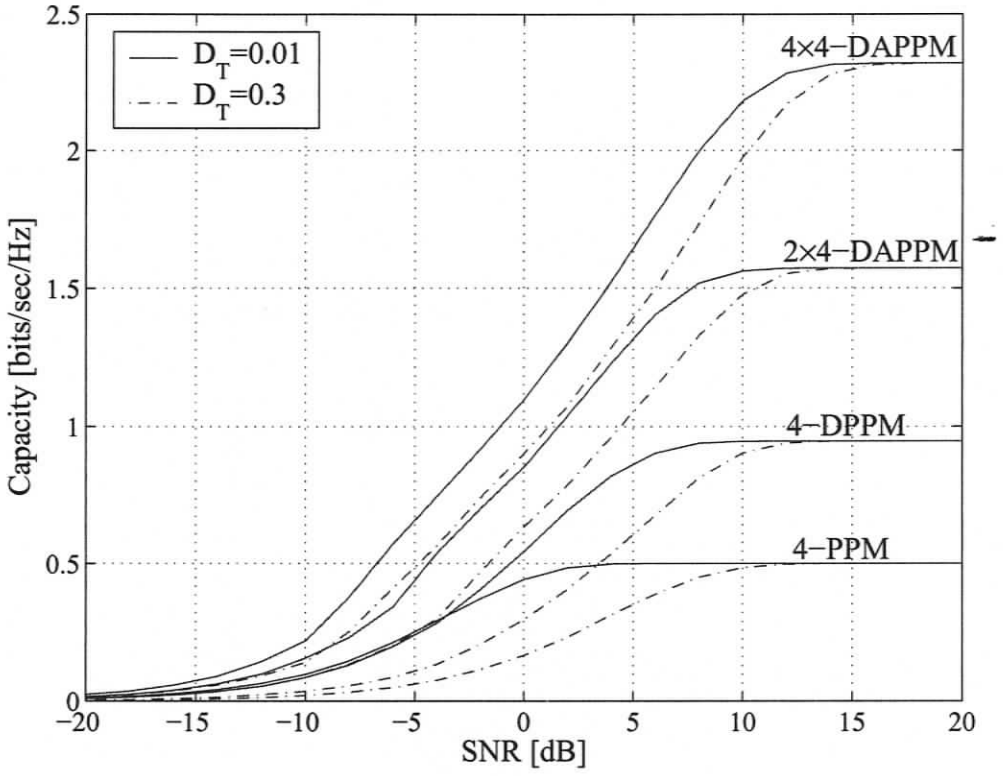

Figure 3.12. *Capacity of* 4*-PPM,* 4*-DPPM,* 2×4*-DAPPM and* 4×4*-DAPPM with soft-decision decoding as a function of SNR over a dispersive channel with* $D_T = 0.01$ *and* 0.3.

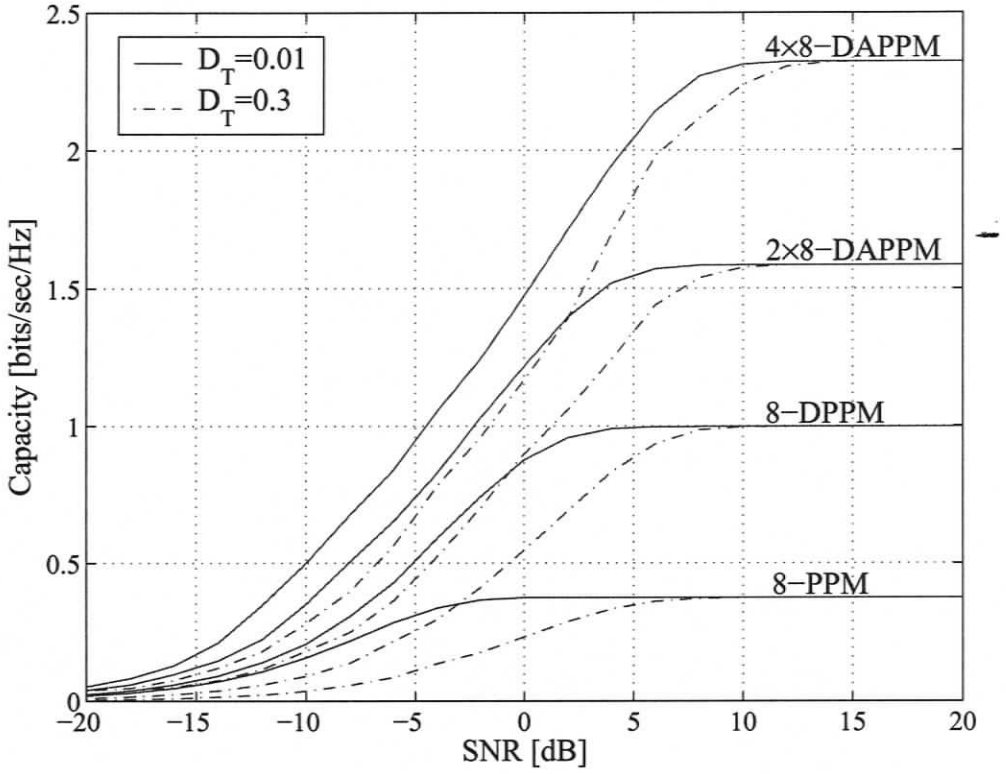

Figure 3.13. *Capacity of* 8*-PPM,* 8*-DPPM,* 2×8*-DAPPM and* 4×8*-DAPPM with soft-decision decoding as a function of SNR over a dispersive channel with* $D_T = 0.01$ *and* 0.3.

Chapter 4

Soft-Decision Decoding for Differential Pulse-Position Modulation

4.1 Introduction

In Chapter 3, it was shown that soft-decision decoding requires much less transmit power than hard-decision decoding, especially when the channel is susceptible to multipath dispersion. In a PPM system, maximum-likelihood sequence detection (MLSD) is the optimal soft-decision decoding algorithm [67, 68]. MLSD in a PPM system requires waiting until all the sampled outputs associated with the transmission of one PPM symbol have been received. Then, the received symbol is decoded by choosing the symbol which has the minimum distance from the received symbol. This is feasible for PPM modulation because PPM is isochronous, that is, each symbol is transmitted within a constant duration of time. However, this technique cannot be applied to anisochronous modulation such as DPPM, DAPPM and DH-PIM, in which the duration of a transmitted symbol varies, and the receiver does not know the boundary of a symbol until an "on" chip is detected. Nevertheless, some soft-decision detection algorithms have been developed.

Shiu and Kahn [49] suggested that MLSD can be applied to DPPM by comparing the received frame with all possible sequences. Their performance analysis shows that MLSD can significantly improve the performance of DPPM when the channel is dispersive with high D_T. However, this technique is not feasible because its complexity grows exponen-

tially with the length of the frame.

Wang and Xu [69, 70] introduced soft-decision detection with less complexity and applied it to IDPPM (Improved Differential Pulse-Position Modulation) and DH-PIM. Their idea utilizes the constraint of consecutive "on" chips in IDPPM and DH-PIM symbols. The "off" chips following "on" chip are easily detected as "on" chips due to the multipath dispersion. Therefore at the receiver, if the number of detected consecutive "on" chips violates the rule of IDPPM and DH-PIM symbols, it assumes that there are some "off" chips which were detected as "on" chips. Thus, the detector will select the chips with the maximum amplitude among those chips to be "on" chip, while the rest are "off" chips. However, error correction is quite limited because the algorithm can only correct errors which cause an "off" chip to be detected as an "on" chip, while "on" chips detected as "off" chips remain uncorrected. As a result, although it is better than using hard-decision decoding, their improvement is far from that obtained using MLSD.

In this chapter, we propose soft-decision techniques for DPPM which are less complex than MLSD, but have performance close to that with MLSD. Since DPPM can be represented by a trellis diagram as shown in Chapter 3, the maximum a posteriori (MAP) algorithm and its simplification such as Max-Log-MAP and soft-output Viterbi algorithm (SOVA) can be used. Note that these techniques require knowledge of the channel. In addition, a low complexity soft-decision decoding algorithm which does not need channel knowledge is introduced. Their performance is evaluated and compared with hard-decision detection and MLSD. Also, their complexities are discussed and compared with MLSD.

4.2 Maximum Likelihood Sequence Detection (MLSD)

According to [49], MLSD selects the sequence which maximizes the conditional probability

$$\Pr(\boldsymbol{r}_1^\tau | \boldsymbol{b}_1^\tau) = \left(\frac{1}{\sqrt{2\pi}\sigma}\right)^\tau \exp\left[-\sum_{k=1}^{\tau} \frac{(r_k - b_k)^2}{2\sigma^2}\right]. \tag{4.1}$$

In other words, the MLSD detector selects the sequence $\hat{\boldsymbol{b}}_1^{\tau}$ among all possible sequences which is closest in Euclidean distance to the received sequence $\boldsymbol{r}_1^{\tau}$, i.e. the sequence $\hat{\boldsymbol{b}}_1^{\tau}$ is selected if $\sum_k \parallel r_k - \hat{b}_k \parallel^2$ is minimum. The performance of DPPM with MLSD over nondispersive and dispersive channels is now analysed.

4.2.1 Performance over a nondispersive channel

MLSD selects the chip sequence $\hat{\boldsymbol{b}}_1^{\tau}$ which has minimum-distance compared with the received chip sequence $\boldsymbol{r}_1^{\tau}$. In a DPPM system, minimum-distance errors correspond to an "on" chip deleted and placed elsewhere in the sequence, as long as there is no run of "off" chips greater than $L-1$ in the frame. Thus, the Hamming distance between the detected sequence $\hat{\boldsymbol{b}}_1^{\tau}$ and the transmitted sequence $\boldsymbol{b}_1^{\tau}$ is equal to two. In an F-bit frame, there are $(F/\log_2 L)$ "on" chips and approximately $((L-1)/2)(F/\log_2 L)$ "off" chips. Therefore there are a total of $((L-1)/2)(F/\log_2 L)^2$ sequences that have Hamming distance two from a given chip sequence. However, only half of the "on" chip movements do not result in a run of "off" chips greater than $L-1$. An upper bound on the DPPM frame error rate over an AWGN channel at high SNRs is [49]

$$\text{FER} \approx \left(\frac{L-1}{4}\right)\left(\frac{F}{\log_2 L}\right)^2 \cdot Q\left(RP_t\sqrt{\frac{(L+1)\log_2 L}{4R_bN_0}}\right). \tag{4.2}$$

4.2.2 Performance over a dispersive channel

We define an error event as $\bar{e}$ when the leading and ending entries of $\bar{e}$ are nonzero. We define $e_k = b_k - \hat{b}_k$ as the input error sequence associated with an error event and $e_k \in \{-1, 0, 1\}$. For an error event, $\sum_k e_k$ must be zero in order to have the correct number of received symbols. The frame error rate can be approximately upper bounded by

$$\text{FER} \approx \sum_{\bar{e}\in\mathcal{E}} \Pr(\bar{e}), \tag{4.3}$$

where $\Pr(\bar{e})$ is the probability of error event $\bar{e}$ and $\mathcal{E}$ is the set of error events. In a DPPM system, if $e_k = 1$, then $b_k = 0$, and $e_k = -1$ if $b_k = 1$. Because each symbol is assigned to

different waveforms with different numbers of "off" chips, the distribution of $b_k = 0$ and $b_k = 1$ is not uniform. The probabilities of $e_k = -1$ and $e_k = +1$ can be calculated as

$$\Pr(e_k = -1) = \frac{2L}{L(L+1)}, \tag{4.4}$$

and

$$\Pr(e_k = +1) = 1 - P_{(-1)}. \tag{4.5}$$

Thus, the probability of a particular error event $\bar{e}$ is given by

$$\Pr(\bar{e}) \approx \left[\prod_k \Pr(e_k \neq 0)\right] \cdot Q\left(\frac{1}{2}\sqrt{\frac{\sum_k \mid e_k \otimes g_k \mid^2}{N_0}}\right), \tag{4.6}$$

where g_k is the equivalent discrete-time channel impulse response given in (3.21).

4.3 Optimal and Sub-Optimal Maximum a Posteriori (MAP) Decoding Algorithms

4.3.1 The MAP algorithm

Unlike MLSD, a maximum a posteriori (MAP) detector selects the sequence $\hat{\boldsymbol{b}}_1^\tau$ if it yields the maximum a posteriori probability $\Pr(\boldsymbol{b}_1^\tau|\boldsymbol{r}_1^\tau)$ [71]. Assuming that the channel input b_k has an identical, independent distribution (iid),

$$\Pr(\boldsymbol{b}_1^\tau|\boldsymbol{r}_1^\tau) = \prod_{k=1}^{\tau} \Pr(b_k|\boldsymbol{r}_1^\tau). \tag{4.7}$$

To select the sequence having the maximum of $\Pr(\boldsymbol{b}_1^\tau|\boldsymbol{r}_1^\tau)$ is equivalent to select the sequence that has the maximum of $\Pr(b_k|\boldsymbol{r}_1^\tau)$ for each channel input, i.e.

$$\max \Pr(\boldsymbol{b}_1^\tau|\boldsymbol{r}_1^\tau) = \prod_{k=1}^{\tau} \max \Pr(b_k|\boldsymbol{r}_1^\tau). \tag{4.8}$$

Consequently, if b_k is a binary signal, the detector chooses $\hat{b}_k = 1$ when $\Pr(b_k = 1|\boldsymbol{r}_1^\tau) > \Pr(b_k = 0|\boldsymbol{r}_1^\tau)$; otherwise, it chooses $\hat{b}_k = 0$. We define $L(b_k)$ as the log-likelihood ratio

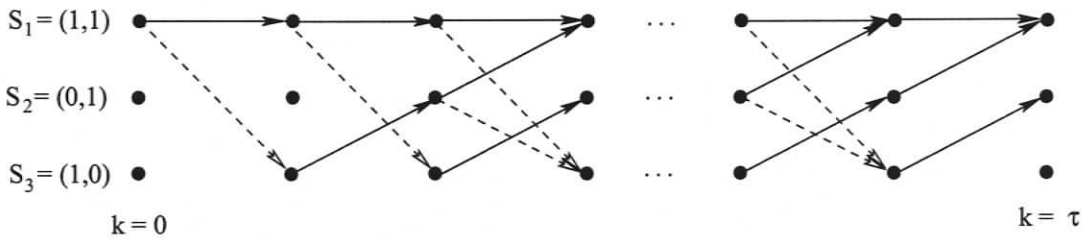

Figure 4.1. *Trellis diagrams for 2−DPPM systems over a dispersive channel with 3 taps. The dashed and solid lines represent transitions between two states forced by* $b_k = 0$ *and* 1, *respectively.*

(LLR) which can be calculated as

$$L(b_k) = \ln \left[\frac{\Pr(b_k = 1 | \boldsymbol{r}_1^\tau)}{\Pr(b_k = 0 | \boldsymbol{r}_1^\tau)} \right]. \tag{4.9}$$

Therefore the detector chooses $\hat{b}_k = 1$ if $L(b_k) > 0$ and $\hat{b}_k = 0$ otherwise. This algorithm cannot be applied directly to DPPM since the channel input is not iid. Next, the MAP algorithm is modified for use with DPPM.

DPPM over a noisy channel can be represented by a trellis diagram as shown in Fig. 4.1. If $(m-1) > (L-1)$, the states must not contain any run of zeros exceeding $(L-1)$. Therefore the number of states can be computed as

$$n(\mathcal{S}) = a(m + L + 1), \tag{4.10}$$

where $a(j)$ is a function which can be determined as follows

$$a(j) = \begin{cases} 0, & 0 \le j \le L-1 \\ 1, & j = L \\ \sum_{i=j-L}^{j-1} a(i), & j > L \end{cases}. \tag{4.11}$$

Conversely, if $(m-1) \le (L-1)$, besides the binary number of length $(m-1)$, the states are represented as $L - m$ states containing $(m-1)$ consecutive zeros. Accordingly, the number of states is

$$n(\mathcal{S}) = 2^{m-1} + L - m. \tag{4.12}$$

For the transition from past state $s_{k-1} = s'$ to present state $s_k = s$ corresponding to channel input b_k, the log-likelihood can rewritten as

$$L(b_k) = \ln \left[\frac{\Pr_{b_k=1}(s', s|\boldsymbol{r}_1^\tau)}{\Pr_{b_k=0}(s', s|\boldsymbol{r}_1^\tau)} \right]. \tag{4.13}$$

We use a modified BCJR method [64] to calculate the log-likelihood which is given by

$$L(b_k) = \ln \left[\frac{\sum_{\substack{s',s \\ b_k=1}} \alpha_{k-1}(s')\gamma_k(s', s)\beta_k(s)}{\sum_{\substack{s',s \\ b_k=0}} \alpha_{k-1}(s')\gamma_k(s', s)\beta_k(s)} \right]. \tag{4.14}$$

The definitions of $\alpha_k(s)$, $\beta_k(s)$ and $\gamma_k(s', s)$ were given in Chapter 3. We assume that the state sequence starts from the first state and must end at a state resulting from a transition of $b_\tau = 1$, as shown in Fig. 4.1. Therefore $\alpha_0(s)$ and β_τ are initialized as

$$\alpha_0(0) = 1; \quad \alpha_0(s) = 0, \quad \forall s \neq 0 \tag{4.15}$$

and

$$\beta_\tau(s) = \begin{cases} \frac{1}{n(\mathcal{S}_{b_k=1})}; & \forall s \in \mathcal{S}_{b_k=1} \\ 0; & \text{otherwise} \end{cases}, \tag{4.16}$$

where $n(\mathcal{S}_{b_k=1})$ is the number of states in the set of states $\mathcal{S}_{b_k=1}$ for which the transition is forced by $b_k = 1$. In this chapter, we investigate the performance of MAP detection for equiprobable DPPM symbols. Thus, $P(s|s')$, the probability of a transition from s' to s, is calculated as follows [72].

Given that X is a random variable describing the possible number of chips per symbol, we have $\Pr(X = i) = 1/L$ where $i \in \{1, \cdots, L\}$. Let j represent the number of consecutive zeros preceding the instantaneous channel input b_k in state s'. If the transition between two states is forced by $b_k = 1$

$$P(s|s')_{b_k=1} = \frac{\Pr(X = j+1)}{1 - \sum_{i=1}^{j} \Pr(X = i)}. \tag{4.17}$$

If the transition between two states is forced by $b_k = 0$

$$P(s|s')_{b_k=0} = 1 - P(s|s')_{b_k=1}. \tag{4.18}$$

Otherwise, $P(s|s') = 0$.

After the $L(b_k)$ are computed, the most likely positions of the "on" chips can be determined from $L(b_k)$. The detector selects $(F/(\log_2 L))$ positions which have the maximum values of $L(b_k)$ and decides $\hat{b}_k = 1$ according to these positions; otherwise, $\hat{b}_k = 0$. This decision rule is referred to as MAP-I.

Alternatively, in the MAP-II detector, the detector decides $\hat{b}_k = 1$ if

$$L(b_k) \geq \ln\left[\frac{\Pr(b_k = 1)}{\Pr(b_k = 0)}\right] = \ln\left[\frac{2}{L-1}\right], \tag{4.19}$$

and decides $\hat{b}_k = 0$ otherwise. Note that

$$\ln\frac{\Pr(b_k = 1)}{\Pr(b_k = 0)} \neq 0. \tag{4.20}$$

Since each symbol is assigned to different waveforms with different numbers of "off" chips, the probabilities of $\Pr(b_k = 1)$ and $\Pr(b_k = 0)$ can be calculated as

$$\Pr(b_k = 1) = \frac{2}{L+1} \text{ and } \Pr(b_k = 0) = \frac{L-1}{L+1}. \tag{4.21}$$

4.3.2 The Max-Log-MAP algorithm

We can reduce the LLR computation in the MAP algorithm by using the approximation

$$\ln\left(\sum_i e^{x_i}\right) \approx \max_i(x_i). \tag{4.22}$$

The log-likelihood ratio in (4.13) can then be rewritten as

$$\begin{aligned} L(b_k) &= \ln\left[\frac{\sum_{\substack{s',s \\ b_k=1}} \alpha_{k-1}(s')\gamma_k(s',s)\beta_k(s)}{\sum_{\substack{s',s \\ b_k=0}} \alpha_{k-1}(s')\gamma_k(s',s)\beta_k(s)}\right] \\ &= \ln\left[\sum_{\substack{s',s \\ b_k=1}} \alpha_{k-1}(s')\gamma_k(s',s)\beta_k(s)\right] - \ln\left[\sum_{\substack{s',s \\ b_k=0}} \alpha_{k-1}(s')\gamma_k(s',s)\beta_k(s)\right] \\ &\approx \max_{\substack{s',s \\ b_k=1}}[\ln\alpha_{k-1}(s') + \ln\gamma_k(s',s) + \ln\beta_k(s)] - \max_{\substack{s',s \\ b_k=0}}[\ln\alpha_{k-1}(s') + \ln\gamma_k(s',s) + \ln\beta_k(s)]. \end{aligned} \tag{4.23}$$

We will apply this approximation in calculating the forward recursion, $\ln(\alpha_k(s))$ and the backward recursion, $\ln(\beta_k(s))$ as follows.

$$\begin{aligned}\ln(\alpha_k(s)) &= \ln \sum_{s'} \gamma_k(s', s) \cdot \alpha_{k-1}(s') \\ &\approx \max_{s'} (\ln \gamma_k(s', s) + \ln \alpha_{k-1}(s')),\end{aligned} \tag{4.24}$$

and

$$\begin{aligned}\ln(\beta_{k-1}(s')) &= \ln \sum_{s} \gamma_k(s', s) \cdot \beta_k(s) \\ &\approx \max_{s} (\ln \gamma_k(s', s) + \ln \beta_k(s)).\end{aligned} \tag{4.25}$$

From (3.13) and (3.38), $\ln(\gamma_k(s', s))$ can be calculated as

$$\begin{aligned}\ln(\gamma_k(s', s)) &= \ln(Pr(r_k|b_k)P(s|s')) \\ &= \ln\left(\frac{1}{\sqrt{2\pi}\sigma}\right) - \frac{1}{2\sigma^2}\left(r_k - \sum_{i=0}^{m-1} g_i b_{k-i}\right)^2 + \ln(P(s|s')),\end{aligned} \tag{4.26}$$

where $\ln\left(\frac{1}{\sqrt{2\pi}\sigma}\right)$ is constant and can be omitted. Note that, $\ln(P(s|s'))$ cannot be expressed in term of $L(b_k)$.

4.3.3 The soft-output Viterbi algorithm (SOVA)

Basically, the Viterbi algorithm performs maximum likelihood decoding by selecting a path which yields a minimum distance between the received sequence and the trellis path. The chosen path is called the survivor. Hagenauer and Hoeher [73] presented a modified Viterbi algorithm for iterative decoding, the so-called Soft-In/Soft-Out Viterbi Algorithm (SOVA). The maximum likelihood path can be decided by choosing the largest probability

$$p(\boldsymbol{s}_1^{k(i)}, \boldsymbol{r}_1^k) = p(\boldsymbol{s}_1^{(k-1)(i)}, \boldsymbol{r}_1^{k-1}) \cdot p(s^{(i)}, r_k|s'^{(i)}), \tag{4.27}$$

where $s_1^{k(i)}$ denotes the i-th-state sequence for each state s and each time k. The path metric of the ith path at time k is defined as

$$\begin{aligned} M_k(s^{(i)}) &\triangleq \ln p(\boldsymbol{s}_1^{k(i)}, \boldsymbol{r}_1^k) \\ &= \ln p(\boldsymbol{s}_1^{(k-1)(i)}, \boldsymbol{r}_1^{k-1}) + \ln p(s^{(i)}, r_k | s'^{(i)}) \\ &= M_{k-1}(s'^{(i)}) + \ln \gamma_k(s'^{(i)}, s^{(i)}), \end{aligned} \tag{4.28}$$

where $s^{(i)}$ is the state of path i at time k and $s'^{(i)}$ is the state of path i at time $k-1$. $M_0(s)$ is initialized as

$$M_0(s) = 0; \quad \alpha_0(s) = 0, \quad \forall s \neq 0. \tag{4.29}$$

Since there are several paths to reach a state s at time k, the path with the higher metric is selected as the survivor, so that

$$M_k(s) = \max_{s'}(M_{k-1}(s'^{(i)}) + \ln \gamma_k(s'^{(i)}, s^{(i)})). \tag{4.30}$$

The receiver selects the maximum likelihood path at the end of the frame by choosing the path with highest $M_\tau(s)$ and $s \in \mathcal{S}_{b_k=1}$.

4.3.4 Simulation results

Figs. 4.2 and 4.3 present the frame error rate for MAP-I, Max-Log-MAP, SOVA, hard-decision decoding, and the upper bound for MLSD. It can be seen that over an AWGN channel, the performance of the MAP and Max-Log-MAP detectors are almost identical and they offer a 2dB gain relative to hard-decision decoding. While SOVA is inferior to MAP and Max-Log-MAP, it requires 0.5 dB less transmit power than a hard detector. When the channel is dispersive with high D_T, MAP, Max-Log-MAP and SOVA outperform a hard-decision detector by about 12 dB and 16 dB for 4-DPPM and 16-DPPM systems, at a FER of $= 10^{-4}$. It is also shown that their performance is very close to the MLSD upper bound.

Fig. 4.4 compares the performance of 4-DPPM with MAP-I and MAP-II detectors. The decisions with the MAP-II detector are based on the assumption that the chips b_k are

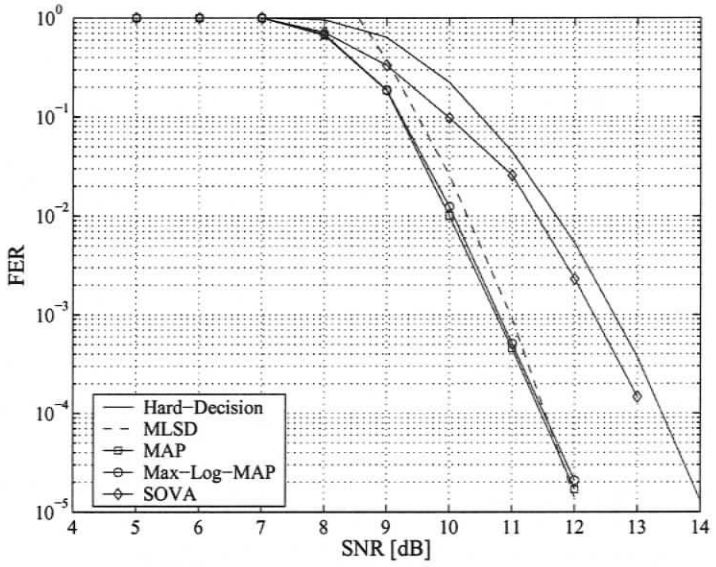

(a)

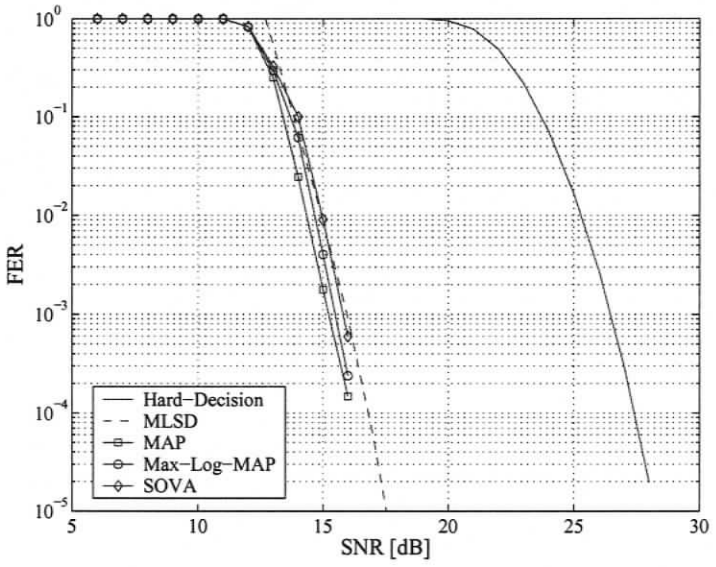

(b)

Figure 4.2. *Performance comparison of different decoding algorithms in 4-DPPM system on a dispersive channel (a)* $D_T = 0.01$ *and (b)* $D_T = 0.3$.

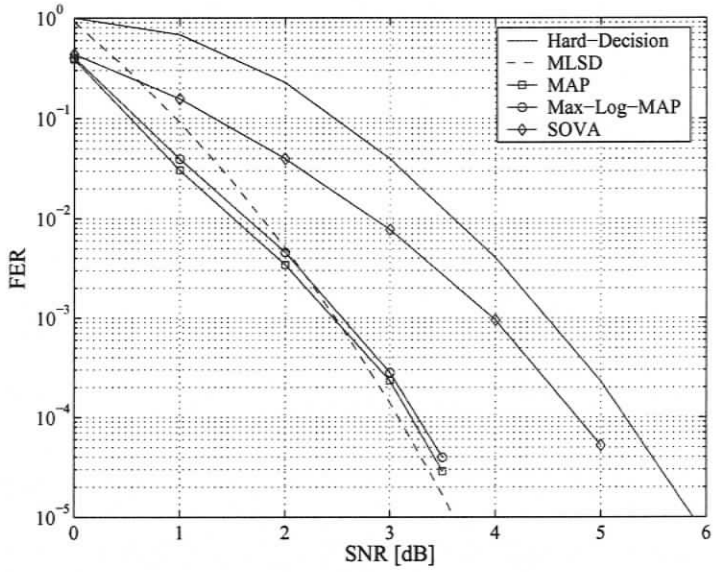

(a)

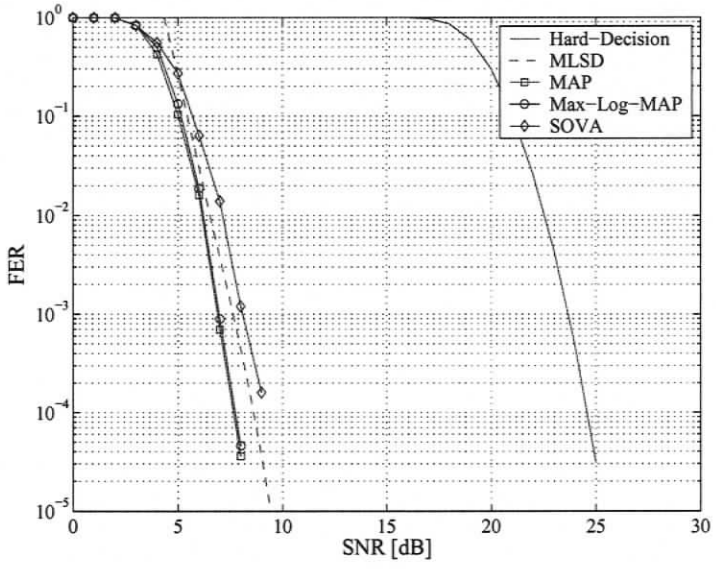

(b)

Figure 4.3. *Performance comparison of different decoding algorithms in 16-DPPM system on a dispersive channel (a)* $D_T = 0.01$ *and (b)* $D_T = 0.2$.

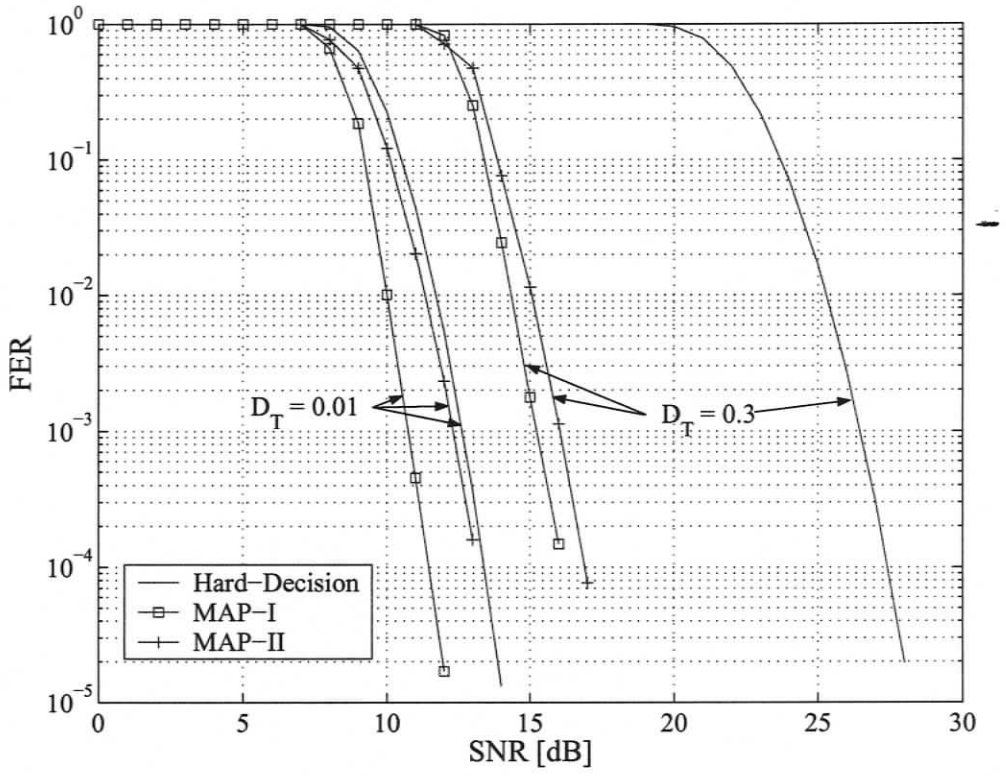

Figure 4.4. *Performance comparison of MAP-I and MAP-II detectors in a 4-DPPM system on a dispersive channel.*

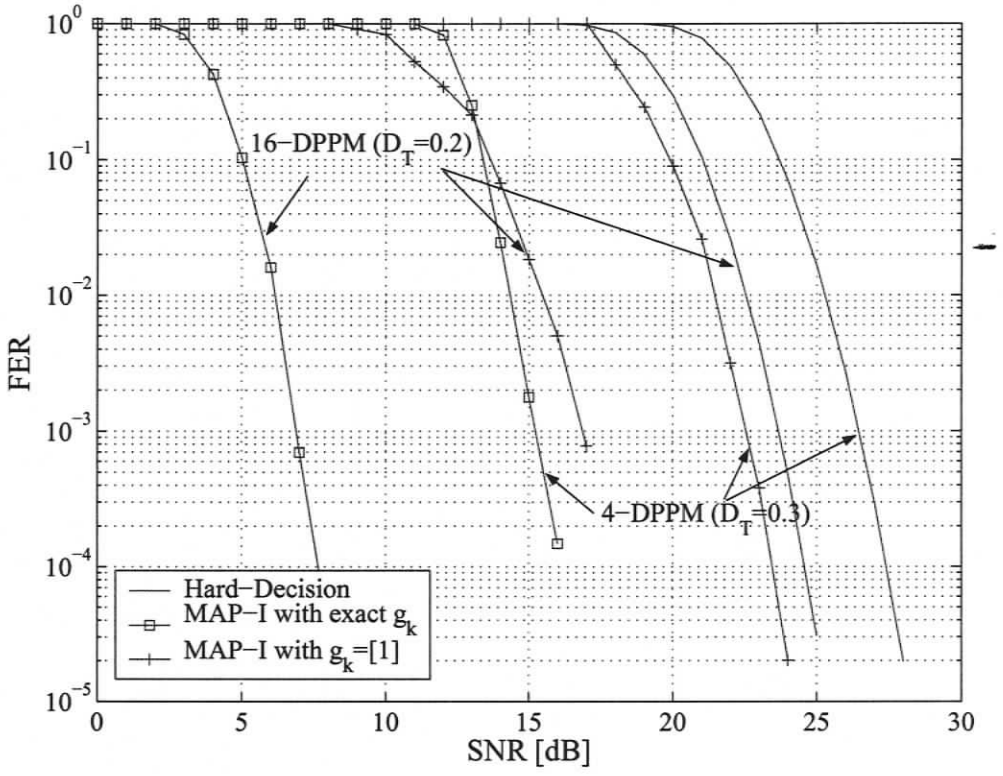

Figure 4.5. *Performance comparison of MAP-I detector with perfect and mismatched channel estimation (set the impulse response as $g_k = [1]$) in a 4- and 16-DPPM system on a dispersive channel.*

independent, which causes the MAP-II detector performance to be worse. The degradation relative to the MAP-I detector is about 1.5 dB when $D_T = 0.01$ and about 1 dB when $D_T = 0.3$.

Fig. 4.5 shows the effect of channel estimation on a DPPM system with a MAP-I detector. For the worst case, there is no channel estimation and the discrete-impulse response is always set as $g_k = [1]$. The performance of MAP is much degraded as it can achieve only 4 dB gain and 5.5 dB gain for 4-DPPM and 16-DPPM over a dispersive channel with high D_T. In other words, the performance is degraded about 10 dB compared with a MAP detector with perfect channel knowledge.

4.4 Sub-optimal Soft-Decision Decoding

It is shown that the optimal and sub-optimal MAP decoding algorithms significantly improve DPPM performance. However, their performance depends on knowledge of the channel and their complexity increases when D_T is high. In this section, we propose a soft-decision decoding which has complexity much lower than that of MLSD and MAP algorithms.

Although the advantage of using variable-length symbols is that the receiver does not need symbol synchronization, a single-chip error not only affects the corresponding symbol but also subsequent symbols and it causes insertion and deletion errors [74] as follows.

- Insertion error:

  As we use the "on" chip to indicate the end of a symbol, if a transmitted "off" chip is received as an "on" chip, this causes an additional symbol to be inserted and the next symbol to be demodulated in error. As a result, there is an extra symbol at the receiver, as shown in Fig. 4.6(b).

- Deletion error:

  If the noise causes a transmitted "on" chip to be received as an "off" chip, the symbol associated with the error chip is deleted and the following symbol is demodulated

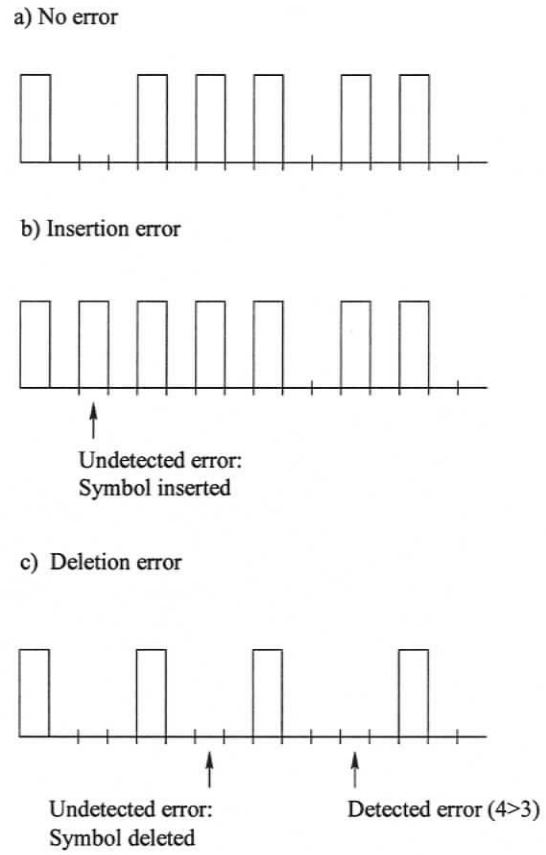

Figure 4.6. *Types of DPPM errors when $L = 4$: (a) No error, (b) Insertion error and (c) Deletion error.*

incorrectly. Note that if error chips cause a run of "off" chips longer than $L - 1$, the error is detected; otherwise, it is not detected. Therefore the number of received symbols is less than the number of transmitted symbols, as shown in Fig. 4.6(c).

Hence, these errors cause the number of demodulated symbols to differ from the number of transmitted symbols and a substitution error occurs after an insertion/deletion error.

4.4.1 The soft-decision decoding algorithm

First, we use hard decoding to verify if a received chip r_k is an "on" or "off" chip according to

$$\hat{b}_k = \begin{cases} 0, \text{ iff } r_k < \theta \\ 1, \text{ iff } r_k \geq \theta \end{cases} . \tag{4.31}$$

When errors are detected, i.e. groups of more than $L-1$ consecutive "off" chips occur, the soft decoding algorithm selects the positions corresponding to the "off" chips with maximum values of r_k and flips these "off" chips to be "on" chips. The number of flipped chips is calculated from $\lfloor n_{\text{off}}/L \rfloor$, which is the minimum possible number of symbols according to the number of consecutive "off" chips, n_{off} so that there is no run of "off" chips exceeding $L-1$.

We assume that the frame synchronizaiton is perfect. After the entire frame is received and the detected errors are corrected, the detector will determine the number of received "on" chips, n_{on}, which defines the total number of received symbols. If n_{on} does not equal $(F/\log_2 L)$, there are still undetected insertion and deletion errors. These errors can be detected using the following steps.

- To correct insertion errors:

  If $n_{\text{on}} > (F/\log_2 L)$, there are inserted symbols which need to be corrected. In another words, we need to find $[n_{\text{on}} - (F/\log_2 L)]$ "off" chips which were received as "on" chips. The position of a possible "off" chip error is determined from the position of a received "on" chip which has the *minimum* value of r_k among all received "on" chips. Then, the "on" chip is flipped to be an "off" chip. However, the position needs to be such that it will not create a run of "off" chips longer than $L-1$.

- To correct deletion errors:

  If $n_{\text{on}} < (F/\log_2 L)$, there are deleted symbols which need to be corrected. In another words, we need to find $[(F/\log_2 L) - n_{\text{on}}]$ "on" chip positions which were detected as "off" chips. The position of a possible "on" chip error is determined from

the position of a received "off" chip which has the *maximum* value of r_k among all received "off" chips. Then, the "off" chip is flipped to be an "on" chip.

In the soft-decision decoding algorithm, instead of comparing all possible sequences ($\approx L^{(F/\log_2 L)}$ sequences) having the same number of chips as the transmitted sequence, we can reduce the complexity by assuming that most of the chips are received correctly. This assumption is valid for high SNRs.

Now, we consider insertion-error correction. Assuming that there are no detected errors and there is one extra detected "on" chip, i.e. $n_{\text{on}} - (F/\log_2 L) = 1$, we need to find the position of an "off" chip which was received as an "on" chip. Given that $\hat{b}_1^{\tau(1)}$ and $\hat{b}_1^{\tau(2)}$ are the possible sequences and the Hamming distance between these sequences is two, $\hat{b}_1^{\tau(1)}$ has one "off" chip located at the position of the received "on" chip having the *minimum* value of r_k among all detected "on" chips, while $\hat{b}_1^{\tau(2)}$ has one "on" chip located at this position and one "off" chip located elsewhere. Therefore $\left(\sum_k \parallel \hat{b}_k^{(1)} - r_k \parallel^2\right) < \left(\sum_k \parallel \hat{b}_k^{(2)} - r_k \parallel^2\right)$, and MLSD would select $\hat{b}_1^{\tau(1)}$ since it yields the minimum Euclidean distance compared with the received sequence. Considering the proposed algorithm, the chip error is assigned to the position with a *minimum* value of r_k among all "on" chips. Thus, soft decoding also selects $\hat{b}_1^{\tau(1)}$ (same as with MLSD). The discussion is the same for deletion-error correction.

4.4.2 Simulation results

Fig. 4.7 shows the performance of soft-decision decoding compared with hard-decision decoding over an AWGN channel. This shows that the power required with soft decoding is less than that for hard decoding by about 2 dB. In addition, the upper bound from (5.20) is a good approximation at high SNRs, i.e. the proposed soft decoding performance is the same as with MLSD.

Figs. 4.8 through 4.11 present the frame error rate with soft-decision decoding compared with hard-decision decoding for a DPPM system with $L = 2, 4, 8$ and 16 over a dispersive channel with different values of D_T. The soft-decision system needs to transmit

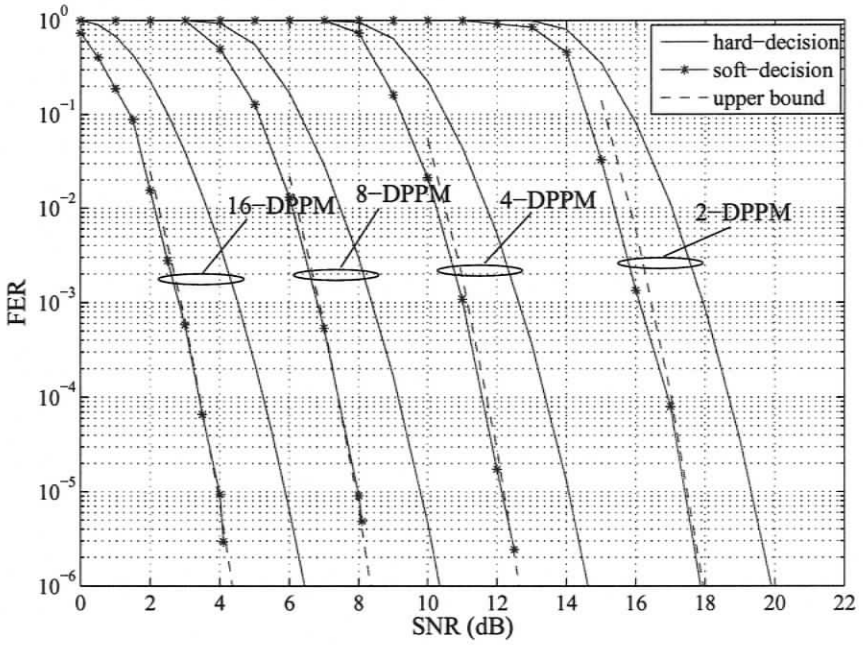

Figure 4.7. *Frame error rate with hard-decision and soft-decision decoding for a DPPM system with* $L = 2, 4, 8$ *and* 16 *on a nondispersive channel.*

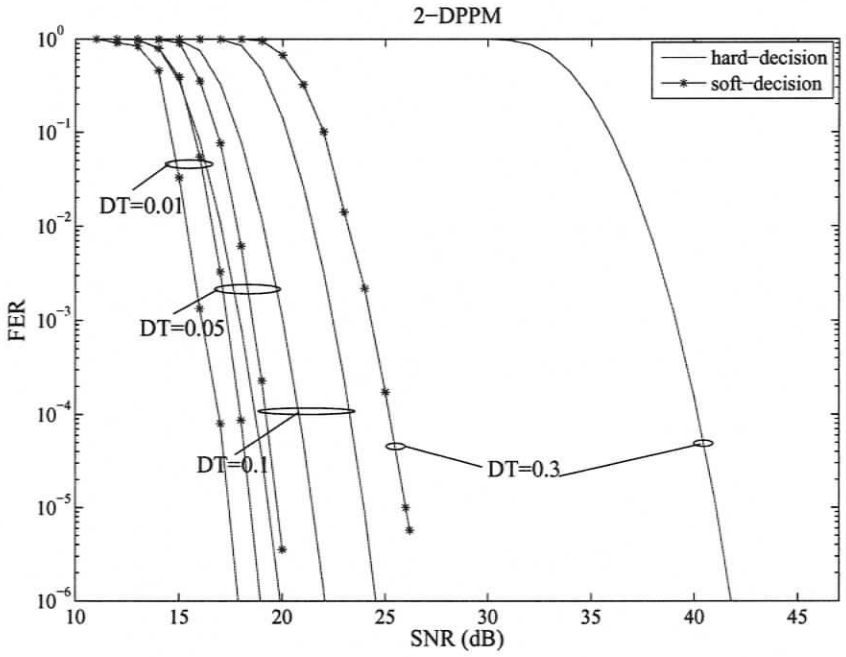

Figure 4.8. *Frame error rate with hard-decision and soft-decision decoding for a 2-DPPM system on a dispersive channel with* $D_T = 0.01, 0.05, 0.1$ *and* 0.3.

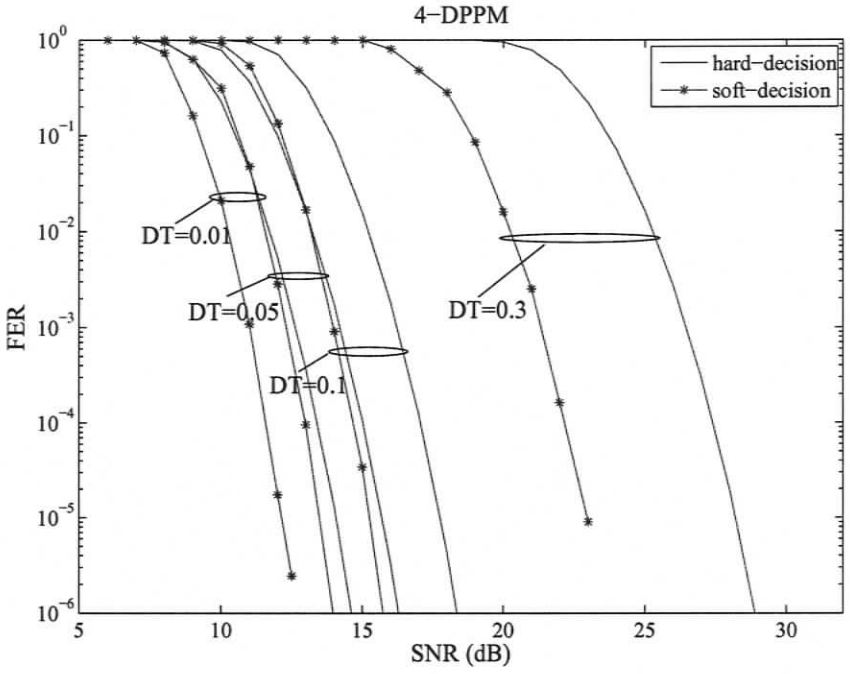

Figure 4.9. *Frame error rate with hard-decision and soft-decision decoding for a 4-DPPM system on a dispersive channel with* $D_T = 0.01, 0.05, 0.1$ *and* 0.3.

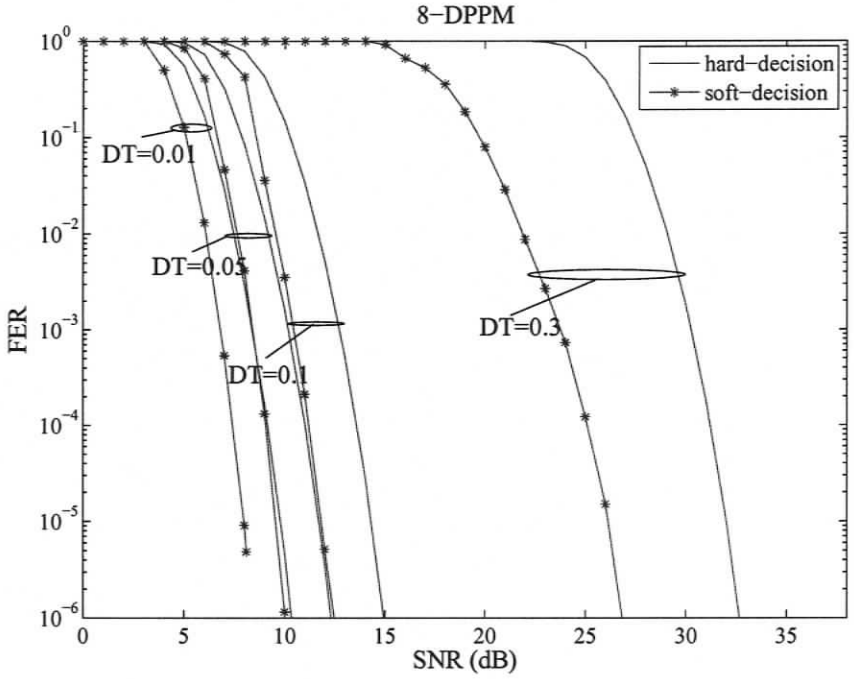

Figure 4.10. *Frame error rate with hard-decision and soft-decision decoding for a 8-DPPM system on a dispersive channel with* $D_T = 0.01, 0.05, 0.1$ *and* 0.3.

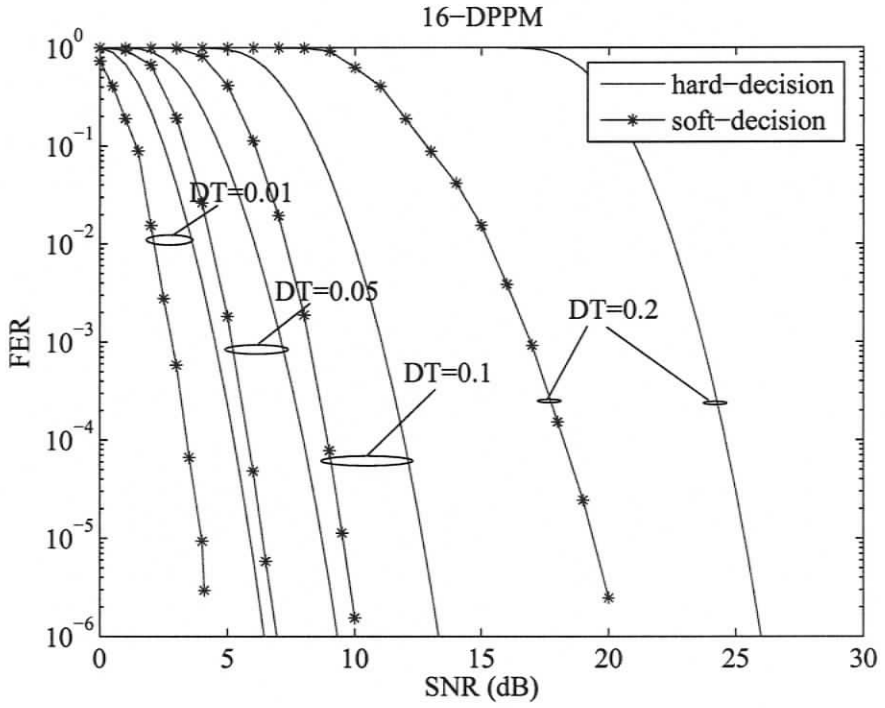

Figure 4.11. *Frame error rate with hard-decision and soft-decision decoding for a 16-DPPM system on a dispersive channel with* $D_T = 0.01, 0.05, 0.1$ *and* 0.2.

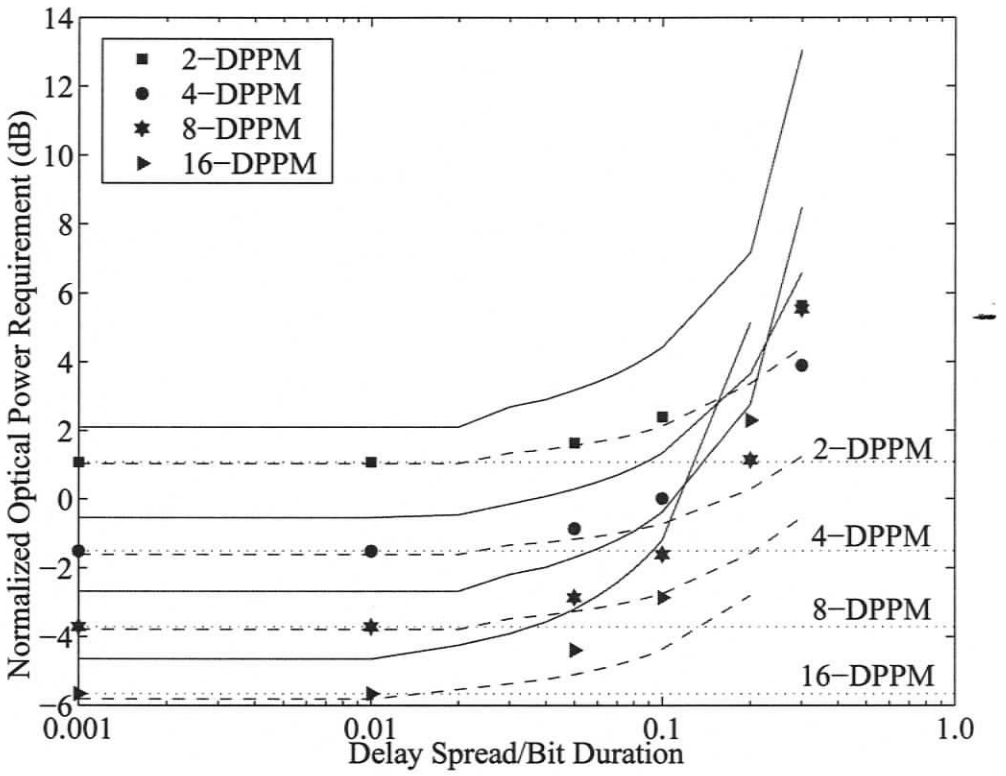

Figure 4.12. *Average optical-power required to transmit a 1-kB frame with a* 10^{-6} *frame-error rate for DPPM systems with* $L = 2, 4, 8$ *and* 16. *The solid lines represent the performance with hard-decision decoding. The dashed and dotted lines represent the upper bounds with soft-decision decoding on dispersive and nondispersive channels, respectively. The reference level (0 dB) is the optical power required for OOK on a nondispersive channel.*

much less power than the hard-decision system when D_T is high, especially when $L = 2$.

Fig. 4.12 presents the optical power penalty for hard-decision and soft-decision decoding in DPPM systems according to D_T. Moreover, it also compares the performance of MLSD from (5.20) and (5.21) with the proposed algorithm. This shows that soft decoding has performance very close to that with MLSD when $D_T \leq 0.1$. However, the power requirements for MLSD are less than for soft-decision decoding when $D_T > 0.1$ (especially when L is high), because the algorithm efficiency still depends on the threshold decision and correcting detected errors in the first step of the algorithm.

4.5 Complexity and Performance Comparisons

In this section, a comparison of the complexity and performance for all soft-decision decoding algorithms described above is given. The complexity is evaluated by the (approximate) required number of operations to decode one received frame.

Since MLSD needs to compare the received sequence with all possible sequence and select the most likely sequence which has minimum Euclidean distance from the received sequence, it requires $L^{(F/\log_2 L)}$ comparisons and each comparison requires τ multiplications and $2\tau - 1$ additions, where τ is the chip length per frame.

Next, we consider the proposed soft-decision algorithm. First, τ comparisons according to (4.31) are needed. Because of the multipath dispersion, "off" chips tend to be detected as "on" chips, so we assume that there are no detected errors. Then, the detector requires τ additions to determine the number of undetected insertion and deletion errors $\epsilon = |n_{\text{on}} - F/\log_2 L|$. To find the most likely chip error positions, the receiver needs approximately $(\epsilon\tau)$ comparisons. As a result, the complexity of this algorithm is not exponential in the frame length, and so is much less than with MLSD.

According to the MAP algorithms, the complexity depends on the number of states $n(\mathcal{S})$ in (4.10) and (4.12). Note that the complexity of the MAP algorithm significantly increases when the channel is more affected by intersymbol interference, while the complex-

Table 4.1. *Complexity of soft-decision decoding for DPPM systems.*

Operation	Additions	Multiplications	Comparisons
MLSD†	$2\tau - 1$	τ	$L^{(F/\log_2 L)}$
MAP	$8\tau n(\mathcal{S})$	$12\tau n(\mathcal{S})$	$\frac{F}{\log_2 L}\left(\tau - \frac{F}{\log_2 L}\right)$
Max-Log-MAP	$10\tau n(\mathcal{S})$		$8\tau n(\mathcal{S}) + \frac{F}{\log_2 L}\left(\tau - \frac{F}{\log_2 L}\right)$
SOVA	$6\tau n(\mathcal{S})$		$n(\mathcal{S})(2\tau + 1)$
Proposed	τ		$\tau(\epsilon + 1)$

† Note that, only for MLSD, the number of additions and multiplications is calculated for each comparison.

ity of MLSD and the proposed algorithm is independent of the channel. The complexity of all algorithms is summarized in Table 4.1.

In Table 4.2, we compare the performance of all soft-decision algorithms by considering the achieved gain relative to hard-decision decoding at FER=10^{-4}. Over a channel with low D_T, the proposed algorithm yields the same performance as the MAP detector and is better than SOVA. Moreover, its complexity is much less than that of the MAP detector. The proposed algorithm performs worse than the MAP algorithm when channel has intersymbol interference. However, it can achieve more gain than the MAP algorithm when the channel impulse response is unknown at the receiver.

4.6 Conclusions

A DPPM system over an intersymbol interference channel can be represented by a trellis diagram. Thus, the MAP, Max-Log-MAP and SOVA algorithms can be used to combat

Table 4.2. *The achieved gain [dB] for MAP, Max-Log-MAP, SOVA with perfect channel knowledge, MAP with $g_k = [1]$, and the proposed algorithm over a dispersive channel.*

system	4-DPPM		16-DPPM	
D_T	0.01	0.3	0.01	0.2
MAP	2	12	2	16.5
Max-Log-MAP	2	11.75	2	16.5
SOVA	0.4	11.5	0.5	14
MAP with $g_k = [1]$	2	4	2	5.5
proposed	2	5	2	6.5

ISI. First, MAP detectors with two different decision rules were presented. Then, Max-Log-MAP and SOVA were adapted to improve the performance of a DPPM system. Their error performance was compared with that with a hard-decision detector and MLSD. It was shown that excellent performance can be obtained which is superior to that with hard-decision decoding, and close to that with MLSD. Over a low dispersive channel, the MAP-I and Max-Log-MAP detectors require approximately 2 dB less transmit power than a hard detector, while the MAP-II and SOVA detectors require almost the same power as a hard detector. However, those detectors provide superb performance in high dispersive channels, i.e. the power requirement is about 10 dB less than with a hard-decision detector. In addition, the performance of MAP algorithms is degraded when the channel impulse response is unknown at the receiver.

Next, we proposed a novel soft decoding algorithm for a DPPM system over optical wireless communications. Its performance was evaluated on both nondispersive and dispersive channels and compared with MLSD and hard decoding. When the channel is

nondispersive or dispersive with low D_T, performance is similar to that with MLSD. In addition, soft decoding requires approximately 2 dB less power than hard decoding. The soft decoding performance is also better than hard decoding when the channel is dispersive with high D_T, although it requires more transmit power than MLSD. The performance of the proposed algorithm is independent of knowledge of the channel.

Finally, we compared the complexity of the soft-decision algorithms. It was shown that they can achieve superb performance (almost the same as MLSD) with much lower complexity.

Chapter 5

Forward Error-Control Coding for Differential Pulse-Position Modulation

5.1 Introduction

Forward error-control coding has been used to increase the power efficiency of optical wireless system modulation schemes such as PPM, MPPM and OPPM. In [74, 75], a Reed-Solomon (RS) code was used with PPM modulation and it was shown that the power required is significantly decreased. Takahashi *et al.* [76] studied the improvement when using an RS code in an MPPM system. The RS coded MPPM system yields a higher power efficiency of more than twice that of RS coded PPM. Convolutional codes have also been applied in OOK and PPM systems and the performance of trellis coded OPPM was examined in [43, 75]. Furthermore, the effect of imperfect chip synchronization on MPPM systems with an RS code and a convolutional code were investigated by Sato *et al.* [77]. Although coded MPPM performs better than an uncoded system at the same bit rate when timing offset is small, its performance becomes worse when the timing offset is large. In [78, 79], Yamamoto and Ohtsuki employed turbo coding in an optical wireless system with binary PPM (BPPM) to yield better performance.

Nevertheless, techniques which can correct errors in PPM, MPPM and OPPM systems cannot be applied directly to anisochornous modulation schemes like DPPM, DAPPM and DH-PIM$_\alpha$ systems due to the variable-length symbols which lead to insertion and deletion

Table 5.1. *Insertion/deletion errors in a 4-DPPM system.*

Transmitted bits	01	00	10	01	11	00	01	00
Transmitted symbols	1	0	2	1	3	0	1	0
Transmitted chips	01	1	001	01	0001	1	01	1
Received chips	00	1	001	01	0011	1	00	1
Received symbols	†_	2	2	1	‡20	0	†_	2

† Note that one symbol is deleted and followed by a substitution error.

‡ Note that one symbol is inserted and followed by a substitution error.

errors. Such errors cause the number of received symbols to differ from the number of transmitted symbols. An example of the occurrence of insertion and deletion errors in a 4-DPPM system is given in Table 5.1.

The error-control coding techniques which can correct insertion and deletion errors have been studied for decades. Note that insertion and deletion errors are sometimes referred to as synchronization errors. Such errors were first considered by Golomb *et al.* in 1958 [80]. He introduced block codes, the so called comma-free codes, having the property that the correct block which is next to a synchronization error can always be resynchronized. The codewords in a comma-free dictionary must follow the rule that overlaps of any pair of codewords cannot be a codeword. The construction of comma-free codes was presented in [81]. Scholtz adapted the condition on comma-free codes so that the codeword length can be variable and a code construction algorithm was also given in [82]. Although synchronization can be resumed, the error cannot be corrected and the decoder requires a look-up table.

In 1962, Sellers [83] proposed an error-control coding technique capable of correcting bit insertions or deletions by inserting a special character at fixed periodic intervals into the transmitted message and combining this with a burst-error-correcting code. These codes

can correct single deletion errors or insertion errors, and also substitution errors if no synchronization error occurs in the word. No bounds or simulation results have been obtained, so its efficiency is unknown.

Properties of binary block codes capable of correcting deletions, insertions and substitutions were first presented by Levenshtein in 1966 [84]. The Levenshtein distance between two codewords is defined as the minimal number of deletions and insertions in order to change one codeword into the other. Therefore these codes can correct up to s deletions and insertions if the Levenshtein distance between two codewords is greater than $2s$. The Levenshtein code construction which can correct a single insertion/deletion error was also presented. Levenshtein's works was expanded to correcting synchronization and substitution errors in consecutive words under the condition that both substitution and synchronization errors do not occur in the same word in [85, 86]. Helberg *et al.* [87] extended the Levenshtein theory and constructed codes which can correct multiple random insertion and deletion errors. However, the codes are in a nonsystematic form; therefore it is not easy to apply these to the real system. Ullman suggested inserting the synchronization sequence "011" before and after a codeword in order to correct errors that can be determined from the synchronization sequence [88]. Thus, a single synchronization error can be corrected and there is no need for table look-up. A systematic block code with fewer parity bits than the above codes, and its encoder and decoder, were presented in [89]. These codes can correct single synchronization errors. While most of the literature has focused on binary codes, Tenengolts proposed non-binary codes with a systematic form which are capable of correcting a single deletion or insertion [90].

Some concatenated codes have been suggested in the literature. An array code comprised of comma-free codes, which can be used for resynchronization, and Reed-Muller codes, which can correct random errors, was introduced in [91]. Thus, this array code is able to correct bursts of insertions, deletions and substitutions, however; its code rate is low. Another concatenated code combining watermark codes and low-density parity-check (LDPC) codes over non-binary fields was presented in [92]. In addition, convolutional

coding was modified to be used in a channel with insertions and deletions. In [93], new states corresponding to the insertions or deletions were added in the trellis diagram of the decoder while the encoder was unchanged. Both the encoder and decoder were adjusted in [94]. However, the ability to correct errors is limited to only insertions or deletions.

Previous work has resulted in complicated codes and offer low code rates. Hence, the objective of this chapter is to determine a concatenated code with low complexity and a high code rate to correct insertion and deletion errors that occur in DPPM systems and also to combat ISI.

A marker code is used as the inner code to locate the insertions and/or deletions. Its vicinity including the errors will be erased from the received sequence. Because Reed-Solomon code is capable of correcting erasures, we select an (n, k) Reed-Solomon code as the outer code to correct burst errors and erasures which result from the insertion and deletion errors. Examples are considered for both nondispersive and dispersive channels. In addition, the performance of hard-decision and soft-decision decoding of the coded DPPM system is evaluated based on both analytical and simulation results.

5.2 Concatenated Coding for DPPM Systems

The concatenated code system is shown in Fig. 5.1. From a binary data source, kq bits enter the RS encoder as k Q-ary symbols ($Q = 2^q$). The encoder adds $n - k$ parity symbols to obtain an n symbol codeword. These symbols are then transformed to L-ary symbols. One Q-ary symbol consists of approximately m L-ary symbols and may be a noninteger, i.e. $m \approx \log_2 Q / \log_2 L = q/M$. Thus, the n Q-ary symbols are transformed to nm L-ary symbols. A block of $M = \log_2 L$ bits is mapped to one of L distinct waveforms according to DPPM coding rules. Then, markers are inserted every δ L-ary symbols, i.e. the markers are inserted after every δ "on" chips. The marker is assigned to be different from the DPPM waveforms. It is comprised of L "off" chips followed by an "on" chip so that its total chip length is $L + 1$. Note that the chip duration of a marker is also equal to that of a DPPM

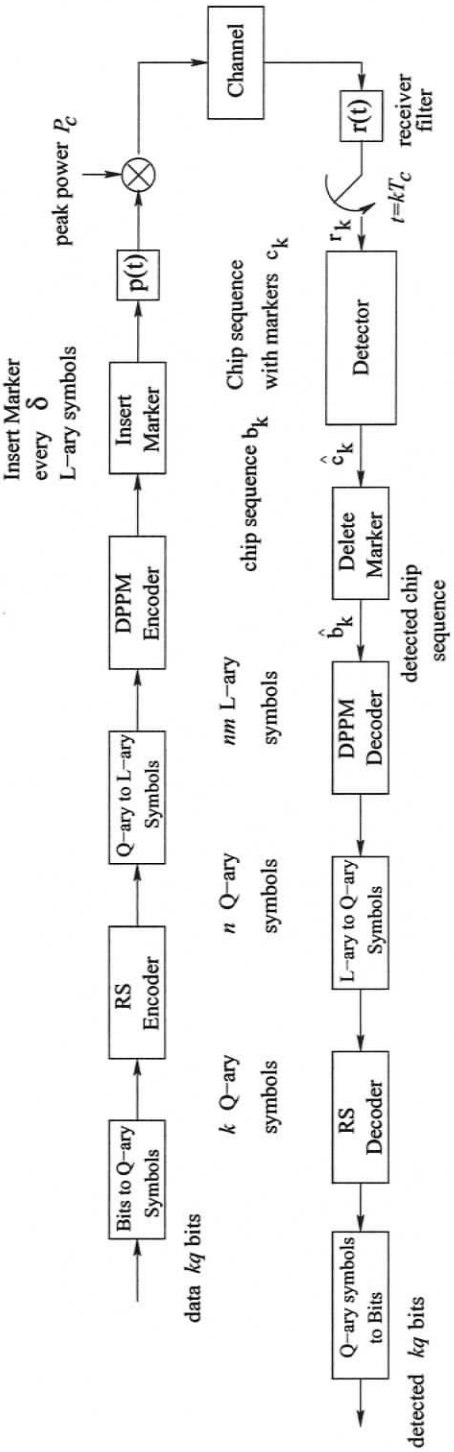

Figure 5.1. *Block diagram of a DPPM system with concatenated coding.*

symbol. Thus, the bandwidth of the coded DPPM system is

$$\mathrm{W} = \frac{(L+1)(1+(0.5\delta+1)N_i)R_b}{kq}, \tag{5.1}$$

where

$$N_i = \frac{nm}{\delta} \tag{5.2}$$

is the number of intervals in a codeword. Thus, the code rate of the concatenated marker and (n, k) RS code is

$$R = \frac{kq}{2M(1+(0.5\delta+1)N_i)}. \tag{5.3}$$

The chip sequence with markers $\boldsymbol{c}_1^\tau$ will be transmitted using a rectangular pulse shape $\underline{p}(t)$ with peak power

$$P_c = \frac{(L+1)(0.5nm+N_i-1)P_t}{nm+N_i-1}, \tag{5.4}$$

where P_t is the average transmit power.

At the receiver, the received signal is passed through a receive filter $r(t) = p(-t)$ and a detector. Then, the receiver attempts to locate the markers and delete them from the received chips, and transforms the remaining chips into L-ary symbols. Next, these symbols are formed into Q-ary symbols. The transmitted data is then obtained by decoding the received Q-ary symbols according to an RS decoding algorithm. Note that the RS decoding is hard-decision decoding.

Given an RS symbol size of $q = 8$ bits and uncoded message length $k = 233$ symbols, the RS codeword length is $n = 2^q - 1 = 255$ symbols and the minimum distance is $d_{\min} = n - k + 1 = 33$. As a result, the code can correct up to $t = \lfloor (d_{\min} - 1)/2 \rfloor = \lfloor (n-k)/2 \rfloor = 16$ symbol errors. In addition, up to e errors and s erasures can be corrected where $2e + s = n - k = 32$. This means that with erasures-only correction, 32 errors can be corrected if the error locations are known. The implemented RS code has generator polynomial $g(x) = x^8 + x^4 + x^3 + x^2 + 1$. We assign one codeword per frame and assume that the frame synchronization is perfect.

5.3 Hard-Decision Decoding Algorithms

First, we consider a receiver with hard decision decoding. At the receiver, the marker locations must be determined correctly so that the Reed-Solomon decoder can correct errors and/or erasures efficiently. Note that the Berlekamp-Massey algorithm is used to decode the Reed-Solomon code. Two decoding algorithms are presented below.

5.3.1 Algorithm I

Step 1: At the receiver, the filter output r_k is compared to the detection threshold θ to estimate the transmitted chips c_k

$$\hat{c}_k = \begin{cases} 0, \text{ iff } r_k < \theta \\ 1, \text{ iff } r_k \geq \theta \end{cases} . \tag{5.5}$$

Step 2: The marker locations are determined by searching the detected sequence $\hat{c}_1^{\tau}$ for possible markers. Two possible marker locations are selected if there are δ DPPM symbols and the interval between these markers does not contain more than $L-1$ consecutive "off" chips. Hence, we assume that those markers and symbols are received correctly and it is defined as a valid interval. Otherwise, the received symbols between the selected markers are erased. Below is an example of how to locate the markers in a 4-DPPM system with $\delta = 12$. The receiver attempts to determine the markers by searching for "00001". The interval between the possible markers in the first case is a valid interval because there is no run of "off" chips greater than 3 and the number of symbols is 12. In the second case, there is a run of 6 "off" chips and the number of symbols is only 10. Thus, this interval is defined as an erasure.

case 1:

$$\ldots \underbrace{00001}_{\text{marker}} \underbrace{0100100010110011100101 1001}_{\text{valid interval}} \underbrace{00001}_{\text{marker}} \ldots$$

case 2:

$$\ldots \underbrace{00001}_{\text{marker}} \underbrace{0100100000010011100101 1001}_{\text{erasure}} \underbrace{00001}_{\text{marker}} \ldots$$

If the number of unerased symbols is less than km, there is not enough information for the RS decoder to correct the errors. The algorithm then stops and the frame is declared in error.

***Step 3*:** After the markers have been recovered, the number of erased symbols n_{es} within the invalid intervals is determined. This step is important because although the location of the markers selected in the previous step is correct, if n_{es} is determined incorrectly, the followed symbols will be shifted and the RS decoder cannot correct the erasures. In this step, the number of erased symbols n_{es} is determined from the number of chips n_c within those intervals. For a given number of chips n_c, n_{es} can take on many values. All possible numbers of symbols will be assigned as

$$n_{es} = j\delta \tag{5.6}$$

if

$$j\delta + (j-1)(L+1) \leq n_c \leq j\delta L + (j-1)(L+1) \tag{5.7}$$

because the invalid interval may have a multiple of δ DPPM symbols and markers instead of containing only δ DPPM symbols. For example, in a 4-DPPM system with $\delta = 12$, if the number of chips is $n_c = 40$, the invalid interval may contain only 12 DPPM symbols or 24 DPPM symbols plus a marker. Hence, the number of erased symbols within the interval can be possibly 12 or 24. Hence, there might be more than one potential transmitted sequence. Then we obtain the possible chip sequences $\hat{\boldsymbol{b}}_1^{\tau(l)}, 0 \leq l < N_s$ where N_s is the number of possible chip sequences.

***Step 4*:** The possible sequences $\hat{\boldsymbol{b}}_1^{\tau(l)}$ which have the sum of the number of symbols from valid intervals and the number of erased symbols assigned from the third step not equal to nm are discarded. For those sequences $\hat{\boldsymbol{b}}_1^{\tau(l)}$ which generate nm L-ary symbols, the location of the erased DPPM symbols is determined. Then, the DPPM symbols are transformed into RS symbols and RS decoding is performed. Let $C^{(l)}$ be the decoded codeword from $\hat{\boldsymbol{b}}_1^{\tau(l)}$.

***Step 5*:** To select which sequence is the most likely transmitted sequence, we modify the algorithm presented in [95]. The decoded RS codewords $C^{(l)}$ are transformed back to chip sequences with markers $\hat{\mathbf{c}}_1^{\tau(l)}$. Then, we determine the distance between $\hat{\mathbf{c}}_1^{\tau(l)}$ and the received signal r_k as

$$\rho^{(l)} = \sum_k (\hat{c}_k^{(l)} - r_k)^2 \tag{5.8}$$

and the correct codeword is chosen as the $C^{(l)}$ for which $\rho^{(l)}$ is a minimum.

In summary, the decoder attempts to determine the positions of the markers and deletes them from the received chip sequence. Then, the remaining errors and/or erasures for each potential sequence are corrected by the RS decoder. Finally, the receiver chooses the decoded codeword $C^{(l)}$ which gives the minimum $\rho^{(l)}$ to obtain the best estimate of the transmitted kq bits of data.

5.3.2 Algorithm II

We can reduce the complexity of *Algorithm I* by modifying the condition to determine n_{es} in the third step. Rather than assigning all possible numbers of symbols to n_{es}, the detector choose the most likely number of symbols n_{es}. Consequently, the number of possible chip sequences is just one, i.e. $N_s = 1$. The third step of Algorithm I is changed as follows:

***Step 3*:** For a given number of chips n_c and number of "on" chips n_{on} between those selected markers from the second step, $n_{es} = j\delta$ if

$$n_c \leq j\delta L + (j-1)(L+1) \text{ and } n_{\text{on}} \leq j\delta + (j-1) + \Psi, \tag{5.9}$$

where $0 \leq \Psi \leq \delta$. Then we obtain one possible chip sequence $\hat{\mathbf{b}}_1^{\tau}$. If this sequence generates nm L-ary symbols, the algorithm continues to the fourth step; otherwise, it stops and the frame is declared in error.

Note that in this case the decoded codeword from the fourth step is presumed to be the transmitted codeword and the fifth step is discarded.

5.4 Analysis and Simulation Results for a Hard-Decision Coded DPPM System

A single-chip error corrupts the symbol associated with that chip and also shifts the following symbols. According to the decoding algorithm, if any received chips are in error, the interval associated with those chips is in error and the decoder will erase the corresponding $\lceil \delta/m \rceil$ Q-ary symbols.

We assume that all of the error intervals can be detected and erased. Since the RS code can correct up to $n-k$ erased symbols, the concatenated code can correct

$$T = \left\lfloor \frac{n-k}{\lceil (\delta/m) \rceil} \right\rfloor \tag{5.10}$$

erasure intervals, so the FER can be determined as

$$\text{FER} = 1 - \sum_{i_s=0}^{T} P(i_s) \tag{5.11}$$

where $P(i_s)$ is the probability of erasure intervals i_s. This depends on the interval error rate

$$P_{ie} = 1 - (1 - P_{ce})^{(0.5\delta(L+1))} \tag{5.12}$$

and the marker error rate

$$P_{me} = 1 - (1 - P_{ce})^{(L+1)} \tag{5.13}$$

where P_{ce} is the chip error rate. The chip error rate over a nondispersive channel for DPPM is given by [49]

$$P_{ce} = Q\left[\frac{rP_c}{(2\sqrt{WN_0})} \right]. \tag{5.14}$$

where r is the photodetector responsivity.

When the channel is dispersive, the received chip is affected not only by noise, but also previous and subsequent chips. Let s_j be an m-chip segment randomly taken from a DPPM sequence, $p(s_j)$ be the probability of occurrence of s_j, and $I(s_j)$ the receiver filter

output (excluding noise) of the next-to-last chip of s_j. The chip error rate over a dispersive channel can be calculated as [49]

$$P_{ce} = \sum_j p(s_j)\epsilon(s_j), \tag{5.15}$$

where $\epsilon(s_j)$ is the error probability of the next-to-last chip of s_j and

$$\epsilon(s_j) = \begin{cases} Q\left(\frac{(\theta - I(s_j))P_c}{\sqrt{N_0 W}}\right), & \text{if the next-to-last chip is an "off" chip.} \\ Q\left(\frac{(I(s_j) - \theta)P_c}{\sqrt{N_0 W}}\right), & \text{otherwise.} \end{cases} \tag{5.16}$$

Figs. 5.2 through 5.5 compare the performance of uncoded and coded DPPM systems using *Algorithm I* over a nondispersive channel as a function of SNR. The coded system performs better than the uncoded system, e.g., the coding gain is approximately 4 dB when the code rate is approximately 0.7 for a DPPM system with $L > 2$. We also show the frame error rate when all markers are located correctly (RS-perfect M), and when only some markers are located correctly (RS-M), via both analytic and simulation results. For large L, the performance of RS-perfect M and RS-M is much different than for low L. The reason is that when L is high, the marker length is also high which increases the probability of a marker error. When the code rate is low, i.e. the markers are inserted more frequently, the RS-M analytic performance differs from the simulation results. The reason is that when the number of L-ary symbols within an interval is low, the selected markers from the second step are located incorrectly more often. Thus, the performance of coded DPPM system can be improved by decreasing the code rate. However, the coded DPPM system with further low code rate can experience an error floor at high SNR. In an 8-DPPM system, the analysis and simulation results differ because m, the number of L-ary symbols per Q-ary symbol, is a noninteger. This result is confirmed by using $q = 6$ instead of $q = 8$ bits per RS symbol. In Fig. 5.6, the analysis and simulation results yield the same performance because m is an integer.

Fig. 5.7 presents the performance of coded 4-ary DPPM systems with different code rates when using *Algorithm I* and *Algorithm II* and only some markers are located correctly

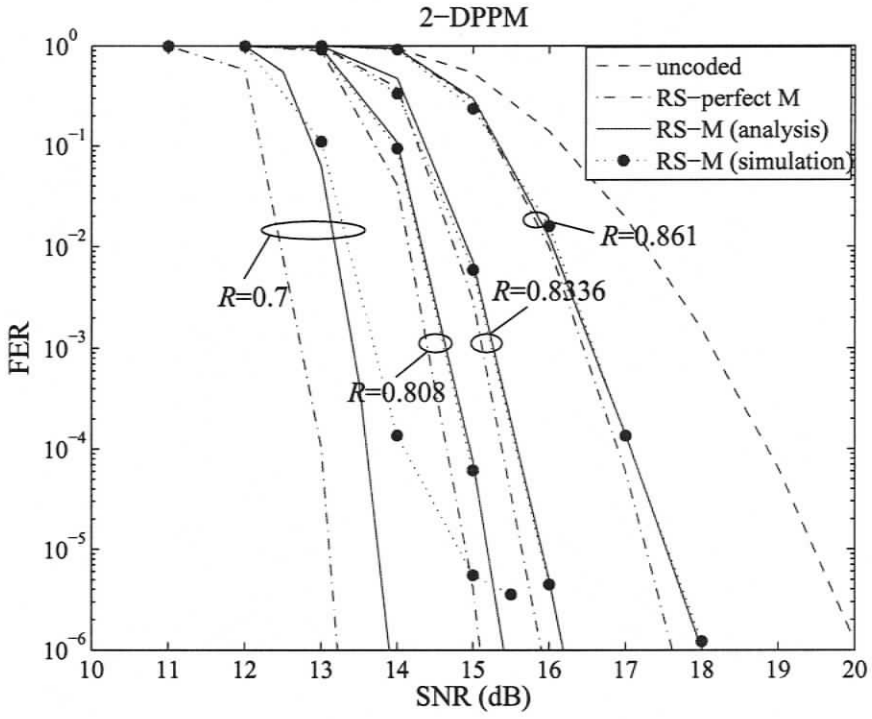

Figure 5.2. *Frame error rate of uncoded and coded 2-DPPM systems using* Algorithm I *over a nondispersive channel.*

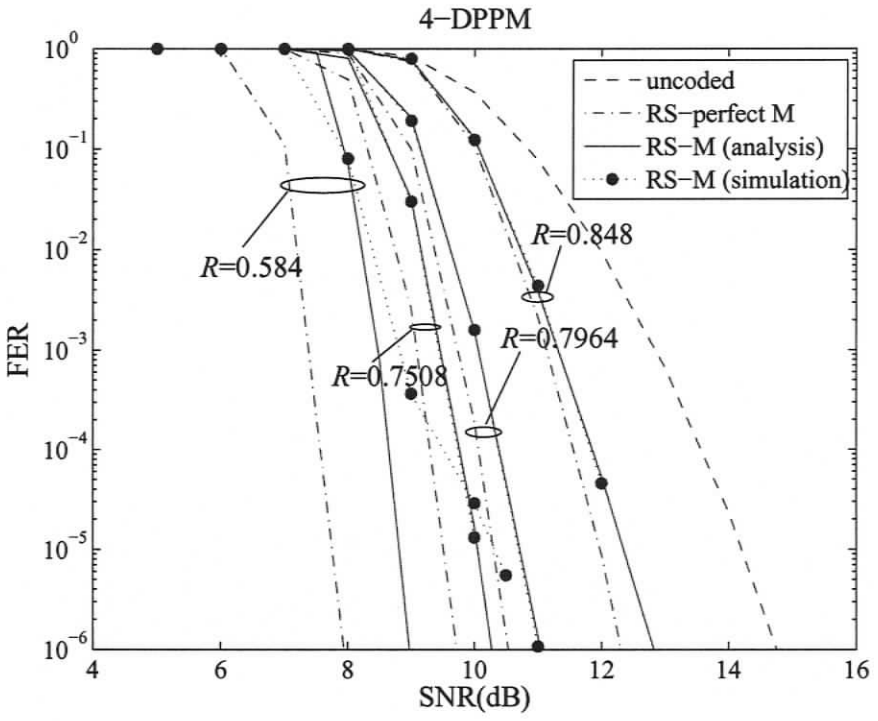

Figure 5.3. *Frame error rate of uncoded and coded 4-DPPM systems using* Algorithm I *over a nondispersive channel.*

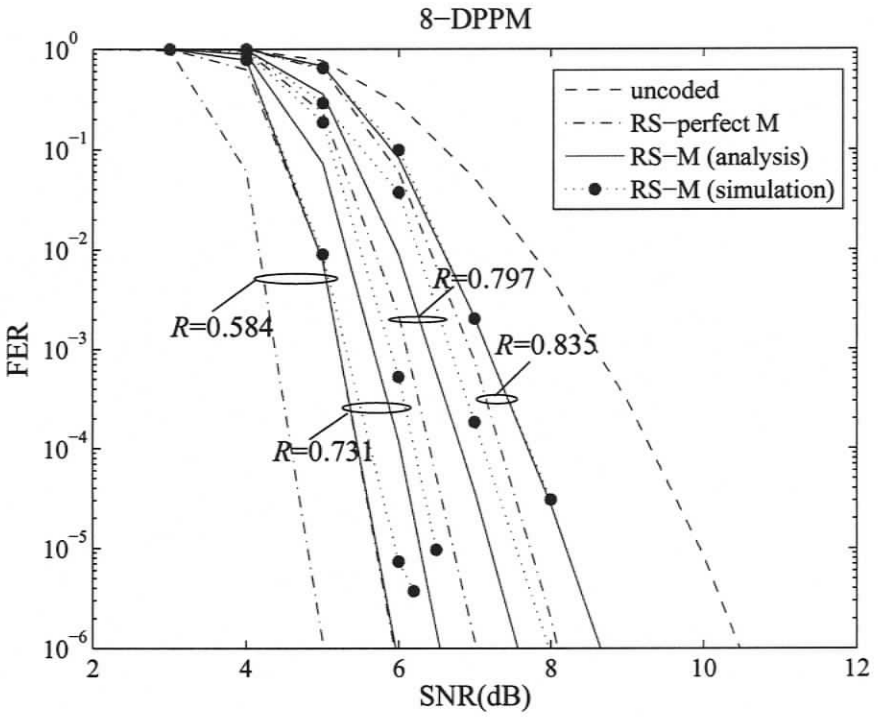

Figure 5.4. *Frame error rate of uncoded and coded 8-DPPM systems using* Algorithm I *over a nondispersive channel.*

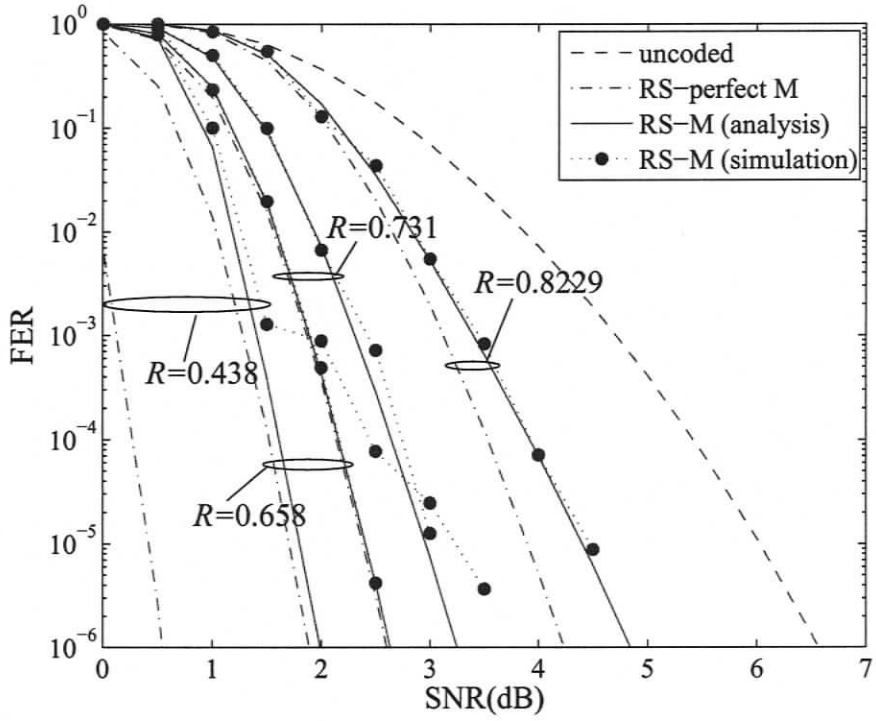

Figure 5.5. *Frame error rate of uncoded and coded 16-DPPM systems using* Algorithm I *over a nondispersive channel.*

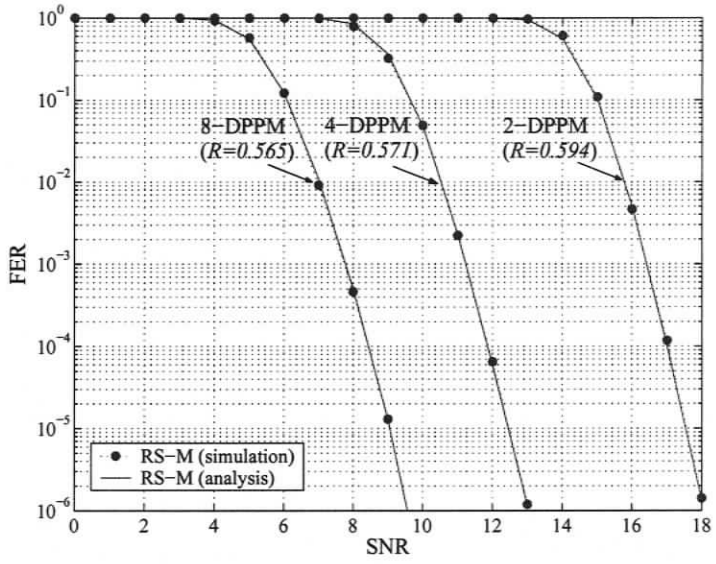

Figure 5.6. *Frame error rate of coded 2,4 and 8-DPPM systems with a* $(63, 39)$ *RS code over a nondispersive channel.*

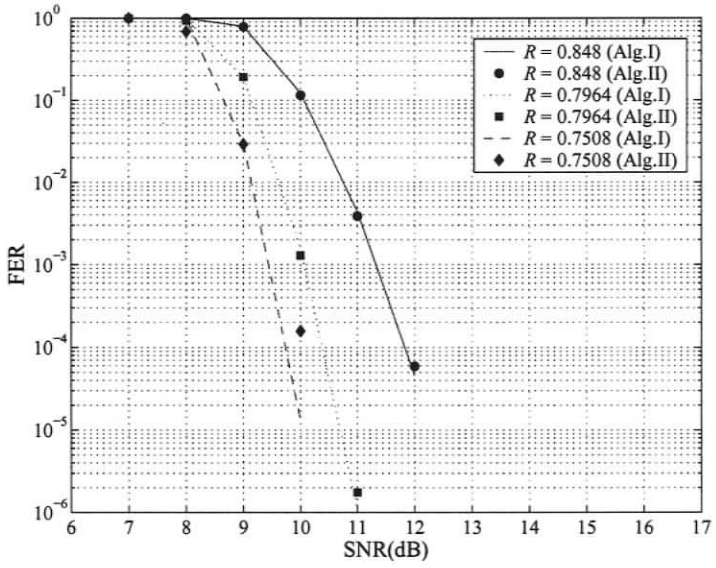

Figure 5.7. *Comparison of the performance of* Algorithm I *and* Algorithm II *in an (RS-M) coded 4-DPPM system over a nondispersive channel for different code rates.*

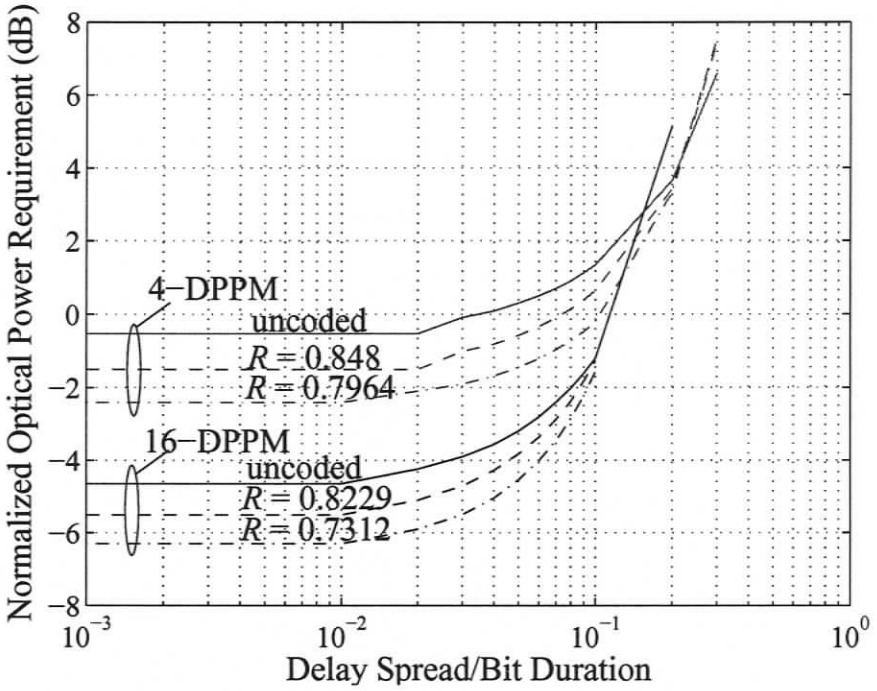

Figure 5.8. *Average optical-power requirements to transmit a kq-bits packet at* 10^{-6} *frame-error rate using coded 4- and 16-DPPM with different code rates compared to uncoded. The reference level (0 dB) is the optical power required for kq-bits with OOK modulation on a nondispersive channel.*

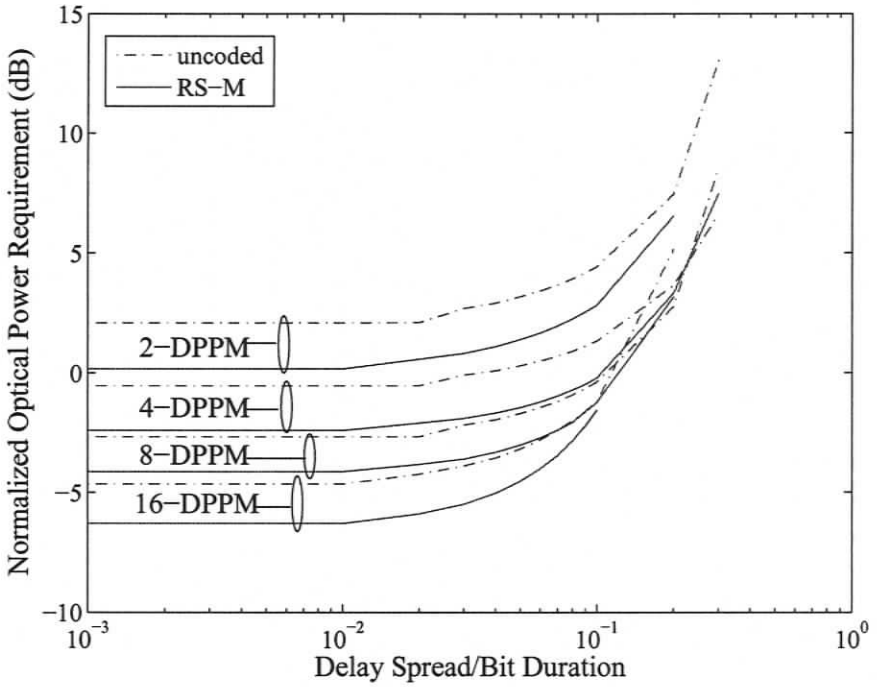

Figure 5.9. *Average optical-power requirements to transmit a kq-bit frame at* 10^{-6} *frame error rate using coded 2,4,8,16-DPPM systems with* $\delta = 40, 20, 20$ *and* 10*, respectively, compared to uncoded systems. The reference level (0 dB) is the optical power required for OOK on a nondispersive channel.*

(RS-M). At a high code rate, *Algorithm II* is nearly as power efficient as *Algorithm I*. However, when the code rate is low, its performance becomes slightly worse than that of *Algorithm I*. Figs. 5.8 and 5.9 show that coded DPPM performs better than uncoded DPPM at low D_T. As D_T increases, the performance of coded DPPM approaches that of uncoded DPPM.

5.5 Soft-Decision Decoding Algorithm

We now apply the suboptimal soft-decision algorithm proposed in Chapter 4 for the coded system. The first and second steps of the soft-decision decoding algorithm are the same as the hard-decision decoding algorithm, and the remaining steps are described as follows:

***Step 3*:** After some markers have been recovered from the second step, we use the condition in (5.9) to determine $n_{es} = j\delta$, the number of erased symbols. Note that j is the number of erasure intervals. Then, we obtain one possible chip sequence $\hat{b}_1^{\tau}$. If the sequence generates nm L-ary symbols, the algorithm continues to the next step. However, if the sequence generates L-ary symbols greater than nm, we assume that some of the selected markers from the second step are incorrect. In this step, we try to delete some of those markers. The two closest markers, i.e. the number of chips between them is smallest, are selected. The one with the higher Euclidean distance from the received chips r_k is deleted and n_{es} is reassigned. If it still cannot generate nm L-ary symbols or the number of generated symbols is less than nm, the process stops and the frame is declared in error.

***Step 4*:** In this step, we first determine $j-1$ markers within the j erasure intervals. We assume that the z-th marker is located between $((z+1)\delta + z) - \Phi$ symbols from the beginning of the interval and $((j-z-1)\delta + j - z - 2) - \Phi$ symbols from the end

of the interval, where $z = 0, 1, .., j-2$ and $0 \leq \Phi \leq \delta$.

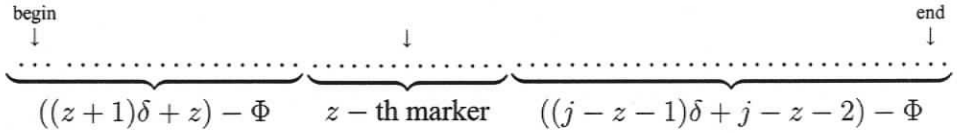

We define n_{on}^{b} as the number of "on" chips before the marker, n_{on}^{a} as the number of "on" chips after the marker, and n_e^m as the number of error chips within the marker. We assume that there are probable error chips which are given by

$$|((z+1)\delta + z) - n_{on}^{b}| + n_e^m + |((j-z-1)\delta + j - z - 2) - n_{on}^{a}|, \qquad (5.17)$$

if the marker is selected. There are several possible z-th markers. We select some of the possible markers with minimum probable error chips as marker candidates. Next, the chips between those selected markers are detected by the soft-decision detector as described in Chapter 4. However, since the number of symbols in an interval is equal to δ, the undetected errors are assigned as insertions if $N_s > \delta$; otherwise, they are deletions. Again, there are a number of possible chip sequences for the j erasure intervals. The sequence with minimum $\rho_{(l)}$, which is determined by

$$\rho^{(l)} = \sum_k (\hat{b}_k^{(l)} - r_k)^2 \qquad (5.18)$$

is selected and assigned as the transmitted chip sequence of the j-erasure intervals.

***Step 5*:** The detected DPPM symbols are transformed into RS symbols and RS decoding is performed to obtain the best estimate of the transmitted kq bits of data.

Note that this technique is still based on hard-decision decoding. Thus, the thresholds θ in (5.5) and Ψ in (5.9) should be optimized in order to appropriately select markers in the second step, assign the number of erased symbols in the third step, and correct the detected errors in the fourth step.

5.6 Analysis and Simulation Results for Soft-Decision Coded DPPM System

To analyse the performance of the coded DPPM system with soft-decision decoding is complicated. Therefore we assume that every marker is located correctly and its performance is only affected by the efficiency of the soft-decisions and the RS decoder. Let the error in soft-decision decoding cause every symbol within the erasure interval to be in error, then the sequence can be corrected only if there are no more than $T = \left\lfloor \frac{n-k}{2\lceil(\delta/m)\rceil} \right\rfloor$ error intervals. The corresponding frame error rate is

$$\text{FER} = 1 - \sum_{i=0}^{T} \binom{N_i}{i} (P_{ie})^i (1 - P_{ie})^{N_i - i} \tag{5.19}$$

where P_{ie} is the probability that an interval is in error after soft-decision decoding and can be calculated as described in the next section. Note that we analyze the performance over nondispersive and dispersive channels following the procedure presented in [49, 65], which was used to analyze the performance of an MLSD detector.

5.6.1 Performance over a nondispersive channel

As discussed in Chapter 4, an upper bound on the probability of an interval error over an AWGN channel at high SNRs can be computed as

$$P_{ie} \approx \left(\frac{L-1}{4}\right) \cdot \delta^2 \cdot Q\left(RP_t\sqrt{\frac{(L+1)\log_2 L}{4R_b N_0}}\right). \tag{5.20}$$

Fig. 5.10 shows the performance of soft decoding compared to hard decoding over a nondispersive channel. This shows that the power required with soft decoding is less than that for hard decoding by about 2 dB. The performance of the soft-decision system with RS-M performs close to that with RS-perfect M. Moreover, the upper bound from (5.19) with $P_{ie} =$ (5.20) is a good approximation at high SNRs.

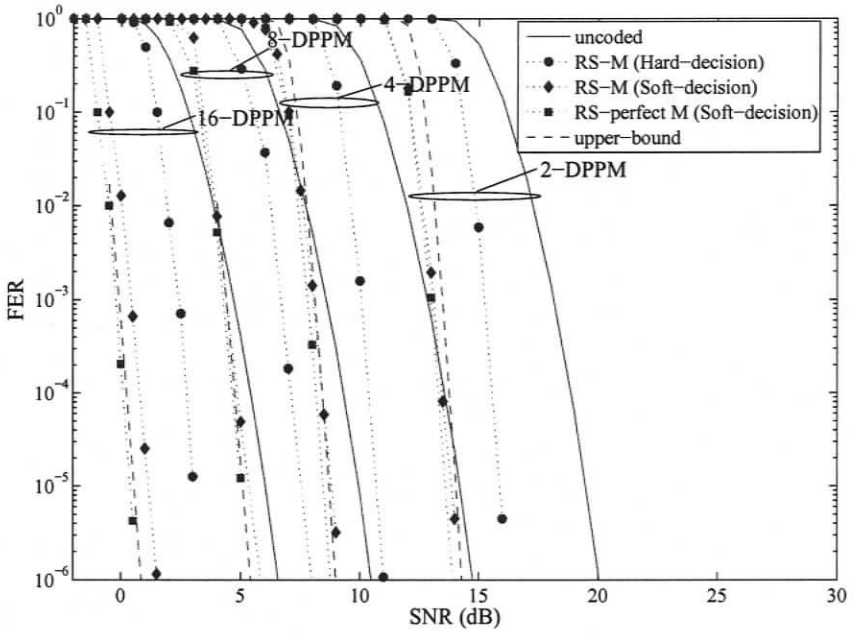

Figure 5.10. *Comparison of the performance of hard-decision and soft-decision decoding for coded 2,4,8,16-DPPM systems with* $\delta = 40, 20, 20$ *and* 10*, respectively, over a nondispersive channel.*

5.6.2 Performance over a dispersive channel

The probability of an interval error can be approximately upper bounded by

$$P_{ie} \approx \sum_{\bar{e} \in S} P(\bar{e}) \tag{5.21}$$

where $P(\bar{e})$ is the probability of error event $\bar{e}$ which can be calculated by (4.6). Note that the thresholds θ and Ψ are optimized in the simulation results.

Fig. 5.11 presents the frame error rate with soft-decision decoding compared to hard-decision decoding for a 4-DPPM system over a dispersive channel for different values of D_T. It also shows the performance of the system when every marker is received correctly. The soft-decision system needs to transmit much less power than the hard-decision system when D_T is high. Due to high intersymbol interferene, the receiver frequently selects the wrong markers and this affects the performance of soft-decision decoding. As a result, (RS-perfect M) outperforms (RS-M) when D_T is high.

Fig. 5.12 presents the optical power penalty for hard-decision and soft-decision DPPM systems according to D_T. Moreover, it also compares the performance of an (RS-perfect M) DPPM system with MLSD from the analysis to an (RS-M) DPPM system with the proposed soft-decision algorithm from simulation. This shows that (5.19) with $P_{ie} =$ (5.20) is a good approximation for soft-decision decoding performance over a dispersive channel when $D_T \leq 0.01$. Consequently, the proposed algorithm has performance close to that of an MLSD system. When D_T is higher, the power required from (5.19) with $P_{ie} =$ (5.21) is much less than the simulation results because the hard decoding still influences the efficiency of selecting markers and soft decoding.

5.7 Conclusions

In this chapter, we proposed a novel concatenated code, comprising a marker code as the inner code and a Reed-Solomon (RS) code as the outer code, to correct insertion and deletion

errors in differential pulse-position modulation (DPPM) for wireless infrared communications. A hard-decision decoding algorithm was presented. The performance over both nondispersive and dispersive channels was analyzed and compared with simulation results. The coded DPPM system outperforms the uncoded system and the coding gain over a nondispersive channel is about 4 dB when the code rate is about 0.7. Over a dispersive channel, although the coded system performs better than the uncoded system, the power penalty increases faster than that of an uncoded system when the ratio of delay spread to bit duration is high. Finally, we presented a soft decoding algorithm for the coded DPPM system, and evaluated its performance by analysis and simulation on both nondispersive and dispersive channels. The analysis is a good approximation when the channel is nondispersive or dispersive with $D_T \leq 0.1$. It was shown that soft decoding requires approximately 2 dB less power than hard decoding. Its performance is also better than hard decoding when the channel is dispersive with high D_T. Moreover, the performance of the proposed soft-decision decoding is close to MLSD when D_T is low. However, the (RS-perfect M) DPPM system with MLSD has exceptional performance when D_T is very high.

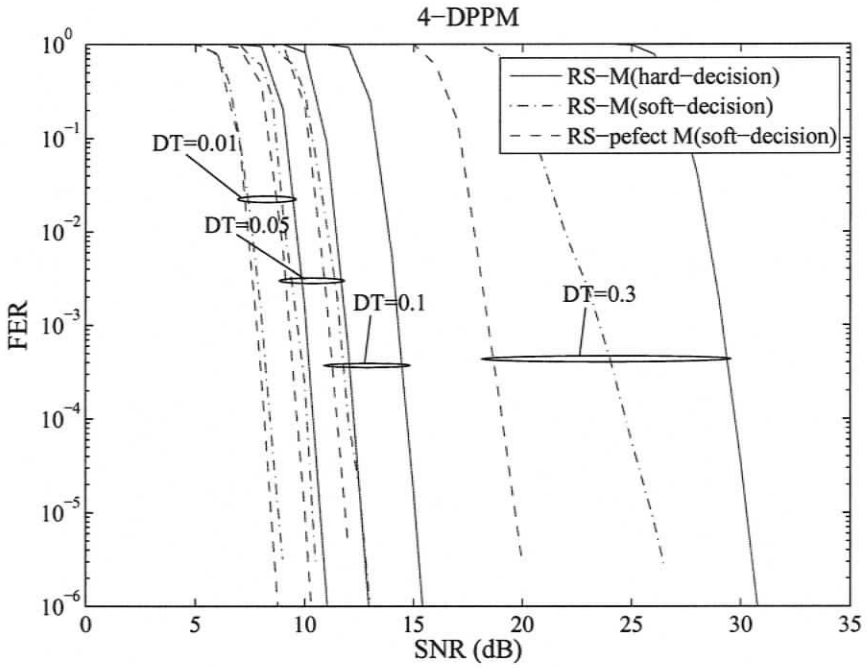

Figure 5.11. *Comparison of the performance of hard-decision and soft-decision decoding for a coded 4-DPPM system with* $\delta = 20$ *on a dispersive channel with* $D_T = 0.01, 0.05, 0.1$ *and* 0.3.

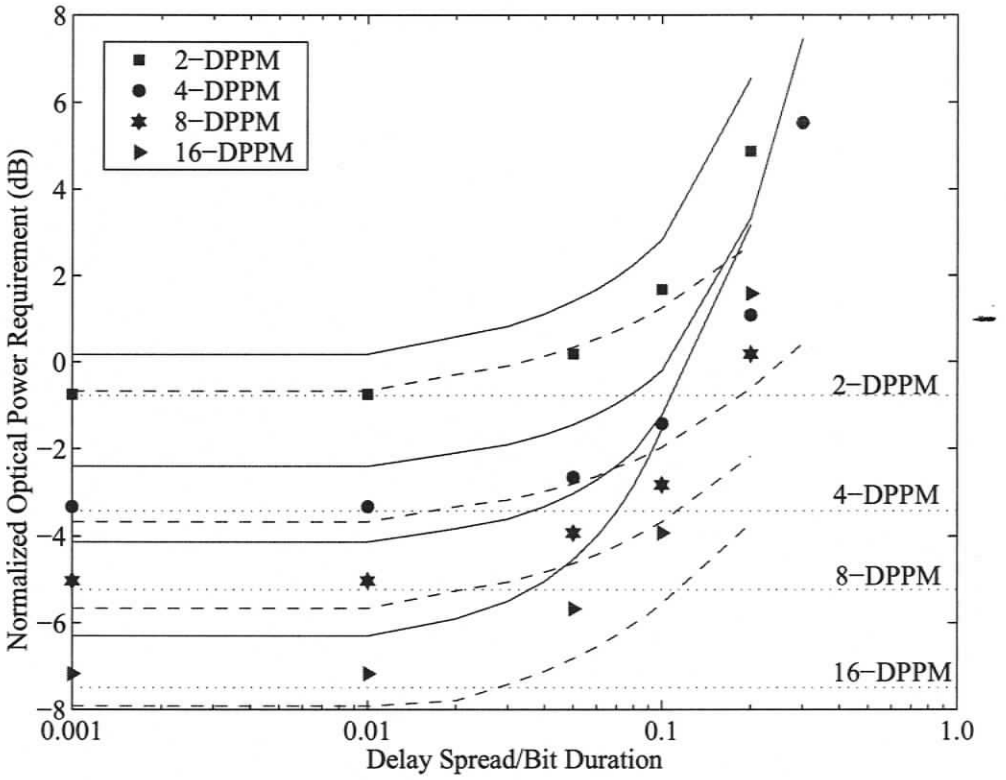

Figure 5.12. *Average optical-power requirements to transmit a kq-bit frame with 10^{-6} frame error rate for coded 2,4,8,16-DPPM systems with $\delta = 40, 20, 20$ and 10, respectively. The solid line represents the performance of a hard-decision system. The dashed and dotted line represents the upper bounds for a soft-decision system on dispersive and nondispersive channels, respectively. The reference level (0 dB) is the optical power required for OOK on a nondispersive channel.*

Chapter 6

Summary and Future Work

6.1 Summary

As the number of mobile users is increasing dramatically, the technology which can support access to high-speed networks must be investigated. Generally, radio technology has been exploited; however, optical systems have been considered as another option for wireless local area networks (WLANs) because it provides some advantages over radio system such as virtually unlimited and worldwide unregulated bandwidth and high security. Nonetheless, some drawbacks, e.g, path loss and multipath dispersion, hinder the utilization of optical systems in WLANs. Although indoor optical wireless communications (OWC) were introduced in 1979, this research area has not gained much attention until recently. There are still a lot of issues which need to be explored and developed such as transceiver design, channel modeling, and physical layer and higher-layer protocols, to enhance the performance of OWC.

In this thesis, an OWC system with anisochronous modulation, e.g. differential pulse position (DPPM) and differential amplitude pulse-position modulation (DAPPM), have been developed. The advantages of using such modulation are that it offers a good compromise between power and bandwidth efficiency and symbol synchronization is not required. The channel capacity of DPPM and DAPPM systems was calculated by using expectation-maximization. It was shown that the DPPM and DAPPM systems provide higher capacity than PPM system and the capacity convergence of DAPPM system is $\log_2(A+1)$

bits/sec/Hz, while the capacity convergence of PPM is zero when L is large. Since DPPM and DAPPM have better bandwidth efficiency than PPM, they are more robust to intersymbol interference than PPM. At constant SNR, soft-decision decoding yields higher capacity than hard-decision decoding especially when the channel suffers from multipath dispersion.

Since the DPPM system cannot exploit maximum-likelihood sequence detection used in a system with pulse-position modulation (PPM) to improve its performance, the maximum a posteriori (MAP) algorithm and its simplification such as Max-Log-MAP and soft-output Viterbi algorithm (SOVA) were modified for soft-decision decoding in the system. It was shown that their performance is closed to that of MLSD with lower complexity if the receiver knows the channel model. A novel soft-decision decoding algorithm was also proposed. The technique was motivated by the assumption that most of the chips are received correctly when SNR is high so that the chip-error positions can be located. Over a channel with low D_T, its performance is similar to that with MLSD. Although, over high dispersive channel, it requires more transmit power than MLSD, it performs better than MAP algorithm when the channel model cannot be estimated.

To improve the performance of DPPM system, the error-control coding was also considered. Since the variable-length symbols in a DPPM system lead to insertion/deletion errors, a conventional error-control coding cannot be exploited. The concatenation of marker and Reed-Solomon codes in order to correct such errors was introduced. The concatenated code decoding algorithms with hard-decision and soft-decision detection were presented. It was shown that the coded DPPM system with hard-decision decoding over nondispersive channel achieves approximately 4 dB gain when the code rate is about 0.7. However, its performance approaches that of uncoded DPPM as the ISI increases. Then, a soft-decision detector is employed to combat ISI. Over AWGN, the soft-decision system requires 2 dB gain relative to the hard-decision system and it also provides a performance improvement in high dispersive channels.

6.2 Future Work

Since DAPPM has the same self-symbol synchronization as DPPM, the conventional soft-decision decoding and error control coding which can be used in PPM cannot be applied to DAPPM. However, we can modify the soft-decision decoding algorithms introduced in Chapter 4 and the proposed concatenated code in Chapter 5 for DAPPM.

It was shown that the performance of MAP, Max-Log-MAP and SOVA can be much improved if the receiver has the ability to estimate the exact channel impulse response. The channel model can be estimated without a training sequence by using blind channel estimation. The basic idea is that the output from the symbol estimator based on the forward-backward recursion (BCJR algorithm) is fed back to channel estimator to improve the initial channel estimates [96, 97]. Since DPPM can be represented in a trellis diagram, the BCJR algorithm can be exploited to estimate received chips, so the channel model can be estimated iteratively by the blind channel estimator. However, an adaptation is needed due to the non-equiprobable input signal.

The insertion, deletion and substitution errors that exist in a DPPM system can be corrected using the proposed concatenated Reed-Solomon (RS) and marker code. If bursts of errors occur, the errors cannot be corrected and retransmission of the data frame corresponding to the errors is required. This can be done by an automatic repeat request (ARQ) protocol. When an error is detected at the receiver, a retransmission request is generated. However, the channel throughput decreases if the channel is significantly corrupted by noise and errors occur often. Thus, a hybrid between forward error correction (FEC) and ARQ is preferable [71]. FEC has the responsibility to correct the most frequently error patterns and detect less frequently occurring patterns. A detectable but uncorrectable error pattern initiates a request to the transmitter to retransmit the data. ARQ has been employed in an OWC system with PPM [98, 59]. The utilization of ARQ in a DPPM system has not been considered in the literature and so is a stimulating research area for future work.

Since users share the same channel, multiple access algorithms have been researched.

The performance of time-division multiple access (TDMA) and code-division multiple access (CDMA) with OOK for indoor OWC was examined [99]. The analysis showed that TDMA is comparable to CDMA. Although the complexity of TDMA is less than that of CDMA, it cannot be used in a DPPM or DAPPM system where symbols have no fixed length so users cannot communicate independently and simultaneously. In addition, the interference between users severely degrades the performance of the whole network due to intersymbol interference. Therefore CDMA might be a good candidate for multiple access in such modulation systems. The CDMA can be directly applied and the system should be analysed and compared with other systems with different modulation schemes.

Bibliography

[1] F. R. Gfeller and U. H. Bapst, "Wireless in-house data communication via diffuse infrared radiation," *Proceedings of the IEEE*, vol. 67, no. 11, pp. 1474–1486, November 1979.

[2] D. C. O'Brien and M. Katz, "Optical wireless communications within fourth-generation wireless systems [Invited]," *Journal of Optical Networking*, vol. 4, no. 6, pp. 312–322, June 2005.

[3] J. R. Barry, *Wireless Infrared Communications.* Norwell, MA: Kluwer, 1994.

[4] J. M. Kahn and J. R. Barry, "Wireless infrared communications," *Proceedings of the IEEE*, vol. 85, no. 2, pp. 265–298, February 1997.

[5] A. M. Street, P. N. Stavrinou, D. C. O'Brien, and D. J. Edwards, "Tutorial review: indoor optical wireless systems-a review," *Optical and Quantum Electronics*, vol. 29, pp. 349–378, 1997.

[6] A. Mahdy and J. Deogun, "Wireless optical communications: a survey," in *Proceedings of the IEEE Wireless Communications and Networking Conference (WCNC)*, vol. 4, 21-25 March 2004, pp. 2399–2404.

[7] International Electrotechnical Commission (IEC), "IEC 60825-1 edition 1.2, safety of laser products," *International Standard*, August 2001.

[8] A. Boucouvalas, "Indoor ambient light noise and its effect on wireless optical links," *IEE Proceedings Optoelectronics*, vol. 143, no. 6, pp. 334–338, December 1996.

[9] S. Hranilovic, *Modulation and Constrained Coding Techniques for Wireless Infrared Communication Channels.* M.A.Sc. thesis, University of Toronto, ON, Canada, 1999.

[10] Y. Tanaka, *A Study on Optical Wireless Communication Systems and Their Applications.* Ph.D. dissertation, Keio University, Kanagawa, Japan, 2002.

[11] D. O'Brien, G. Faulkner, E. Zyambo, K. Jim, D. Edwards, P. Stavrinou, G. Parry, J. Bellon, M. Sibley, V. Lalithambika, V. Joyner, R. Samsudin, D. Holburn, and R. Mears, "Integrated transceivers for optical wireless communications," *IEEE Journal of Selected Topics in Quantum Electronics*, vol. 11, no. 1, pp. 173–183, January-February 2005.

[12] M. Sakai, T. Sasao, K. Yamada, S. Toguchi, and T. Iwamoto, "A micro optical wireless module for high-definition images and broadband wireless access," in *Proceedings of the International Conference on Consumer Electronics (ICCE)*, 7-11 January 2006, pp. 43–44.

[13] P. Eardley and D. Wisely, "1 Gbit/s optical free space link operating over 40 m - system and applications," *IEE Proceedings on Optoelectronics*, vol. 143, no. 6, pp. 330–333, December 1996.

[14] G. Tourgee, G. Nykolak, P. Szajowski, and H. Presby, "2.5 Gbit/s free space optical link over 4.4 km," *IEE Electronics Letters*, vol. 35, no. 7, pp. 578–579, April 1999.

[15] G. Yun and M. Kavehrad, "Spot-diffusing and fly-eye receivers for indoor infrared wireless communications," in *Proceedings of the IEEE International Conference on Selected Topics in Wireless Communications*, 25-26 June 1992, pp. 262–265.

[16] M. Pakravan, E. Simova, and M. Kavehrad, "Holographic diffusers for indoor infrared communication systems," *International Journal of Wireless Information Networks*, vol. 4, no. 4, pp. 259–274, October 1997.

[17] S. Jivkova and M. Kavehrad, "Receiver designs and channel characterization for multi-spot high-bit-rate wireless infrared communications," *IEEE Transactions on Communications*, vol. 49, no. 12, pp. 2145–2153, December 2001.

[18] J. Kahn, J. Barry, W. Krause, M. Audeh, J. Carruthers, G. Marsh, E. Lee, and D. Messerschmitt, "High-speed non-directional infrared communication for wireless local-area networks," in *Proceedings of the IEEE Conference on Signals, Systems and Computers*, vol. 1, 26-28 October 1992, pp. 83–87.

[19] J. Barry, J. Kahn, W. Krause, E. Lee, and D. Messerschmitt, "Simulation of multipath impulse response for indoor wireless optical channels," *IEEE Journal on Selected Areas in Communications*, vol. 11, no. 3, pp. 367–379, April 1993.

[20] J. Carruthers and J. Kahn, "Modeling of nondirected wireless infrared channels," *IEEE Transactions on Communications*, vol. 45, no. 10, pp. 1260–1268, October 1997.

[21] J. Carruthers and S. Carroll, "Statistical models for indoor optical wireless channels," *Special Issue of the International Journal of Communication Systems: Indoor Optical Wireless Communication Systems and Networks*, vol. 18, no. 3, pp. 267–284, April 2005.

[22] N. M. Aldibbiat, Z. Ghassemlooy, and R. McLaughlin, "Dual header pulse interval modulation for dispersive indoor optical wireless communication systems," *IEE Proceedings - Circuits, Devices and systems*, vol. 149, no. 3, pp. 187–192, June 2002.

[23] IrDA, "http://www.irda.org," September 2004.

[24] R. T. Valadas, A. R. Tavares, and A. M. de Oliveira Duarte, "The infrared physical layer of the IEEE 802.11 standard for wireless local area networks," *IEEE Communications Magazine*, vol. 36, no. 12, pp. 107–112, December 1998.

[25] T. Komine and M. Nakagawa, "Integrated system of white LED visible-light communication and power-line communication," *IEEE Transactions on Consumer Electronics*, vol. 49, no. 1, pp. 71–79, February 2003.

[26] G. Edwards, "http://www.engadget.com/2005/06/29/kansai-airport-tries-delivering-content-using-visible-light/," June 2005.

[27] NEC corporation, "http://www.nec.co.jp/press/en/9710/2102.html," October 1997.

[28] JVC, "http://www.jvc.com/press," September 2004.

[29] Clarinet Systems, "http://www.clarinetsys.com/," April 2006.

[30] N. P. Schmitt, "Wireless optical NLOS communication in aircraft cabin for inflight entertainment distribution," in *Proceedings of the DTI-Workshop on Photonic Wireless Communication*, 26-28 April 2005.

[31] D. Kedar and S. Arnon, "Urban optical wireless communication networks: the main challenges and possible solutions," *IEEE Communications Magazine*, vol. 42, no. 5, pp. 2–6, May 2004.

[32] A. Gumaste and T. Antony, *First Mile Access Networks and Enabling Technologies.* Indianapolis, IN: Cisco Press, 1994.

[33] TereScope Product Line, "http://www.mrv.com/products/line/terescope.php," April 2006.

[34] Cablefree Solutions, "http://www.cablefreesolutions.com/products.htm," April 2006.

[35] fSONA optical wireless, "http://www.fsona.com/," April 2006.

[36] LightPointe, "http://www.lightpointe.com/home.cfm," April 2006.

[37] M. Akanegawa, Y. Tanaka, and M. Nakagawa, "Basic study on traffic information system using LED traffic lights," *IEEE Transactions on Intelligent Transportation Systems*, vol. 2, no. 4, pp. 197–203, December 2001.

[38] P. F. Szajowski, G. E. Tourgee, J. W. Robinson, G. Nykolak, A. J. Rigas, B. B. Brown, H. M. Presby, and J. J. Auborn, "Eight-channel video broadcast feed service using free-space optical wireless technology at Sydney 2000 Olympic Games," *Proceedings of SPIE*, vol. 4214, pp. 1–10, November 2000.

[39] M. Aljada, K. Alameh, and K. Al-Begain, "Distributed wireless optical communi-

cations for humanitarian assistance in disasters," in *Proceedings of the Third IEEE International Workshop on Electronic Design, Test and Applications (DELTA)*, 17-19 January 2006, pp. 321–326.

[40] H. Hemmati, *Deep Space Optical Communications*. Deep space communications and navigation series: Jet Propulsion Laboratory California Institute of Technology, 2005.

[41] J. Hamkins and B. Moision, "Selection of modulation and codes for deep space optical communications," *Proceedings of SPIE*, vol. 5338, pp. 123–130, June 2004.

[42] J. M. Kahn, J. R. Barry, M. D. Carruthers, J. B. Krause, and G. W. Marsh, "Non-directed infrared links for high-capacity wireless LANs," *IEEE Personal Communications*, vol. 1, no. 2, pp. 12–25, Second Quarter 1994.

[43] H. Park and J. R. Barry, "Modulation analysis for wireless infrared communications," in *Proceedings of the IEEE International Conference on Communications (ICC)*, vol. 2, 18-22 June 1995, pp. 1182–1186.

[44] J. M. Kahn and J. R. Barry, "Wireless infrared communications," *Proceedings of the IEEE*, vol. 85, no. 2, pp. 265–298, February 1997.

[45] A. M. Street, P. N. Stavrinou, D. C. O'Brien, and D. J. Edwards, "Indoor optical wireless systems - a review," *Optical and Quantum Electronics*, vol. 29, pp. 349–378, 1997.

[46] J. Zhang, "Modulation analysis for outdoors applications of optical wireless communications," in *Proceedings of the International Conference on Communication Technology Proceedings (WCC-ICCT)*, vol. 2, 21-25 August 2000, pp. 1483–1487.

[47] D. Chadha and P. K. Rathore, "Performance of pulse modulation schemes for infrared wireless communications," in *Proceedings of the Asia-Pacific Microwave Conference*, 3-6 December 2000, pp. 946–949.

[48] D. Zwillinger, "Differential PPM has a higher throughput than PPM for the band-limited and average-power-limited optical channel," *IEEE Transactions on Information Theory*, vol. 34, no. 5, pp. 1269–1273, September 1988.

[49] D. Shiu and J. M. Kahn, "Differential pulse-position modulation for power-efficient optical communication," *IEEE Transactions on Communications*, vol. 47, no. 8, pp. 1201–1209, August 1999.

[50] Z. Ghassemlooy, A. R. Hayes, N. L. Seed, and E. D. Kaluarachchi, "Digital pulse interval modulation for optical communications," *IEEE Communications Magazine*, vol. 36, no. 12, pp. 95–99, December 1998.

[51] A. R. Hayes, Z. Ghassemlooy, N. L. Seed, and R. McLaughlin, "Baseline-wander

effects on systems employing digital pulse-interval modulation," *IEE Proceedings-Optoelectronics*, vol. 147, no. 4, pp. 295–300, August 2000.

[52] Z. Ghassemlooy, A. R. Hayes, and B. Wilson, "Reducing the effects of intersymbol interference in diffuse dpim optical wireless communications," *IEE Proceedings-Optoelectronics*, vol. 150, no. 5, pp. 445–452, October 2003.

[53] N. M. Aldibbiat, Z. Ghassemlooy, and R. McLaughlin, "Performance of dual header-pulse interval modulation (DH-PIM) for optical wireless communication systems," *Proceedings of SPIE*, vol. 4214, pp. 144–152, February 2001.

[54] S. Hranilovic and D. A. Johns, "A multilevel modulation scheme for high-speed wireless infrared communications," in *Proceedings of the IEEE International Symposium on Circuits and Systems (ISCAS)*, vol. 6, 30 May-2 June 1999, pp. 338–341.

[55] J. G. Proakis, *Digital Communications*. New York: McGraw-Hill, 1995.

[56] L. W. Couch, *Digital and Analog Communication Systems*. New Jersey: Prentice Hall, 1997.

[57] H. Park and J. R. Barry, "Performance analysis and channel capacity for multiple-pulse position modulation on multipath channels," in *Proceedings of the IEEE International Symposium on Personal, Indoor and Mobile Radio Communications (PIMRC)*, vol. 1, 15-18 October 1996, pp. 247–251.

[58] S. Dolinar, D. Divsalar, J. Hamkins, and F. Pollara, "Capacity of pulse-position modulation (PPM) on Gaussian and Webb channels," *LPL TMO Progress Report*, pp. 42–142, August 2000.

[59] K. Akhavan, *Rate-Adaptive Code Combining over Time and Space for Wireless Radio Frequency and Infrared Communication Systems*. Ph.D. dissertation, The Pennsylvania State University, PA, USA, 2000.

[60] A. Kavcic, "On the capacity of Markov sources over noisy channels," in *Proceedings of the IEEE Global Telecommunications Conference (GLOBECOM)*, vol. 5, 25-29 November 2001, pp. 2997–3001.

[61] R. G. Gallager, *Information Theory and Reliable Communication*. New York, NY: John Wiley and Sons, 1968.

[62] R. E. Blahut, *Principles and Practice of Information Theory*. Cambridge, MA: Addison-Wesley, 1987.

[63] Z. Zhang, T. M. Duman, and E. M. Kurtas, "Achievable information rates and coding for MIMO systems over ISI channels and frequency-selective fading channels," *IEEE Transactions on Communications*, vol. 52, no. 10, pp. 1698–1710, October 2004.

[64] C. Berrou and A. Glavieux, "Near optimum error correcting coding and decoding: turbo-codes," *IEEE Transactions on Communications*, vol. 44, no. 10, pp. 1261–1271, October 1996.

[65] G. D. Forney, "Maximum-likelihood sequence estimation of digital sequences in the presence of intersymbol interference," *IEEE Transactions on Information Theory*, vol. 18, no. 3, pp. 363–377, May 1972.

[66] A. Kato and K. Zeger, "On the capacity of two-dimensional run length constrained channels," *IEEE Transactions on Information Theory*, vol. 45, no. 4, pp. 1527–1540, July 1999.

[67] M. D. Audeh, J. M. Kahn, and J. R. Barry, "Performance of pulse-position modulation on measured non-directed indoor infrared channels," *IEEE Transactions on Communications*, vol. 44, no. 6, pp. 654–659, June 1996.

[68] K. Akhavan, M. Kavehrad, and S. Jivkova, "High-speed power-efficient indoor wireless infrared communication using code combining - Part I," *IEEE Transactions on Communications*, vol. 50, no. 7, pp. 1098–1109, July 2002.

[69] J. Wang, Z. Xu, and W. Hu, "Improved DPPM modulation for optical wireless communications," *Proceedings of SPIE*, vol. 5281, pp. 483–490, May 2004.

[70] Z. Xu, J. Wang, and L. Shen, "A novel soft decoding technology in diffuse optical wireless networks employing DH-PIM," *Proceedings of SPIE*, vol. 5640, pp. 504–512, January 2005.

[71] S. B. Wicker, *Error Control Systems for Digital Communication and Storage*. Eaglewood Cliffs, NJ: Prentice-Hall, 1995.

[72] E. Zehavi and J. K. Wolf, "On runlength codes," *IEEE Transactions on Information Theory*, vol. 34, no. 1, pp. 45–54, January 1988.

[73] J. Hagenauer and P. Hoeher, "A Viterbi algorithm with soft-decision outputs and its applications," in *Proceedings of the IEEE Global Telecommunications Conference (GLOBECOM)*, vol. 3, 27-30 November 1989, pp. 1680–1686.

[74] R. E. Peile, "Error correction, interleaving and differential pulse position modulation," *International Journal of Satellite Communications*, vol. 6, pp. 173–187, April-June 1988.

[75] K. Akhavan, M. Kavehrad, and S. Jivkova, "High-speed power-efficient indoor wireless infrared communication using code combining - Part II," *IEEE Transactions on Communications*, vol. 50, no. 9, pp. 1495–1502, September 2002.

[76] M. Takahashi, H. Yashima, I. Sasase, and S. Mori, "Capacity and effects of Reed-

Solomon codes on multi-pulse PPM in optical communications," *IEICE Transactions on Communications*, vol. E72, no. 11, pp. 1198–1203, November 1989.

[77] K. Sato, T. Ohtsuki, and I. Sasase, "Coding for multi-pulse PPM with imperfect slot synchronization in optical direct-detection channels," *IEICE Transactions on Communications*, vol. E78-B, no. 6, pp. 916–922, June 1995.

[78] N. Yamamoto and T. Ohtsuki, "SOVA-based iterative decoding of turbo coded OOK and turbo coded BPPM," in *Proceedings of the IEEE International Symposium on Personal, Indoor and Mobile Radio Communications (PIMRC)*, vol. 1, 15-18 September 2002, pp. 369–373.

[79] T. Ohtsuki, "Turbo-coded atmospheric optical communication systems," in *Proceedings of the IEEE International Conference on Communications (ICC)*, vol. 5, 28 April-2 May 2002, pp. 2938–2942.

[80] S. W. Golomb, B. Gordon, and L. R. Welch, "Comma-free codes," *Canadian Journal of Mathematics*, vol. 10, no. 2, pp. 202–209, 1958.

[81] W. L. Eastman, "On the construction of comma-free codes," *IEEE Transactions on Information Theory*, vol. IT-11, no. 2, pp. 263–267, April 1965.

[82] R. A. Scholtz, "Maximal and variable word-length comma-free codes," *IEEE Transactions on Information Theory*, vol. IT-15, no. 2, pp. 300–306, March 1969.

[83] J. F. R. Sellers, "Bit loss and gain correction code," *IRE Transactions on Information Theory*, vol. 8, pp. 35–38, January 1962.

[84] V. I. Levenshtein, "Binary codes capable of correcting deletions, insertions, and reversals," *Soviet Physics-Doklady*, vol. 10, no. 8, pp. 707–709, February 1966.

[85] L. Calabi and W. Hartnett, "A family of codes for the correction of substitution and synchronization errors," *IEEE Transactions on Information Theory*, vol. IT-15, no. 1, pp. 102–106, January 1969.

[86] E. Tanaka and T. Kasai, "Synchronization and substitution error-correcting codes for the Levenshtein metric," *IEEE Transactions on Information Theory*, vol. IT-22, no. 2, pp. 156–162, March 1976.

[87] A. S. J. Helberg and H. C. Ferreira, "On multiple insertion/deletion correcting codes," *IEEE Transactions on Information Theory*, vol. 48, no. 1, pp. 305–308, January 2002.

[88] J. D. Ullman, "Near-optimal, single-synchronization-error-correcting code," *IEEE Transactions on Information Theory*, vol. IT-12, no. 4, pp. 418–424, October 1966.

[89] K. Saowapa, H. Kaneko, and E. Fujiwara, "Systematic deletion/insertion error correcting codes with random error correction capability," in *Proceedings of the In-*

ternational Symposium on Defect and Fault Tolerance in VLSI Systems (DFT), 1-3 November 1999, pp. 284–292.

[90] G. Tenengolts, "Nonbinary codes, correcting single deletion or insertion," *IEEE Transactions on Information Theory*, vol. IT-30, no. 5, pp. 766–769, September 1984.

[91] P. A. H. Bours, *Codes for Correcting Insertion and Deletion Errors*. Ph.D. dissertation, Eindhoven Technology University, Eindhoven, The Netherlands, 1994.

[92] M. C. Davey and D. J. C. Mackay, "Reliable communication over channels with insertions, deletions, and substitutions," *IEEE Transactions on Information Theory*, vol. 47, no. 2, pp. 687–697, February 2001.

[93] M. F. Mansour and A. H. Tewfik, "Convolutional codes for channels with substitutions," in *Proceedings of the IEEE Global Telecommunications Conference (GLOBECOM)*, vol. 2, 17-21 November 2002, pp. 1051–1055.

[94] T. G. Swart and H. C. Ferreira, "Insertion/deletion correcting coding schemes based on convolution coding," *Electronics letters*, vol. 38, no. 16, pp. 871–872, August 2002.

[95] H. Tanaka and K. Kakigahara, "Simplified correlation decoding by selecting possible codewords using erasure information," *IEEE Transactions on Information Theory*, vol. 29, no. 5, pp. 743–748, September 1983.

[96] A. A. Khan, *Iterative Decoding and Channel Estimation over Hidden Markov Fading Channels*. M.A.Sc. thesis, the Virginia Polytechnic Institute and State University, VN, USA, 2000.

[97] R. R. Lopes and J. R. Barry, "The extended-window channel estimator for iterative channel-and-symbol estimation," *EURASIP Journal on Wireless Communications and Networking*, vol. 2005, no. 2, pp. 92–99, 2005.

[98] T. Ozugur, M. Naghshineh, P. Kermani, and J. A. Copeland, "On the performance of arq protocols in infrared networks," *International Journal of Communication systems*, vol. 13, pp. 617–638, 2000.

[99] G. W. Marsh and J. M. Kahn, "Channel reuse strategies for indoor infrared wireless communications," *IEEE Transactions on Communications*, vol. 45, no. 10, pp. 1280–1290, October 1997.

[100] A. Kato and K. Zeger, "A comment regarding: "on the capacity of two-dimensional run length constrained channels"," June 2005.

[101] R. W. D. Nickalls and R. H. Dye, "The geometry of the discriminant of a polynomial," *The Mathematical Gazette*, vol. 80, pp. 279–285, July 1996.

[102] L. B. W. Jolley, *Summation of Series.* New York, NY: Dover publications, 1996.

[103] G. E. Andrews, *The Theory of Partitions.* Cambridge, England: Cambridge University Press, 1998.

Appendix A

The Channel Capacity Convergence of $A \times L$-DAPPM as L Grows

This appendix presents a proof of (3.33), the channel capacity limit of DAPPM when L is large, and (3.34), the rate of convergence, as mentioned in Chapter 3, by adapting the proof of the capacity limit for run-length codes described in [66, 100]. Kato and Zeger showed that the capacity of a $(0, k)$ run-length code (equivalent to the DPPM system) converges to one when k grows. We extend their work to determine the channel capacity convergence when the multilevel technique is applied to DPPM, i.e., the DAPPM system. The characteristic equation of the transition matrix **B**, (3.29), for DAPPM over a noiseless channel is

$$f(X) = X^{L+1} - (A+1)X^L + A = 0. \tag{A.1}$$

Then, the capacity is the base-two logarithm of its largest real root λ_{max}, i.e.,

$$C_{\text{DAPPM}} = \log_2 \lambda_{max}. \tag{A.2}$$

Nickalls and Dye showed in [101] that, given a real polynomial $f(X)$ of degree n with no repeated roots, β is the largest real root of $f(X)$ if

- when $X > \beta$, $f(X)$ has the same sign as a_n and
- when $X \leq \beta$, $f(X)$ has the sign of $-a_n$,

where a_n is the coefficient of the highest-degree term. In other words, the derivative of $f(X)$ has the same sign as a_n. Because a_n in (A.1) is equal to 1, we need to find X such

that $f'(X) > 0$. The derivative of $f(X)$ is

$$f'(X) = (L+1)X^L - (A+1)(L)X^{L-1}. \tag{A.3}$$

Therefore, $f'(X) > 0$ if

$$X > (A+1) - \frac{(A+1)}{L+1}. \tag{A.4}$$

We assume that the largest real root of $f(X)$ is the proximity to $(A+1)$. Thus, we let

$$X_\alpha = (A+1)(1 - \alpha(A+1)^{-L-1}), \tag{A.5}$$

and

$$f(X_\alpha) = A - \alpha(1 - \alpha(A+1)^{-L-1})^L, \tag{A.6}$$

where $\alpha \geq 0$.

In the case of $\alpha = A$,

$$X_A = (A+1) - \frac{A}{(A+1)^L} > (A+1) - \frac{(A+1)}{L+1}, \tag{A.7}$$

when L is very large. Therefore, $f'(X) > 0$ for all $X \geq X_A$. Considering $f(X_A)$, we can see that

$$f(X_A) = A - A\left(1 - \frac{A}{(A+1)^{L+1}}\right)^L > 0. \tag{A.8}$$

In the case of $\alpha > A$, it is seen that $X_\alpha < X_A$ and

$$\lim_{L\to\infty} f(X_\alpha) = A - \alpha, \tag{A.9}$$

because $(1 - \alpha(A+1)^{-L-1})^L = 1$. Consequently, $\lim_{L\to\infty} f(X_\alpha) < 0$ when $\alpha > A$.

Considering large L, the largest real root λ_{max} is located as

$$X_\alpha < \lambda_{max} < X_A, \tag{A.10}$$

and the capacity is bounded by

$$\log_2 X_\alpha < \log_2 \lambda_{max} < \log_2 X_A. \tag{A.11}$$

Therefore,

$$\log_2(A+1)+\log_2\left(1-\frac{\alpha}{(A+1)^{L+1}}\right) < C_{\text{DAPPM}} < \log_2(A+1)+\log_2\left(1-\frac{A}{(A+1)^{L+1}}\right), \tag{A.12}$$

and thus

$$\lim_{L\to\infty} C_{\text{DAPPM}} = \log_2(A+1), \tag{A.13}$$

so we can conclude that the capacity of $A \times L$-DAPPM converges to $\log_2(A+1)$ when L grows.

Since [102]

$$\ln(1-x) = -\sum_{n=1}^{\infty}\frac{x^n}{n}, \tag{A.14}$$

$$\begin{aligned}\log_2 X_\alpha &= \log_2(A+1)+\log_2\left(1-\frac{\alpha}{(A+1)^{L+1}}\right) \\ &= \log_2(A+1)-(\log_2 e)\sum_{n=1}^{\infty}\frac{\alpha^n(A+1)^{-n(L+1)}}{n}.\end{aligned} \tag{A.15}$$

Then, (A.12) can be rearranged as

$$\sum_{n=1}^{\infty}\frac{A^n(A+1)^{-(n-1)(L+1)}}{n} \le \frac{\log_2(A+1)-C_{\text{DAPPM}}}{(\log_2 e)(A+1)^{-L-1}} \le \sum_{n=1}^{\infty}\frac{\alpha^n(A+1)^{-(n-1)(L+1)}}{n} \tag{A.16}$$

$$A \le \frac{\log_2(A+1)-C_{\text{DAPPM}}}{(\log_2 e)(A+1)^{-L-1}} \le \sum_{n=1}^{\infty}\alpha^n(A+1)^{-(n-1)(L+1)}.$$

If $x < 1$, [102]

$$\sum_{n=0}^{\infty}x^n = \frac{1}{1-x}, \tag{A.17}$$

then

$$A \le \frac{\log_2(A+1)-C_{\text{DAPPM}}}{(\log_2 e)(A+1)^{-L-1}} \le \frac{\alpha}{1-\alpha(A+1)^{-L-1}}. \tag{A.18}$$

For all $\alpha \ge A$

$$A \le \lim_{L\to\infty}\frac{\log_2(A+1)-C_{\text{DAPPM}}}{(\log_2 e)(A+1)^{-L-1}} \le \lim_{L\to\infty}\frac{\alpha}{1-\alpha(A+1)^{-L-1}} = \alpha \tag{A.19}$$

and

$$\lim_{L\to\infty} \frac{\log_2(A+1) - C_{\text{DAPPM}}}{(\log_2 e)(A+1)^{-L-1}} = A \tag{A.20}$$

$$\lim_{L\to\infty} [\log_2(A+1) - C_{\text{DAPPM}}] = \frac{A\log_2 e}{(A+1)^{L+1}}.$$

Accordingly, the rate of converge of the C_{DAPPM} as L grows is $\frac{A\log_2 e}{(A+1)^{L+1}}$.

Appendix B

Frame Error Rate of Coded DPPM with Hard-decision Detection

In this appendix, the frame error rate of a coded DPPM system mentioned in (5.11) is derived. According to the detection algorithm, the errors can be corrected if the number of erasure intervals in the received frame is less or equal to $T = \left\lfloor \frac{n-k}{\lceil(\delta/m)\rceil} \right\rfloor$. Let P_{ce} be the chip error rate, the interval error rate is

$$P_{ie} = 1 - (1 - P_{ce})^{(\delta\bar{L})}, \tag{B.1}$$

and the marker error rate is

$$P_{me} = 1 - (1 - P_{ce})^{(L+1)}. \tag{B.2}$$

The frame error rate can be calculated as

$$FER = 1 - \sum_{i_s=0}^{T} P(i_s), \tag{B.3}$$

where $P(i_s)$ is the probability that i_s intervals are erased and can be determined as follows.

A partition is a way of writing an integer i_s as a sum of positive integers where the order of the addends is not significant and n_p define as the number of ways of doing so [103]. For example, if $i_s = 3$, $n_p = 3$, all partitions can be written as

$$\begin{aligned} 3 &= 3 \\ &= 2+1 \\ &= 1+1+1 \end{aligned} \tag{B.4}$$

or

$$\mathbf{p} = \begin{bmatrix} 3 & 0 & 0 \\ 1 & 1 & 0 \\ 0 & 0 & 1 \end{bmatrix} \tag{B.5}$$

where $\mathbf{p}$ is an $n_p \times i_s$ matrix and p_{ij} is the number of addends equal to j in the ith partition. Let each addend represent the number of successive erasure intervals. The above example can be interpreted that, in a received frame,

- there is only one three-consecutive erasure interval.
- there is a two-consecutive erasure interval and a one-erasure interval which are not next to each other.
- there are three nonadjacent erasure intervals.

There are several interval and marker error patterns which create a j-successive-erasure interval. Suppose $j = 2$, then the intervals and marker error patterns are

$$\begin{array}{ll} I\ M\ I & I\ M\ I \\ I\ M & I\ M \\ M\ I & I\ M \\ & M\ I \\ & M \end{array} \tag{B.6}$$

Note that the cross over I (interval) and M (marker) means they are in error. Only patterns on the right-hand side will be assigned as a 2-successive-erasure interval and the summation of the probability of those patterns is the probability of a j-consecutive erasure interval $P(j)$ occurring.

Let $n_m^{(i)}$ be the number of markers within the erasures in the i-th partition, i.e.

$$n_m^{(i)} = \sum_{j=2}^{i_s} (j-1) p_{ij}, \tag{B.7}$$

and $n_i^{(i)}$ be the number of consecutive interval erasures in the i-th partition, i.e.

$$n_i^{(i)} = \sum_{j=1}^{i_s} p_{ij}. \tag{B.8}$$

Then, the probability $P(i_s)$ can be calculated as

$$P(i_s) = \sum_{i=1}^{n_p} \left[n^{(i)} (1 - P_{ie})^{N_i - n_i^{(i)}} (1 - P_{me})^{N_i - 1 - n_m^{(i)}} \right] \sum_{j=1}^{i_s} p_{ij} P(j), \tag{B.9}$$

where N_i is the number of intervals in a codeword and $n^{(i)}$ is the total number of ways of arranging erasures in the i-th partition in a frame when no erasures are allowed to be next to each other.